Inferencing with motion artifacts - bed based BCG and MRI case studies

by

Alaleh Alivar

B.S., Shiraz University, Iran, 2011

M.S., Shiraz University of Technology, Iran, 2014

AN ABSTRACT OF A DISSERTATION

submitted in partial fulfillment of the
requirements for the degree

Doctor of Philosophy

Department of Electrical and Computer Engineering
College of Engineering

KANSAS STATE UNIVERSITY
Manhattan, Kansas

2019

Abstract

A signal is a physical quantity which differs with respect to time, space, or other independent variables and contains information about a physical phenomenon. In biomedical applications, analysis and evaluations of signals acquired with bio-measurement tools help with health monitoring and treatment. Biomedical signals may be easily affected by noise arising due to imprecision in measuring instruments, uncertainty within the systems, patient movements, or interference from external sources. Therefore, in many cases, it is necessary to process the signal in order to reduce or eliminate unwanted signals and improve reliability of inferencing. Motivated by these factors, the present dissertation addresses some key challenges associated with inferencing with motion artifacts in two biomedical sensing modalities as 1D and 2D signals: (1) ballistocardiogram (BCG), and (2) magnetic resonance imaging (MRI).

In the first case study, we determine the effect of motion artifacts on a bed-based BCG signal as a 1D biomedical signal. Specifically, we develop a motion detection algorithm followed by a motion artifact removal system using an unobtrusive contact-less electromechanical film based ballistocardiogram sensor integrated into a smart bed system. Furthermore, we leverage the results from the motion detection algorithm to define a restlessness metric that enables us to quantify sleep quality. We demonstrate the use of this algorithm using data from individuals with autism spectrum disorder (ASD) with a collaboration with Heartspring, Wichita, Kansas. Additionally, we illustrate the value of using the restlessness metric along with other indicators of sleep to predict daytime behaviors in this specific population.

In the second case study, we focus on identifying temperature changes due to device or organ movement in proton resonance frequency shift (PRFS) MR-thermometry as 2D biomedical sensing modality. Firstly, we develop an enhanced hybrid method suitable for MRI thermometry in the presence of motion during microwave thermal therapy for heating using diffuse

sources such as needle- and catheter-based microwave applicators. The presented model-based method uses the sparsity of wavelet coefficients of the phase shift based on the fact that heat-induced phase shifts exhibit a correlation structure due to smoothness. Secondly, we propose a new robust motion correction algorithm based on robust principal component analysis (RPCA) to recover low-rank matrix from sparse errors without the need of modeling. We illustrate the efficiency of both works by comparing the results to the previously presented model-based method and fiber-optic temperature sensors during microwave heating of a tissue-mimicking phantom with a 2.45 GHz directional microwave antenna integrated with 14.1 T high-field MRI.

Inferencing with motion artifacts - bed based BCG and MRI case studies

by

Alaleh Alivar

B.S., Shiraz University, Iran, 2011

M.S., Shiraz University of Technology, Iran, 2014

A DISSERTATION

submitted in partial fulfillment of the
requirements for the degree

Doctor of Philosophy

Department of Electrical and Computer Engineering
College of Engineering

KANSAS STATE UNIVERSITY
Manhattan, Kansas

2019

Approved by:

Co-Major Professor
Dr. Balasubramaniam Natarajan

Approved by:

Co-Major Professor
Dr. Punit Prakash

Copyright

Abstract

A signal is a physical quantity which differs with respect to time, space, or other independent variables and contains information about a physical phenomenon. In biomedical applications, analysis and evaluations of signals acquired with bio-measurement tools help with health monitoring and treatment. Biomedical signals may be easily affected by noise arising due to imprecision in measuring instruments, uncertainty within the systems, patient movements, or interference from external sources. Therefore, in many cases, it is necessary to process the signal in order to reduce or eliminate unwanted signals and improve reliability of inferencing. Motivated by these factors, the present dissertation addresses some key challenges associated with inferencing with motion artifacts in two biomedical sensing modalities as 1D and 2D signals: (1) ballistocardiogram (BCG), and (2) magnetic resonance imaging (MRI).

In the first case study, we determine the effect of motion artifacts on a bed-based BCG signal as a 1D biomedical signal. Specifically, we develop a motion detection algorithm followed by a motion artifact removal system using an unobtrusive contact-less electromechanical film based ballistocardiogram sensor integrated into a smart bed system. Furthermore, we leverage the results from the motion detection algorithm to define a restlessness metric that enables us to quantify sleep quality. We demonstrate the use of this algorithm using data from individuals with autism spectrum disorder (ASD) with a collaboration with Heartspring, Wichita, Kansas. Additionally, we illustrate the value of using the restlessness metric along with other indicators of sleep to predict daytime behaviors in this specific population.

In the second case study, we focus on identifying temperature changes due to device or organ movement in proton resonance frequency shift (PRFS) MR-thermometry as 2D biomedical sensing modality. Firstly, we develop an enhanced hybrid method suitable for MRI thermometry in the presence of motion during microwave thermal therapy for heating using diffuse

sources such as needle- and catheter-based microwave applicators. The presented model-based method uses the sparsity of wavelet coefficients of the phase shift based on the fact that heat-induced phase shifts exhibit a correlation structure due to smoothness. Secondly, we propose a new robust motion correction algorithm based on robust principal component analysis (RPCA) to recover low-rank matrix from sparse errors without the need of modeling. We illustrate the efficiency of both works by comparing the results to the previously presented model-based method and fiber-optic temperature sensors during microwave heating of a tissue-mimicking phantom with a 2.45 GHz directional microwave antenna integrated with 14.1 T high-field MRI.

Table of Contents

List of Figures

List of Tables

Acknowledgments

The work presented in this thesis would not have been possible without my close association with many people. I take this opportunity to extend my sincere gratitude and appreciation to all those who made this Ph.D thesis possible.

Firstly, I would like to express my sincere gratitude to my advisors *Dr. Bala Natarajan* and *Dr. Punit Prakash* for their continuous support of my Ph.D study and related research, for their patience, motivation, and immense knowledge. Their guidance helped me in all the time of research and writing of this thesis. Besides my advisors, I would like to thank the rest of my thesis committee: *Dr. Steve Warren*, *Dr. David Thompson*, *Dr. Nathan Albin*, and *Dr. Scott DeLoach* , for their insightful comments and encouragement, but also for the questions which incented me to widen my research from various perspectives.

It's my fortune to gratefully acknowledge the support of my dearest friends, *Niloufar Fattahi*, *Arash Soltani*, *Mehrsa Khaleghi*, *Aram Vajdi* for their support and generous care throughout the research tenure. They were always beside me during the happy and hard moments to push me and motivate me. Special thanks are extended to my friends in Wicom group, *Dr. Solmaz Niknam*, *Hazhar Sufi Karimi*, *Reza Barazideh*, *Dr. Wenji Zhang*, *Dr. Kumarsinh Jhala*, and *Dr. Liu Chang*. Their timely help and friendship shall always be remembered.

I acknowledge the people who mean a lot to me, my parents, for showing faith in me and giving me liberty to choose what I desired. I salute you all for the selfless love, care, pain and sacrifice you did to shape my life. Although you hardly understood what I researched on, you were willing to support any decision I made. I would never be able to pay back the love and affection showered upon by my parents. Also I express my thanks to my sisters for their valuable support.

This material is based upon work supported by the National Science Foundation General & Age-Related Disabilities Engineering (GARDE) Program under grants CBET-1067740 and

UNS-1512564. Human subjects work affiliated with this research has been approved by the Kansas State University Institutional Review Board under protocol #7783. I acknowledge *Dr. Wayne Piersel*, *Dr. Janine Kesterson*, *Steve Stoffregen*, *Megan Swett*, and *Shelby Forrest* (Heartspring, Wichita, KS) for their guidance regarding design criteria related to these bed-based instrumentation systems.

Dedication

To my MOM and my DAD

For their patience, their advice, their faith,

Because they always understood.

Chapter 1

Introduction

1.1 Overview and Motivation

A wide variety of diagnostic and medical technologies have been developed to monitor physiological parameters for diagnostic applications as well as to deliver image-guided therapies. However, in many cases, it is necessary to process the signals/images acquired from patients in order to reduce, eliminate or extract artifacts and improve reliability of patient monitoring. Artifacts are a significant problem affecting the fidelity of information and thereby, affect inferencing derived from motion affected signals and/or images. Common sources of artifacts include other physiological processes that may interfere with the signal of interest, patient movements, and the variations due to sensor imperfections. Patient motion is perhaps the largest effect that causes artifacts. Examples include involuntary movements (e.g. respiration, cardiac motion and blood flow, eye movements, etc) and minor subject movements. The detrimental effects of motion artifact are well recognized and vary with signal/image modality. Over the last decade, there have been considerable advances in signal and image processing technologies leading to more effective use of clinical information in the presence of motion artiafcts [2–5]. These technologies can be categorized into three groups: (1) motion prevention, (2) motion artifact detection and reduction, and (3) motion correction.

Motion prevention approaches aim to eliminate the effects of motion before data acquisition,

but unfortunately this may not always be practical. Some examples of motion prevention approaches are training, sedation [6], and breathholding [7]. Although, these methods can be effective, they may (1) limit the time of data collection, (2) reduce quality and resolution, and (3) incur greater costs and health risks. Depending on the specific signal and imaging modality, a number of motion artifact reduction techniques have been proposed [4, 5]. These methods use different hardware and software enhancements in order to deal with motion artifacts. They either improve the design of biomedical sensors so that they are less sensitive to artifacts, or they improve signal processing methods so that the artifacts can be accurately detected and eliminated [4, 8]. In summary, there is an established toolbox of techniques where different tools are applicable to different situations. In some cases, powerful tools are already available; however in other cases, tools still need to be developed and improved. There will be a continuing need to investigate motion artifact effects in clinical applications and get information of interest from the measured signal regardless of any noise and motion.

Motivated by these factors, this dissertation addresses some of the key challenges related to inferencing with motion artifact in two classes of biomedical signals: (1) ballistocardiogram (BCG), and (2) magnetic resonance imaging (MRI). The first case represents a 1-dimensional (1D) time series signal and the second case is imaging data representing a 2-dimensional (2D) signal. In the following sections, background and research questions that need to be addressed in the context of each case study is presented.

Bed-based BCG as a 1-dimensional (1D) Signal:

BCG is a promising, unobtrusive methodology for monitoring cardiac activity and body movements. Every time the heart beats, the body recoils in response to the heart's micro-movements. Unlike other cardiac activity monitoring devices, recording BCG signals can be unobtrusive without requiring any attachment to the subject's body and also, it can be acquired simply and in an inexpensive home environment. However, the reliability of the BCG signal is often unsatisfactory for long-term recordings due to its high sensitivity and

susceptibility to motion artifacts. These motion artifacts can cause significant challenges in further analysis such as heartbeat estimation. In this disseration, we aim to detect and mitigate motion artifacts in bed-based BCG signals, and additionally extract useful information from these motion corrupted signals to make more broader inferences. The goal here is to use a non-intrusive bed-based BCG system in which motion artifacts help to quantify sleep quality in specific populations, such as children with autism spectrum disorder (ASD).

ASD is a condition that impacts a child's development in social communication and repetitive patterns of behaviors [9]. Moreover, children with ASD suffer from several challenging behaviors such as self injury, tantrums, and sleep disturbances [10–14] in which, sleep problems are one of the main concerns for caregivers and parents of these individuals. Based on previous studies, sleep inefficiency can cause major impacts on a child's behaviors. In children with ASD the possible link between sleep problems and challenging behaviors is not well understood since there have been limited techniques for sleep quality assessment in these individuals [15]. Objectively evaluating sleep quality for long term studies makes it possible to help better investigate sleep and daytime behaviors relationship. In this dissertation, the sensor-laden bed system is used in order to quantify sleep quality in children with severe disabilities in longitudinal study using motion artifact detection strategies. In this regard, there are a few key research questions that need to be properly addressed:

Question 1: *How to detect motion artifacts in bed-based BCG signals? How to use the detected motion frames in defining a new sleep quality metric (e.g., restlessness)?*

Question 2: *How can we estimate heart beat or beat-to-beat interval based on bed-based BCG signals in the presence of motion?*

Question 3: *Can we predict daytime behaviors in children with ASD based on quality of sleep? How can the new sleep quality metric derived from the smart bed system impact prediction process?*

Question 4: *As the reverse problem, can we predict night time sleep quality based on daytime behaviors in children with ASD?*

MR Images as a 2-dimensional (2D) Signal:

For the second case study, incorrect temperature changes due to motion artifacts using proton resonance frequency shift (PRFS) during MR- thermometry are investigated. During a thermal therapy procedure, the amount of thermal dose delivered to the tissue is verified and the performance is evaluated using rela time monitoring and image guidance. MRI is one of the most prevalent, reliable , and comprehensive thermal monitoring methods to measure temperature profiles inside the tissue. Using PRFS method, temperature change can be measured by way of phase changes occurring during imaging. PRFS method is the most frequently used technique to perform volumetric thermometry during thermal therapies [16]. However, one of the main drawbacks of the PRFS method is its sensitivity to inter-frame motion and magnetic field drifts, which can result in incorrect estimation of temperature profiles. To address these problems, several techniques have been proposed [17–19]. Among all, hybrid method is the most comprehensive technique based on both weighted combination of baseline images and a polynomial phase shift. While the hybrid method has demonstrated the best performance, it assumes focal heating, which may be valid when using energy modalities such as high intensity focused ultrasound, but does not hold for heating using diffuse sources such as needle- and catheter-based microwave applicators, which have a relatively broad radiation pattern, and are widely used for thermal ablation of tumors in the liver, kidney, and lung. Following this limitation, we seek to address the following research question in this dissertation:

Question 5: *How to robustly correct temperature changes in PRFS MR-thermometry during heating with applicators having diffuse patterns in the presence of motion?*

The contributions of this dissertation to address these fundamental research questions are discussed in the following section.

1.2 Contributions

To address research question 1&2, Chapter 3 of this dissertation proposed a comprehensive system to deal with motion artifacts in BCG signals which includes a motion artifact detection method followed by motion artifact removal technique in bed-based BCG signals. Additionally, a sleep quality indicator, restlessness, is defined based on the proposed motion artifact detection system which doesn't need to be worn or attached to subject's body. Major contributions of this chapter are listed below.

- Propose motion artifact detection by formulating frame by frame detection algorithm based on signal variance in time domain and out-of-band signal energy in frequency domain.
- Propose motion artifact detection using sequential detection algorithm based on processing the signal measurements directly in a sequential manner.
- Quantify sleep quality using a restlessness as a surrogate sleep quality based on results from motion artifact algorithms.
- Develop two motion artifact reconstruction methods based an autoregressive model-based tracking and Wiener smoothing based parameter estimation to estimate heart beat intervals in the presence of motion.

More details related to these contributions are in Chapter 3 and has been published in the following articles:

[20]: A. Alivar, C. Carlson, A. Suliman, S. Warren, P. Prakash, D. Thompson, and B. Natarajan, "Motion detection in bed-based ballistocardiogram to quantify sleep quality," in *GLOBECOM 2017-2017 IEEE Global Communications Conference*, pp. 1–6, IEEE, 2017.

[21]: A. Alivar, C. Carlson, A. Suliman, S. Warren, P. Prakash, D. E. Thompson, and B. Natarajan, "Motion artifact detection and reduction in bed-based ballistocardiogram," *IEEE Access*, 2019.

To address research questions 3&4, Chapter 4 of this dissertation presents predictive mod-

els built using the restlessness metric along with other sleep metrics to find the association between sleep quality and daytime behaviors in children with ASD.

- Investigate whether problematic daytime behavior is associated with poorer sleep quality in individuals with ASD, such that an individual's prior sleep can be used to predict their subsequent daytime behavior. Sleep quality metrics are derived from our previously proposed motion artifact detection.

- Analyze an extensive real-world dataset containing over 200 nightly sleep observations using our smart bed system matched to challenging daytime behaviors (aggression, self-injury, behaviors in class, and behaviors at home) across two severe autistic male subjects from Heartspring residential facility, Wichita, KS.

- Illustrate the value of using the restlessness metric along with other indicators of sleep to predict daytime behaviors.

- Investigate the influence of history of 1-8 nights of sleep on daytime behaviors. A temporal analysis allows us to examine the timescale on which sleep affects daytime behavior in autism.

- Study and develop predictive models for sleep quality changes based on both daytime behavioral and night-time sleep quality variations.

- Study the impact of 1-6 previous day behavioral changes in sleep quality classification models.

More details of this work are discussed in Chapter 4 and are going to be submitted to the following articles:

[22]: A. Alivar, C. Carlson, A. Suliman, S. Warren, P. Prakash, D. E. Thompson, and B. Natarajan, "Smart bed based daytime behavior prediction in children with autism spectrum disorder - a pilot study* (to be submitted to)," *Medical Engineering & Physics*, 2019.

[23]: A. Alivar, C. Carlson, A. Suliman, S. Warren, P. Prakash, D. E. Thompson, and B. Natarajan, "A pilot study on predicting daytime behavior & sleep quality in children

with asd (under review)," IEEE, 2019.

To address research question 5, Chapter 5 of this dissertation introduces two motion correction techniques to overcome the limitation of previous methods in PRFS MR-thermometry:

- Propose an enhanced hybrid MRI thermometry technique suitable for monitoring temperature profiles during microwave thermal therapy. Errors in thermometry are reduced by using a modified model-based phase correction procedure based on correlation structure of heat-induced phase shifts. The proposed method improves the accuracy of the hybrid algorithm for diffuse hot spots.
- Propose a non-model based motion correction using robust principal component analysis (RPCA) to recover low-rank temperature profile image from sparse corrupted motion artifact observations.

More details on both proposed motion correction approaches can be found in Chapter 5 and in the following articles:

[24]: A. Alivar, P. Faridi, P. Prakash, and B. Natarajan, "An enhanced hybrid mri thermometry technique for monitoring microwave thermal therapy," in *Medical Imaging 2019: Image-Guided Procedures, Robotic Interventions, and Modeling*, vol. 10951, p. 109512P, International Society for Optics and Photonics, 2019.

[25]: A. Alivar, P. Prakash, and B. Natarajan, "Reducing sparse motion artifacts in mr-thermometry using robust principal component analysis (to be submitted to)," in *International Symposium on Biomedical Imaging*, IEEE, 2020.

1.3 Organization of This Dissertation

Chapters 2, 3 and 4 are mainly discussing and presenting motion artifacts in 1D signal as bed-based BCG signals and Chapter 5 is presenting results and methods for 2D signals as

MRI images. Specifically, Chapter 2 provides the background on basics of ballistocardiogram waveform with its relation to cardiac functions, various technologies to measure BCG data, and description of the smart bed system used for further BCG signal acquisition. In Chapter 3, two approaches are proposed to detect motion artifacts in BCG signals and further inference with those detected artifacts to introduce a new surrogate sleep quality measure using the smart bed system. Moreover, following the motion artifact detection methods, two parametric models are proposed to reconstruct motion artifacted BCG frames in order to estimate heart beat intervals in the presence of motion. In Chapter 4, statistical models are developed to find the link and correlation between sleep quality and daytime behaviors in children with autism spectrum disorder using sleep features extracted from motion artifacts in BCG signals during sleep. In Chapter 5, Two methods for estimating temperature changes in the presence of motion are proposed for heating using diffuse sources such as needle- and catheter-based microwave applicators. Concluding remarks and future research directions are discussed in Chapter 6.

Chapter 2

The Ballistocardiogram (BCG)

A ballistocardiogram (BCG) is a non-invasive measurement of the recoil forces of the body in reaction to the blood ejected into the vasculature during the cardiac cycle [26]. The BCG signal was first discovered by J.W.Gordan in 1877 [27]. However, 60 years later, the first practical measurement was introduced by Starr in 1939, and then the term "ballistocardiogram" was used in his article [26]. Their setup was in the form of a mechanical table that was spring loaded and BCG was recorded from the body forces. Throughout the 1900s, BCG signals were quite popular. However, due to wide variety of cardiac recording devices, lack of understanding of this waveform, and overly-cumbersome hardware, BCG was faded when medical imaging technologies emerged. Nowadays, improvements in technology could simplify BCG measurement and analysis and it found a place again in medical researches since it can provide a contactless means of evaluating cardiac activities. In this chapter, the basics of BCG waveform with its relation to cardiac functions, different techniques to measure BCG, and our bed-based BCG system which is used for further analysis in the following Chapters 3 and 4, are provided in detail.

2.1 BCG Signal Description

Fig. 2.1 shows two cycles of BCG waveform in which the BCG extrema are named with consecutive letters from H to N for each cycle. The H-K waves form the ventricular systole and L-N waves occur during the diastole. The waves of the BCG signal are a combination of the forces created by the heart and blood flow. The I wave follows ventricular systole and is attributed to the change in direction of blood movement from the headward direction to the footward direction. The recoil force created from blood direction changes towards the head is seen as a strong J wave in BCG signals and K wave is caused by the deceleration of blood flow. The interpretation of L-, M- and N- waves is more uncertain and they are less interesting in terms of this thesis. The combination of all these waves represents the cyclic event of the heart beating. Heartbeat interval or beat-to-beat interval is defined based on J-peak to J-peak interval from BCG signal and R-peak (the principal peak of the ECG) to R-peak interval from ECG signals which is also called as heartbeat interval. More details on heartbeat interval estimation using BCG data are discussed in Chapter 3.

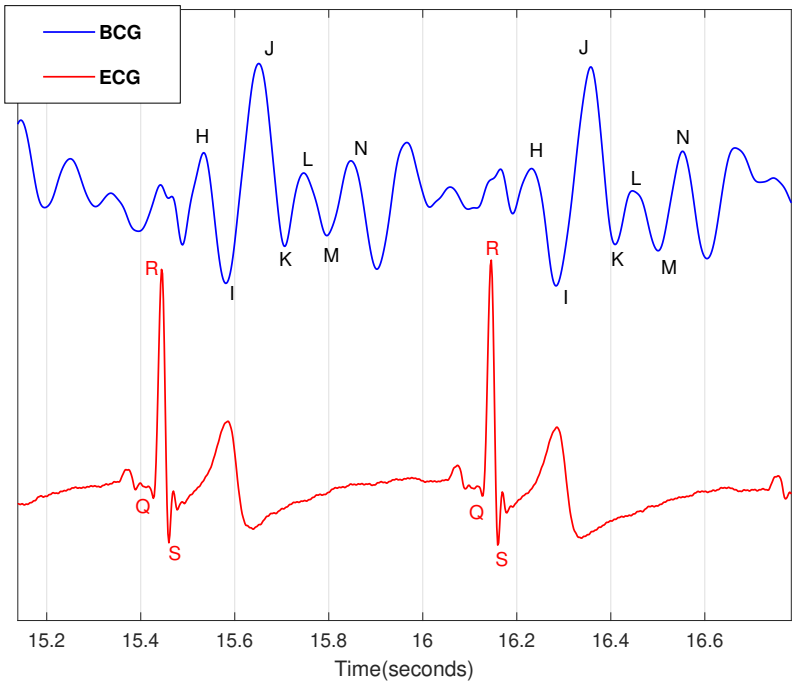

Figure 2.1: A BCG and corresponding ECG signal with two heart cycle.

2.2 BCG Signal Measurement

Recently, modern technology made it possible to renew interest in the BCG and have made the detection of the BCG signal more accessible. Several types of sensors can record the force signals or cardiac vibration signals generated by the heart if they are coupled to the body in one form or another. The most popular method for measuring the BCG is by using a force plate or weighing scale and having the subject stand as still as they can to reduce motion artifacts. Other popular modalities include seat or chair-based systems [28], bed-based systems [29–35], and wearable systems [36, 37]. Bed-based BCG can provide the information on respiration and body movement as well as heartbeats in a more comfortable environment replacing functions done by polysomnography (PSG). Since BCG-based methodology does not require any on-body electrodes. it has advantage over other BCG modalities and ECG. In this thesis, we are quantifying sleep quality in children with ASD using BCG signals. Since, any attached body sensors or wearable devices are not suitable for this population, bed-based BCG measurement is the most appropriate modality for long-term home monitoring of children with ASD. The bed-based BCG systems are incredibly sensitive in order to record the small forces generated by each heartbeat. Thus, these signals are susceptible to any kind of movements that can disrupt the recorded signal. Since in children with ASD, movements during sleep time is common, BCG system is able to capture these motion artifacts while the subject is laying on the bed. In this thesis, we are using these motion artifacts as a useful sleep parameter for further daytime-sleeptime relationship analysis.

2.3 Designed Smart Bed System Description

Our custom bed system includes four electromechanical films (EMFit; L series; 300 mm x 580 mm) and four load cells (TE Connectivity Measurement Specialties; FX1901-0001-0200-L) [**?**]. The sensors are hidden under the mattress and beneath the bed posts, so that the subject is not aware that any changes have been made to their environment. This is a critical aspect of our system, since autistic children are extremely sensitive to even small changes

in their environment. The electromechanical films (EMFis) generate a proportional current in response to an applied changing force. The outputs from the EMFis are conditioned by analog circuitry before being connected to one channel of a National Instruments analog input module, NI 9220 (sixteen 16-bit differential channels). The signal conditioning circuit consists of a charge amplifier, a 2nd order active Sallen-Key low-pass filter with a cutoff frequency of 20 Hz, and a final non-inverting amplification stage. While the bed based BCG data is the only information required for sleep quality analysis, we collect ECG data just for validation purposes in labaratory invironment on three subjects of our team. As mentioned earlier, ECG data collection is invasive and not suited for long term monitoring. However, in this initial stage of validation using the gold standard of ECG is helpful to demonstrate the value of BCG based estimation of physiological parameters. An iWorx ETH-225 bioamplifier with an iWorx ECG module was used to collect the reference ECG data. The output of the ECG module was also connected to one of the NI 9220 analog input channels to gather the BCG and ECG data synchronously. The NI 9220 is connected to a NI 9184 Ethernet chassis. The entire NI acquisition system is controlled by a virtual instrument on a PC running LabVIEW version 14.0.1 which set the sampling rate to 250 Hz for each acquired signal. The virtual instrument does not apply any additional filtering before saving the data to a file on the PC. More details on the bed-system architecture under development at Kansas State University including a preliminary comparison of estimated BCG HBIs compared to the gold standard ECG R-R intervals can be found in [29, 38]. A picture of the bed is illustrated in Fig. 2.2 with four film sensors hidden in the mattress sheet.

Six-Month Study at Heartspring

After we validated the sensor-laden bed system in our laboratory environment for a couple of nights, we placed the designed bed systems in the room of a child with low-functioning autism at Heartspring. Heartspring, a residential school located in Wichita, Kansas, offers a collection of facilities and services for children with a wide range of developmental disabilities [**?**]. There are approximately 62 children in this facility in which most of the them have ASD.

Figure 2.2: Designed bed system with four film sensors (EMFi's).

As a collaboration with Heartspring, we seek solutions to help to create new technologies in order to improve the quality of life for these children. One of the main interests is to understand the relationship between sleep quality and daytime behaviors in these children which motivates the researchers from Kansas State University to design a smart bed system to monitor the nighttime well-being of these individuals in their home environment. Thus, after validating our bed system in laboratory on different subjects of our team, we had a long study of six month for two children with low-functioning autism at Hearspring campus. Two sensor-laden beds were placed in each child's room with one captain's bed and one Endurance bed and the data were collected from March 20, 2018 until beginning of September 2018 under KSU IRB protocol #7783. In order to capture bed entrance and bed exit events, the data were collected from 7:00 pm to 9:00 am for each subject and in total, we had more than 200 nights of data collected from these two children. Additionally, a low-resolutional thermal camera is used in each child's room in order to have information about motion artifacts, sleep and wake times, and diagnose system failures.

2.4 Summary

In this chapter, we introduce BCG as a non-invasive method based on the measurement of micro-movement of heart generated by mechanical activity of the heart. BCG can provide information about body movements, heart rate and respiration rate. Bed-based BCG is one of the techniques that can be used to record BCG data from a subject without any electrodes or sensors attached to the subject's body. Thus, it can be used for long-term home monitoring objectives to measure sleep quality and cardiovascular information.

In the next chapter, we will develop methods to deal with motion artifact in BCG signals by automatically detecting and reconstructing these motion artifacted data.

Chapter 3

Motion Artifact Detection and Reduction in Bed-based BCG

BCG is an inexpensive and unobtrusive method that monitors cardiac activity by recording micro-movements which are caused by the mechanical activity of the heart. Bed-based BCG signals can be recorded by using several EMFis connected to the bed on which the subject is sleeping. Different kinds of sensors have been considered in a bed-based BCG acquisition system [39]. The clean signals measured by EMFi sensors can be used to extract heart rate from the BCG along with respiration rate. However, this system is susceptible to distortion due to motion. The resulting motion artifact can cause significant challenges in heartbeat estimation. In this chapter, we wish to develop a system to automatically detect presence of motion artifact and minimize the effects of motion artifacts in bed-based BCG signals in order to quantify restlessness during sleep for further nocturnal analysis of children with ASD and have a reliable estimation of beat-to-beat interval. Parts of this chapter has been published in [20] [1] and [21] [2].

[1] A. Alivar, C. Carlson, A. Suliman, S. Warren, P. Prakash, D. Thompson, and B. Natarajan, "Motion detection in bed-based ballistocardiogram to quantify sleep quality," in *GLOBECOM 2017-2017 IEEE Global Communications Conference*, pp. 1–6, IEEE, 2017

[2] A. Alivar, C. Carlson, A. Suliman, S. Warren, P. Prakash, D. E. Thompson, and B. Natarajan, "Motion artifact detection and reduction in bed-based ballistocardiogram," *IEEE Access*, 2019

3.1 Related work

Motion artifact detection and removal has received significant interest in many sensing modalities. A multitude of approaches have been proposed for motion artifact detection and removal in electrocardiogram (ECG) signals. These include linear filtering [40], adaptive filtering [41], wavelet denoising [42] and Bayesian filtering methods [43] for detection and adaptive filtering[44], wavelet-based [42] for motion artifact removal. Adami et al. [45] proposed a movement detection approach based on energy of load cell signals collected from four corners of the bed. A two-stage approach for photoplethysmogram (PPG) data based on higher order statistical features and Neyman-Pearson detection rule as motion artifact detection and a frequency domain independent component analysis (FD-ICA) technique along with period estimation as motion artifact reduction unit is presented in [46]. Removal of motion artifacts to recover artifact-reduced PPG signals has been researched extensively [47–50] . Relative to the efforts for ECG, load cells and PPG signals, motion artifact detection and removal in BCG signal has received very little attention. In [30], sleep and awakening epochs are estimated via ballistocardiography using polyvinylidence fluoride film sensor on a mattress. Here, body movement epochs are identified by comparing the heart rate values to a threshold. These epochs are then used for estimating sleep efficiency and compared to PSG results. In [51], a noise sensor is embedded in a weighing scale to measure body movements while a subject is standing on it. ECG, BCG and motion signals are recorded while the subject is stationary as well as when there is movement. Then, all three signals are postprocessed to achieve two signal estimates: (1) BCG noise which is estimated from the BCG and ECG signals, and (2) motion noise derived from the motion signal. The correlation between BCG noise and motion noise estimates are used to calculate the BCG signal to noise ratio. A load sensor based measurement of BCG signal is used in [31] for heartbeat, respiration measurements and identification of specific types of movement. The authors in [31] extract 14 different features including variance from y-axis of the bed, trajectory length of the central mass points, average values of sensors, average diagonal load sensors energy and average percentage variance of each load sensor. These features are fed into a support

vector machine (SVM) classifier to classify the specific type of movements such as hand, leg and all other movements. However, none of the prior efforts [30, 31, 51] attempt to explicitly differentiate between clean and motion corrupted BCG signals, recover the motion corrupted BCG signals and try to clean the data in order to extract heart rate or beat-to-beat interval. Our objective is to use the reconstruction of motion corrupted BCG signal to extract useful information such as heart rate and respiration rate for further physiological sleep analysis especially in children with ASD.

3.2 Motion Artifact Detection

The purpose of motion artifact detection is to use motion detection to quantify restlessness during sleep for children with ASD. A typical 12 hours BCG signal corrupted with motion is shown in Fig. 3.1. In this figuremore than 60% of the signal is corrupted with motion artifacts and this fact make it necessary to detect and get useful information from these artifacts and not just ignore these frames. Furthermore, in Fig. 3.2, two short length BCG signal are illustrated in which one is clean BCG and the other one is a motion artifacted signal. The proposed approach for detecting motion corrupted BCG signal frames involves 3 stages namely: (1) preprocessing, (2) feature selection and extraction, and (3) decision rule implementation. The proposed algorithms are reported and published [20].

(1) Preprocessing:

In the preprocessing stage, low frequency content is removed via a Butterworth bandpass filter of order 6 (0.5-25 Hz). This filter is applied to the individual EMFi signals. After filtering, each BCG film signal is partitioned into short frames of equal length. In our implementation, frame length is fixed to 1s, similar to other efforts in this field [52]. This choice of frame size also helps preserve the shape of a single heartbeat for calculating physiological parameters that depend on beat-to-beat intervals. This framing procedure is done for all

BCG signals collected.

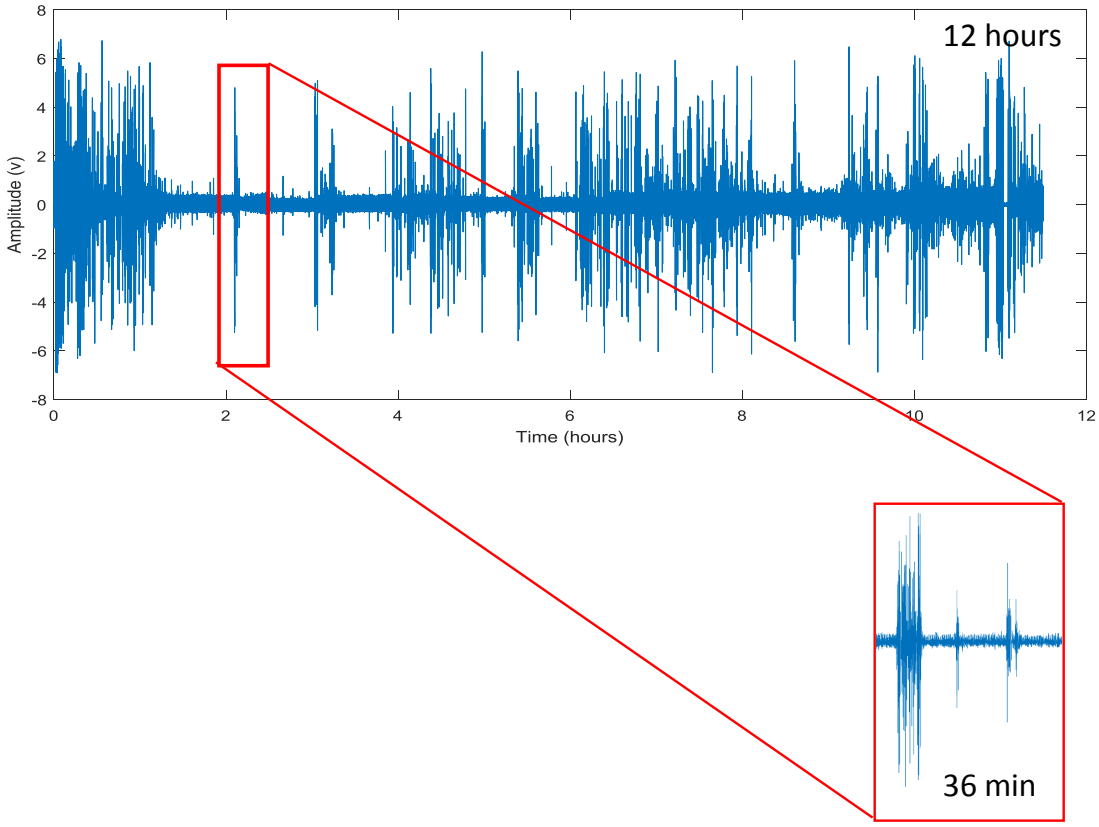

Figure 3.1: A BCG signal illustrating corruption due to motion.

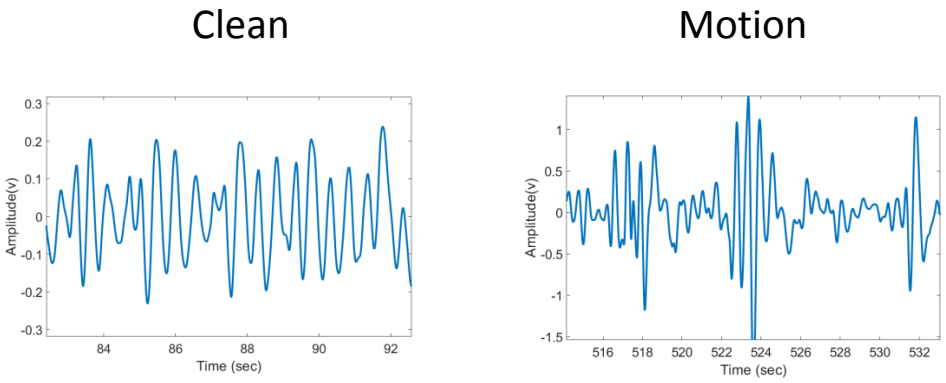

Figure 3.2: Two short length BCG signals: Clean and Motion corrupted.

(2) Feature Selection and Extraction:

The goal of this stage is to identify and extract the BCG signal features that can be used to distinguish between clean and motion corrupted frames based on Neyman-Pearson rule (Frame by frame method). The feature is selected based on a priori analysis of training data. We use BCG data from a child with ASD served by Heartspring and three other subjects, contributing to over 50,000 training data frames. This training data collection was accompanied by manual observation based tagging of motion events.

A. Time-Domain Analysis: After considering multiple statistical features such as median, variance, skewness and kurtosis of the BCG signal, we identified the variance measure to be the most discriminative. Fig. 3.3 shows the distribution of the variance measure. From Fig. 3.3, it is evident that the variance is much higher for motion-corrupted frames than clean frames. We fit an exponential model to the variance distribution as represented in Fig. 3.3. The parameters (λ_0- Clean; λ_1- motion-corrupted) of the fitted exponential distribution are estimated for the four BCG film sensors and provided in Table 3.1.

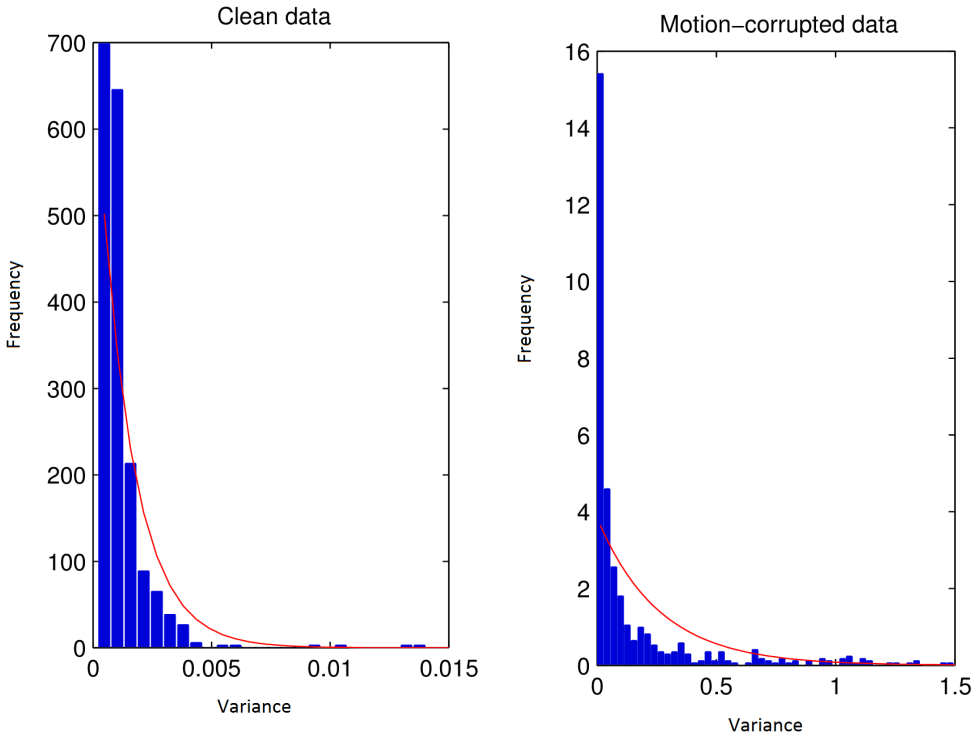

(a) (b)

Figure 3.3: Sample histogram plots of (a) clean and (b) motion-corrupted variance of BCG samples.

Table 3.1: Exponential parameters for clean and motion-corrupted BCG variance features for four film sensors.

Film Sensors	λ_0	λ_1
Film0	5637.5	3.66
Film1	702	3.85
Film2	416.6	4.89
Film3	4246.5	6.66

B. Frequency-Domain Analysis: Analyzing the BCG frames in the spectral domain provides alternative candidate features. By comparing magnitude spectrum of clean and motion-corrupted BCG signal, it is concluded that there is a significant difference between the Fourier

transform components of clean and motion-corrupted data for frequency range greater that 10 Hz which is the out of band range [53]. Therefore, this out-of-band signal energy is another distinguishing feature to consider and the distribution of this feature is plotted in Fig. 3.4. Once again, we can fit an exponential model to this feature and estimate the parameters of the exponential distribution based on training data. The estimated parameter values are given in Table 3.2.

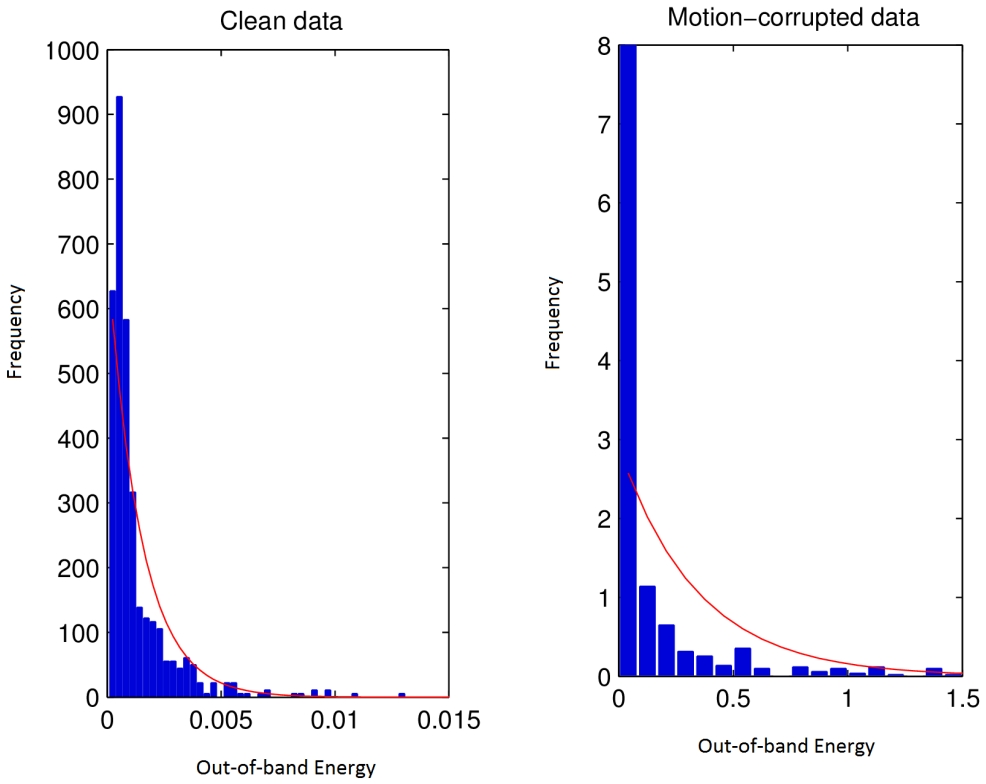

(a) (b)

Figure 3.4: Sample histogram plots of (a) clean and (b) motion-corrupted out-of-band signal energy og BCG samples.

Table 3.2: Exponential parameters for clean and motion-corrupted BCG out-of-band energy measures for four film sensors.

Film Sensors	λ_0	λ_1
Film0	4817.5	1.64
Film1	689	2.91
Film2	470.4	3.77
Film3	3860.6	2.33

We analyze two different decision rules and compare their performance.

3.2.1 Frame by Frame Detection

Neyman Pearson (NP) criteria [54] is used to design the frame by frame decision rule for detecting motion artifacts in a BCG signal. The distinguishing features $\underline{y} = [y_1, y_2]$ are computed for all preprocessed data frames. Here, y_1 denotes variance and y_2 is the out-of-band signal energy. Since an exponential model is used to fit both features, we describe the decision rule derivation for one feature y_1 with the understanding that the detection rule based on y_2 will follow along similar lines. We have a binary hypothesis testing problem where, H_0 corresponds to a clean signal frame, and H_1 corresponds to the case that the signal frame has motion artifacts. That is,

$$\begin{aligned} H_0 &: y_1 \sim P_0 = exp(\lambda_0) \quad \text{[Clean]} \\ H_1 &: y_1 \sim P_1 = exp(\lambda_1) \quad \text{[Motion-corrupted]} \end{aligned} \tag{3.1}$$

The NP criteria aims to maximize the probability of motion detection while constraining the probability of false alarm [54]. The decision rule takes the form of a likelihood ratio test (LRT) where the threshold τ is designed to meet the NP criteria. That is,

$$LRT = L(y) = \frac{p(y_1; H_1)}{p(y_1; H_0)} \underset{H_0}{\overset{H_1}{\gtrless}} \tau \tag{3.2}$$

where, τ is chosen such that $P_1(\Gamma_1)$ is maximized while $P_0(\Gamma_1) \leq \alpha$. Here, $P_j(\Gamma_i)$ indicates the probability of choosing hypothesis H_i when H_j is true. The likelihood ratio for the exponentially distributed feature y corresponds to $L(y) = \frac{\lambda_1}{\lambda_0} e^{y_1(\lambda_0 - \lambda_1)}$. The threshold τ is chosen by setting the probability of false alarm, i.e, $P_0(\Gamma_1) = \alpha$. For the LRT in equation(3.2), the probability of false alarm can be calculated as:

$$\begin{aligned} P_0(\Gamma_1) = P_0(L(y_1) \geq \tau) &= 1 - P_0(L(y_1) < \tau) \\ &= 1 - P_0(\frac{\lambda_1}{\lambda_0} e^{y_1(\lambda_0 - \lambda_1)} < \tau) \\ &= 1 - P_0(y_1 < \ln(\frac{\lambda_0}{\lambda_1}\tau)\frac{1}{\lambda_0 - \lambda_1}) \\ &= exp(1 - \lambda_0 \tau^{'}) \end{aligned} \tag{3.3}$$

where, $\tau^{'} = \ln(\frac{\lambda_0}{\lambda_1})\tau$. Setting $P_0(\Gamma_1) = \alpha$, the modified threshold is $\tau^{'} = \frac{-ln(\alpha)}{\lambda_0}$. The final binary decision ($\delta_{NP}(y_1)$) can be made based on the variance feature for a given α as:

$$\delta_{NP}(y) = \begin{cases} 1 & \text{if } y_1 \geq \tau^{'} \\ 0 & \text{otherwise} \end{cases}, \tag{3.4}$$

The corresponding probability of detection for this decision rule is $P_1(\Gamma_1) = exp(-\lambda_1 \tau^{'})$. As stated earlier, a similar approach can be used to design a hypothesis test based on out-of-band energy feature y_2.

3.2.2 Sequential Detection Rule Formulation

In this approach, the goal is to look at the preprocessed BCG signals and directly process the signal measurements in a sequential manner to determine if the samples contain motion artifacts. Since the preprocessed BCG signals serve as our measurements for sequential detection, it is important to first parameterize the measurements for both clean and motion corrupted BCG signals. Our training data set is used to fit Gaussian distributions for both clean and motion corrupted signals as illustrated in Fig. 3.5. The parameters (μ_0, σ_0^2- Clean; μ_1, σ_1^2- motion-corrupted) of the fitted Gaussian distribution are estimated for the four BCG film sensors and provided in Table 3.3. It is important to note that while our Gaussian assumption for motion corrupted data provides analytical simplicity for deriving the decision rule, this assumption is rather conservative as the actual distribution appears to be heavy tailed (e.g., double exponential or Laplacian). The impact of this assumption is discussed in the result section.

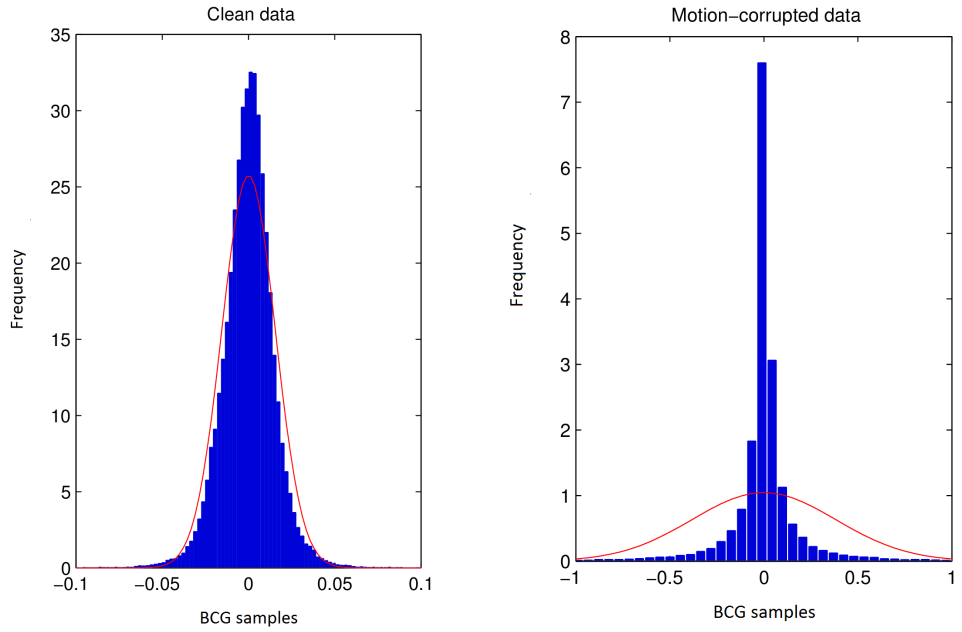

(a) (b)

Figure 3.5: Sample histogram plots of (a) clean and (b) motion-corrupted frames.

Table 3.3: Gaussian parameters for clean and motion-corrupted BCG frames for four film sensors.

Film Sensors	Clean		Motion-corrupted	
	μ_0	σ_0^2	μ_1	σ_1^2
Film0	-2.22e-06	0.0002	7.46e-04	0.27
Film1	-1.07e-04	0.001	-3.77e-04	0.24
Film2	-1.54e-05	0.002	2.33e-04	0.19
Film3	1.86e-05	0.0002	-1.18e-04	0.14

Once again, we formulate a binary hypothesis testing problem as:

$$\begin{aligned} H_0 &: y_i \sim P_0 = N(\mu_0, \sigma_0^2)) \quad \text{[Clean]} \\ H_1 &: y_i \sim P_1 = N(\mu_1, \sigma_1^2) \quad \text{[Motion-corrupted]} \end{aligned} \tag{3.5}$$

For sequential detection, we consider a frame of length 1s with $N = 250$ samples of BCG data (y_i) each modeled as an iid Gaussian with parameters dependent on the presence or absence of motion artifact. The log-likelihood ratio for our binary hypothesis test corresponds to:

$$LLRT(\mathbf{y}) = log\frac{p(\mathbf{y}; H_1)}{p(\mathbf{y}; H_0)} = N.log(\frac{\sigma_0}{\sigma_1}) + \frac{\sum_{i=1}^{N}(y_i - \mu_0)^2}{2\sigma_0^2} - \frac{\sum_{i=1}^{N}(y_i - \mu_1)^2}{2\sigma_1^2}$$

This $LLRT(\mathbf{y})$ for each window is then compared to two quantities an upper threshold A and lower threshold B, which are defined as:

$$\begin{aligned} A &= log(\frac{P_D}{P_{FA}}), \\ B &= log(\frac{1 - P_D}{1 - P_{FA}}) \end{aligned} \tag{3.6}$$

Here, P_D is the desired probability of detection and P_{FA} is the desired probability of false

alarm. If $LLRT(\mathbf{y}) \geq A$, then hypothesis H_1 is accepted and if $LLRT(\mathbf{y}) \leq B$, then hypothesis H_0 is accepted. If $B \leq LLRT(\mathbf{y}) \leq A$, no decision is made while the next measurement is included in the test and the frame is shifted by 1 sample and a new likelihood ratio is computed. The final decision $\delta_S(y)$ for a given A and B is:

$$\delta_S(y) = \begin{cases} 1 & \text{if } LLRT(\mathbf{y}) \geq A \\ \text{No Decision} & \text{if } B \leq LLRT(\mathbf{y}) \leq A \quad , \\ 0 & \text{otherwise } LLRT(\mathbf{y}) \leq B \quad , \end{cases} \tag{3.7}$$

3.3 Motion Artifact Removal

As the next step, we present a novel approach to reconstruct BCG frames from those portions of the data that have been identified to be clean using a prediction based autoregressive model and Wiener smoothing based estimation of the underlying BCG signal parameters [21]. As it is mentioned earlier in Chapter 2, BCG extremas are named with consecutive letters from H to N for each cycle. An ideal BCG heartbeat signal can be modeled as a sinusoid of frequency f_b windowed with a cosine window of length d as shown in Fig. 3.6 [1]. The heartbeat shape $w(t)$ corresponds to:

$$\begin{aligned} w(t) &= A \sin\left(\frac{\pi t}{d}\right). \sin\left(2\pi f_b t\right) \\ \mathrm{A} &= \frac{\mathrm{JK_{amp}}}{2} \\ d &= \frac{\mathrm{JJ_{int}}}{f_s} \\ f_b &= d.f_c - \left(\frac{1}{2d}\right) \end{aligned} \tag{3.8}$$

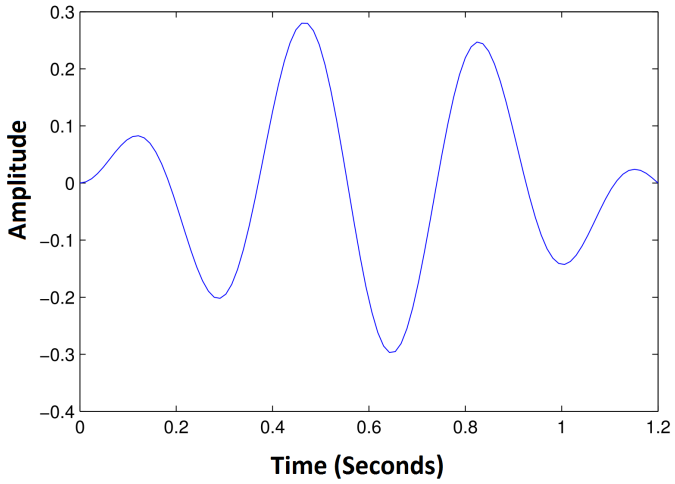

Figure 3.6: BCG signal of an ideal heartbeat [1].

Where, the three parameters that influence $w(t)$ are J-K amplitude which is the amplitude of J-peak to K-peak of the corresponding BCG cycle, J-J interval which is the interval between two consecutive J peaks, and f_c which relates to the most significant frequency component in one BCG cycle. These three parameters that characterize the BCG signal change slowly over time and they are correlated across time. Therefore, if one can track the variation of these parameters through both clean and motion artifacted signal frames, it would be possible to reconstruct the BCG signal over time enabling the continuous monitoring of B-B interval/heart rate. We exploit this idea to design a motion artifact reduction strategy. When a frame is detected as motion corrupted one, J-K amplitude, J-J interval, and the most significant frequency component of the previous (using auto-regressive (AR) model based prediction) frames or previous and future (using Wiener smoother based estimation) frames, are used as the basis for estimation of the new heartbeat frame.

While the motion artifact detection is completed and clean and motion frames are identified, the next step is to reconstruct the original BCG signal from the motion corrupted frames. As previously mentioned, each BCG signal parameter is correlated over time. This motivates the idea of tracking the BCG signal parameters through the motion impacted signal frames. A time series model that captures the dynamics of the signal parameters can help to estimate the parameters of both clean and motion corrupted signal frames. In this work, we suggest

two different methods for parameter estimation namely: (1) AR model-based tracking and (2) Wiener smoother based parameter estimation as discussed in following subsections.

3.3.1 Autoregressive Model

An AR model is used for predicting the current value of a variable of interest using a linear combination of its past values. The general definition for AR(p) model is as follows:

$$\theta_t = \sum_{i=1}^{p} C_i \theta_{t-i} + \epsilon_t \qquad \epsilon_t \sim N(0, \sigma^2) \tag{3.9}$$

Where, C_i are the auto-regression coefficients, θ_t is the series under investigation, p is the filter order, and ϵ_t is the Gaussian process noise. In our motion artifact removal strategy, the $\theta_t = (\theta_{t,1}, \quad \theta_{t,2}, \quad \theta_{t,3})$, where $\theta_{t,i}$ for $i = 1, 2, 3$ corresponds to BCG signal parameters namely: JK_{amp}, JJ_{int}, and f_c. These three parameters are identified using heartbeat information such as J and K peaks and the most significant frequency component. For fitting an AR model to each parameter, we use partial autocorrelation to identify the order of the corresponding AR model. Therefore, in the sample autocorrelation plot (see Fig. 3.7), we look for the delay where the partial autocorrelations essentially become zero. Placing a 95% confidence interval for statistical significance is helpful for this process. As illustrated in Fig. 3.7, the best model order for J-J interval parameter is AR(3). With the same procedure, we conclude that 2nd order AR model is appropriate for the other two BCG signal parameters. Once the model has been identified for each parameter, the AR model predictors can be obtained by finding the estimated coefficients for each parameter using training data.

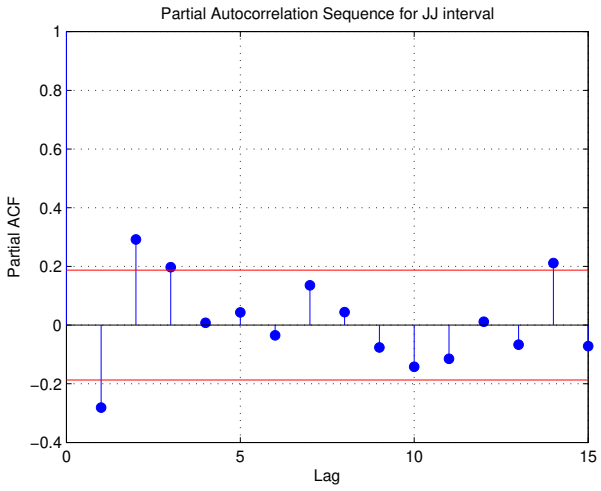

Figure 3.7: Partial autocorrelation plot for J-J interval parameter.

3.3.2 Wiener Smoother Filter

In this approach, we first uncover the underlying correlation over time that is exhibited by the BCG signal parameters. Fig. 3.8, for example, plots the autocorrelation function of the J-J interval parameter. This correlation can be used to estimate signal parameters in motion corrupted frames. In general, consider we have a set of samples θ_n coming from a jointly wide sense stationary (WSS) process (consider $\theta_n = (\theta_{n,1}, \quad \theta_{n,2}, \quad \theta_{n,3})$, where $\theta_{n,i}$ for $i = 1, 2, 3$ corresponds to BCG signal parameters at time n which are JK_{amp}, JJ_{int}, and f_c). The goal is to find the linear estimate of θ_n named as $\hat{\theta}_n$ using the L-most recent and L following samples of θ_n as:

$$\hat{\theta}_n = \mathbf{w}_{opt}^T.\theta_n = \sum_{l=-L+1}^{L-1} w_{opt}(l)\theta_{n-l}, \quad n = 0, 1, ... \tag{3.10}$$

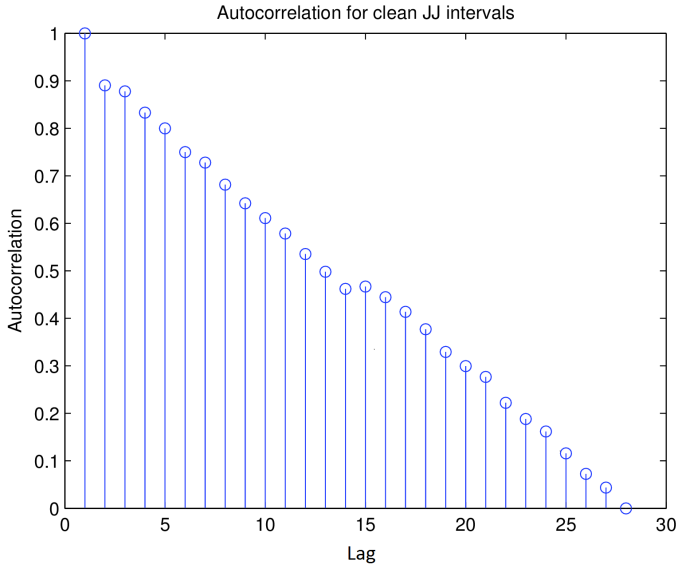

Figure 3.8: Autocorrelation for J-J interval parameters.

Here, $\mathbf{w}_{opt}$ corresponds to the optimal weights which is estimated using equation (3.11), and L is chosen based on the number of samples that exhibit significant autocorrelation (calculated using training data). In Fig. 3.8, for example, if we set a threshold of 0.2 for the autocorrelation, then $L = 20$; if the threshold is 0.1, then $L = 25$. We need to determine the coefficients $w_{opt}(l)$ that minimize the mean squared error (MSE) between $\hat{\theta_n}$ and θ_n. Based on Wiener-Hopf smoothing equations, for computing the optimal smoother weights $\mathbf{w}_{opt}$ corresponds to:

$$\mathbf{w}_{opt} = \mathbf{R}_{\theta}^{-1}.\mathbf{r}_{\theta\theta_l} \tag{3.11}$$

where, $\mathbf{R}_{theta} = E[\theta(n).\theta^T(n)]$ and $\mathbf{r}_{\theta\theta_l} = E[\theta(n).\theta(n-l)]$ are the input autocorrelation matrix and cross correlation vector, respectively. In this study, we use both past and future values of BCG signal parameters to predict the current parameter values. Therefore, $\mathbf{r}_{\theta\theta_l}$ is built based on the lag values of past/future frames with the present one that is to be estimated. These two matrices can be estimated with example autocorrelation function (ACF)s evaluated using the training data. Once the optimal coefficients $\mathbf{w}_{opt}$ are estimated, the

Wiener model for each BCG parameter can be obtained using equation (3.10).

Once the BCG parameters are evaluated for the motion corrupted frames, the BCG signal is reconstructed using equation (3.8) $\hat{w(t)} = \hat{A}\sin(\frac{\pi t}{\hat{d}}).\sin(2\pi\hat{f}_b t)$.

3.4 Experimental Results

3.4.1 Motion Artifact Detection

The proposed motion detection algorithm is tested and validated with data collected from four subjects for a total of over 36,000 test frames. As the ground truth, a team of students were present during the night to record and watch the sleep times and subject's movements via a baby monitor.

We first present the results of the NP test. For $\alpha = 0.005$, the NP decision rule in equation (3.4) is implemented. As an example, three minutes of recorded BCG data from the four films along with the binary decisions based on variance and out-of-band signal energy are illustrated in Fig. 3.9 and Fig. 3.10, respectively. As it is evident from the figures, both features are effective in identifying movement of the subject. By varying the false alarm probability α, one can generate the receiver operating characteristic (ROC) for this test [54]. Fig. 3.11a, 3.11b illustrate the ROC curves for the NP tests based on variance and out-of-band signal energy, respectively. The ROC curves show that, the proposed tests yield high probability of detection even with low probability of false alarm.

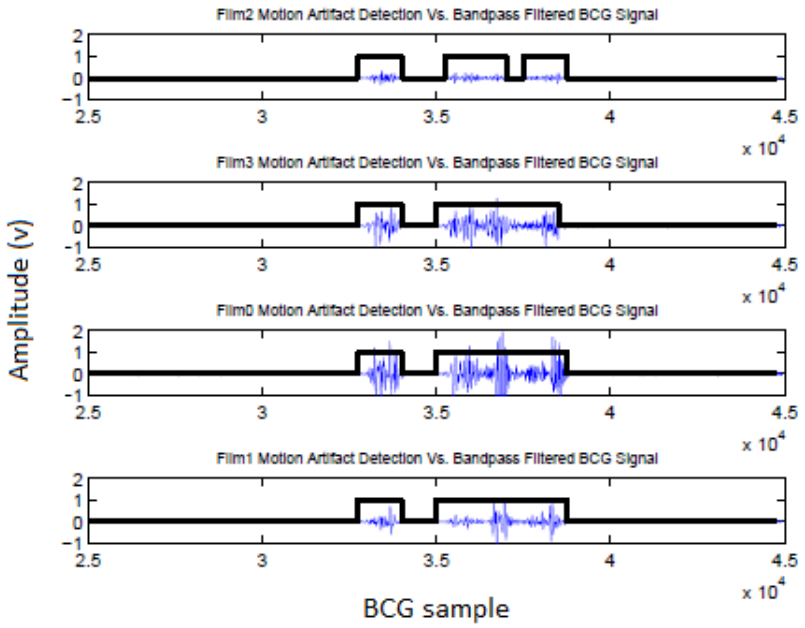

Figure 3.9: Motion artifact detection for four film sensors based on variance.

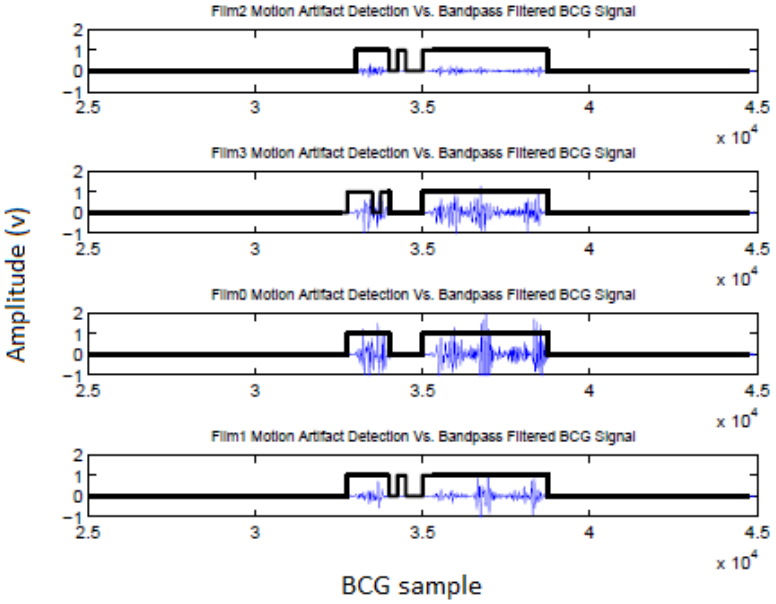

Figure 3.10: Motion artifact detection for four film sensors based on out-of-band energy signal.

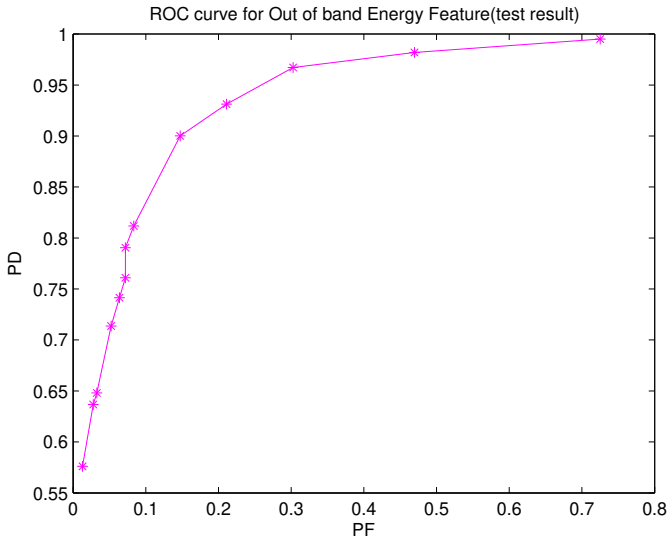

(a)

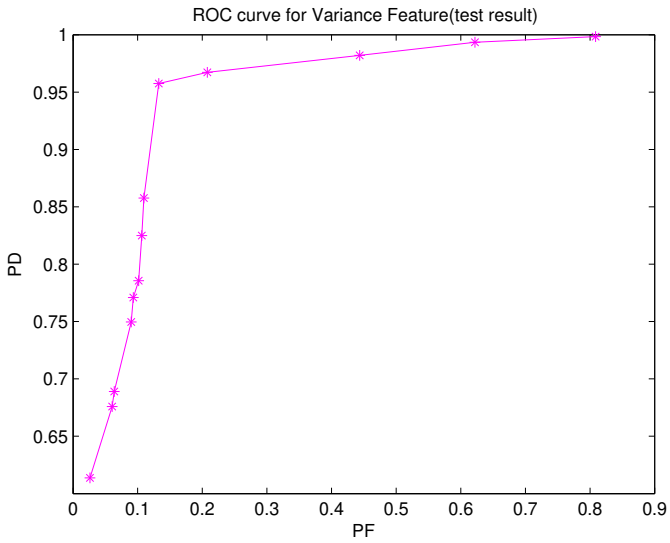

(b)

Figure 3.11: ROC curves for test data plot for (a) out-of-band energy, and (b) variance feature.

In order to improve the system accuracy and efficiency, one can also fuse motion detection decisions based on the two features. This is especially useful when the features lack robustness to ambient noise or other factors. Here we used AND and OR rules to implement a binary classifier. By using an OR rule, both probability of false alarm and probability of detection increase. Conversely, by applying AND operator on two features, both probabilities of detection and false alarm will decrease. Therefore, the choice of using OR and AND

decision fusions depends mainly on preference of the system designer. For each film sensor, AND and OR decision fusions are performed and the results are summarized in Tables 3.4, 3.5, 3.6, and 3.7. It can be easily seen that motion artifact are detected with highly probability (e.g. 94%) while probabilities of false alarm are low.

Table 3.4: Frame by Frame motion detection results on test data for Film2

Film 2				
Probabilities	Individual Analysis		AND Fusion	OR Fusion
	Variance	Energy		
P_d	0.95	0.96	0.93	0.98
P_f	0.03	0.09	0.03	0.09

Table 3.5: Frame by Frame motion detection results on test data for Film3

Film 3				
Probabilities	Individual Analysis		AND Fusion	OR Fusion
	Variance	Energy		
P_d	0.95	0.99	0.95	0.98
P_f	0.09	0.09	0.06	0.12

Table 3.6: Frame by Frame motion detection results on test data for Film0

Film 0				
Probabilities	Individual Analysis		AND Fusion	OR Fusion
	Variance	Energy		
P_d	0.98	0.98	0.98	0.98
P_f	0.33	0.33	0.29	0.37

Table 3.7: Frame by Frame motion detection results on test data for Film1

Film 1				
Probabilities	Individual Analysis		AND Fusion	OR Fusion
	Variance	Energy		
P_d	0.98	0.98	0.98	0.98
P_f	0.33	0.07	0.33	0.07

Next, we apply the sequential detection procedure outlined earlier. First, we calculate the values of the likelihood function $LLRT(\mathbf{y})$ and the corresponding values of upper and lower thresholds. These values are selected based on probabilities of detection and false alarm. Decreasing P_{FA} raises the upper threshold without significantly changing the lower threshold. On the other hand, increasing P_D lowers the lower threshold without significantly changing the upper threshold. We set $P_D = 0.9$, $P_{FA} = 0.1$ and evaluate the lower and upper thresholds. The actual performance based on a comparison with grountruth data is presented in Table 3.8. From the table it is evident that the actual performance is in fact better than the designed performance. One can attribute this to the conservative Gaussian model fit that we have used for the motion artifacted BCG data.

Table 3.8: Sequential motion detection results on test data for four film sensors

Probabilities	Film0	Film1	Film2	Film3
P_d	0.98	0.97	0.96	0.94
P_f	0.027	0.025	0.084	0.055

Finally, the duration of motion corrupted frames can be used to infer the "sleep" and "restlessness" state of the subject. As discussed in [55], continued movements longer than one minute are typically classified as "restlessness" and all other periods during the night are classified as "sleep". Using our proposed motion detection approach, we segmented restlessness and sleep phases of the subject and validated it using manual observation based ground

truth data. The results obtained over an observation period of 19 hours are summarized in Table 3.9. 94% and 95.2% accuracies based on NP and sequential tests in distinguishing the child's sleep and wakefulness state demonstrates the effectiveness of the proposed motion detection algorithm.

Table 3.9: Validation test for restlessness percentage for nineteen hours of EMFi signal.

Detection Method	Restlessness	Accuracy
Neyman-Pearson Test	19.1%	94%
Sequential Test	19.3%	95.2%

3.4.2 Motion Artifact Removal

As the second step and for a different dataset, the proposed motion detection and removal algorithms are tested and validated with data collected from three subjects providing nineteen hours of sleep with corresponding bed-based BCG data. All BCG film sensor data was analyzed individually. Since the results were consistent across all four film sensors, we present the findings from the analysis of Film0. ECG signals are used to establish ground truth values of B-B interval specifically. As a gold standard for comparison, R-peak to R-peak intervals in the ECG signals, which were sampled at 250 Hz and band-limited to 0.5-25 Hz are used.

We first apply the sequential detection procedure outlined earlier to the test data sets and evaluate the lower and upper thresholds by setting $P_D = 0.9$, $P_{FA} = 0.1$. The actual performance based on a comparison with ground truth data is presented in Table 3.10. In this case, ground truth data was generated by examining infrared (IR) images of the subject by using thermal camera and manually identifying motion instances and durations. The frames were fed to a motion detection unit in order to detect the presence of motion artifact and the result for this part of the implementation is binary decisions for all of the BCG frames. The result of motion detection are brought here as probability of detection and false alarm as in Table 3.10. From Table 3.10, it is evident that the proposed sequential

detection approach is very effective in discriminating between clean and motion corrupted frames (with nearly 96% accuracy) for all four film sensors.

As the next step, when the frames are detected as corrupted or clean, the reconstructing procedure using the methods in Chapter. 3.3 are implemented. We applied AR and Wiener filter approaches on the frames identified as motion-corrupted and reconstructed those frames. All BCG film sensor data was analyzed individually. Since the results were consistent across all four film sensors, we present the findings from the analysis of Film0. ECG signals are used to establish ground truth values of B-B interval specifically. As a gold standard for comparison, R-peak to R-peak intervals in the ECG signals, which were sampled at 250 Hz and band-limited to 0.5- 25 Hz are used [56]. It is important to note that while ECG R-peak detection is also susceptible to motion, the detected R-peaks in [56] were determined (experimentally) to be more robust than other two other R-peak detection approaches [57, 58] for our system by comparing R-R intervals from clean ECG signals using the three different methods.

The results of the procedure are illustrated in Tables 3.11 and 3.12 for all three subjects (named as B-B interval (motion)). Additionally, for a complete performance evaluation, we also use both methods to predict the parameters for frames that are detected as clean in the previous step (motion artifact detection) and the corresponding B-B interval (the corresponding results for clean BCG frame reconstruction are mentioned in Tables 3.11 and 3.12 as B-B interval (clean)).

Table 3.10: Performance of sequential motion detection method for four film sensors (results from BCG film0).

Probabilities	Film0	Film1	Film2	Film3
P_d	0.96	0.94	0.95	0.94
P_f	0.065	0.062	0.023	0.014

Table 3.11: B-B Interval performance results of the proposed AR algorithm (results from BCG film0).

Subjects	Data	Mean BCG (s)	Mean ECG (s)	Coverage (%)	Precision (%)
subject 1	B-B interval (clean)	1.07	1.03	87.04	93.41
	B-B interval (Motion)	0.97	1.08	83.32	92.21
subject 2	B-B interval (clean)	1.11	1.23	84.93	93.2
	B-B interval (Motion)	1.12	1.41	82.64	95.3
subject 3	B-B interval (clean)	0.88	0.93	80.24	91.8
	B-B interval (Motion)	1.21	1.22	79.62	90.2
Total average	B-B interval (clean)	1.02	1.06	84.07	92.8
	B-B interval (Motion)	1.1	1.23	81.86	92.57

Table 3.12: B-B Interval performance results of the proposed Wiener smoother algorithm (results from BCG film0).

Subjects	Data	Mean BCG (s)	Mean ECG (s)	Coverage (%)	Precision (%)
subject 1	B-B interval (clean)	1.01	1.03	91.43	95.39
	B-B interval (Motion)	1.09	1.08	88.27	94.33
subject 2	B-B interval (clean)	1.38	1.23	89.22	96.3
	B-B interval (Motion)	1.52	1.41	87.09	95.83
subject 3	B-B interval (clean)	0.99	0.93	84.53	94.2
	B-B interval (Motion)	1.18	1.22	83.22	93.27
Total average	B-B interval (clean)	1.12	1.06	88.39	95.29
	B-B interval (Motion)	1.26	1.23	86.19	94.47

The quality of the reconstructed signal for both clean or motion corrupted frames, is captured by the accuracy of the estimated heartbeat events and heartbeat interval lengths

using a synchronized ECG as benchmark. The differences between BCG J-J intervals and ECG R-R intervals from three subjects and each parameter estimation method are presented in Tables 3.11 and 3.12. The performance of the proposed algorithm is evaluated with parameters including *coverage* and *precision* [52]. Coverage is defined as the ratio of number of detected BCG intervals and number of detected ECG intervals. Then these detected intervals are classified as correct and incorrect ones to measure precision as the ratio of correct ones over all intervals. According to the coverage metric, 91.43% of the B-B intervals have been detected with more than 90% of precision. The Wiener smoothing approach provides a better B-B interval estimate than the AR approach. This can be attributed to the fact that Wiener smoothing uses both past and future frames for estimation but the AR model prediction is based exclusively on the past values. However, it is important to remember that Wiener smoothing relies on the assumption of stationarity of the underlying parameter dynamics.

Fig. 3.13 illustrates an example of peak detection for both ECG signal (black plot) and recovered BCG signal (blue plot) using Wiener smoother estimation method. The pink line shows the motion corrupted part in BCG and the blue line shows the reconstructed heartbeats using the proposed algorithm. This figure presents the alignment of the reconstructed BCG J-peaks with the corresponding ECG R-peaks. Here, the goal is to show how the proposed motion reconstruction algorithm performs by comparing the identified J-peaks with the reference R-peaks. The peak alignment indicates that the algorithm is effective in recovering the heartbeat via BCG data and the B-B intervals are well aligned with the reference ECG data. Fig. 3.12 shows an example of motion reconstruction using the AR approach and motion detection using sequential detection method.

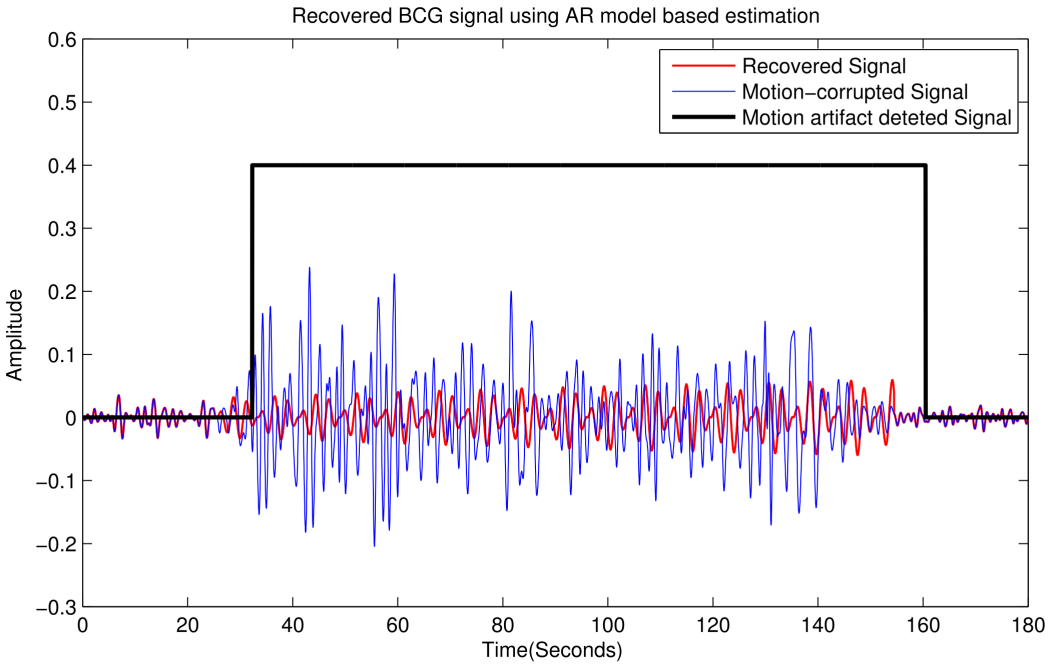

Figure 3.12: Reconstructed BCG signals using AR parametric model estimation (results from BCG film0).

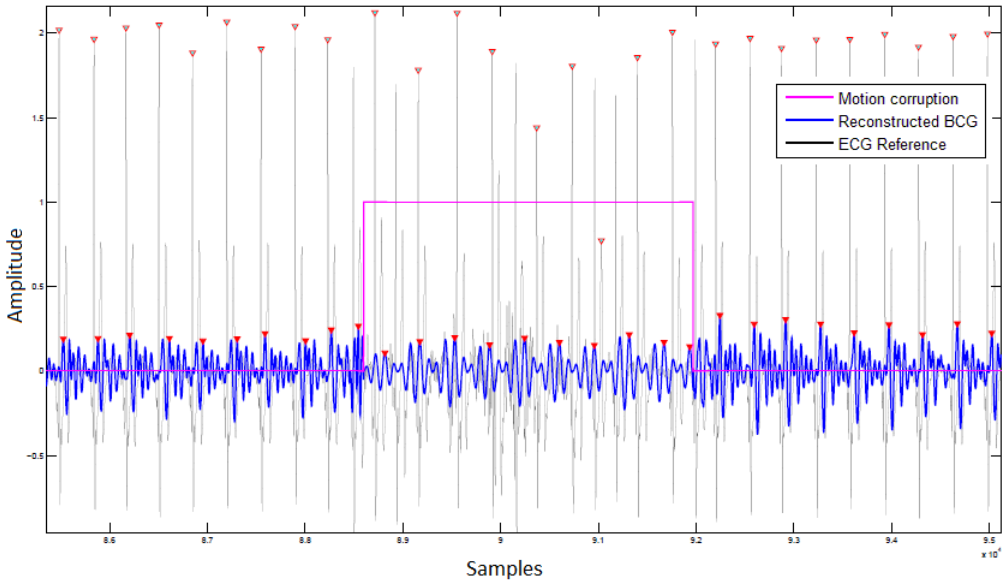

Figure 3.13: Peak Detection in both Recovered BCG and reference ECG data (results from BCG film0).

3.5 Summary

In this chapter, we present a simple yet efficient method for detection and removal of motion artifact in BCG signals. In the detection unit, a sequential decision rule is designed in which successive data frames are compared to upper and lower thresholds to achieve a desired probability of detection and false alarm. If any frame is detected as clean, its three parameters including J-K amplitude, J-J interval, and the most significant frequency component are calculated. If the signal frame is detected as being motion-corrupted, the three signal parameters are estimated using an AR model-based tracking or a Wiener smoother. The efficiency of the methods are illustrated using B-B interval comparison with ECG data based on over nineteen hours of sleep obtained from multiple subjects. The comparisons with ECG reference data indicate that the algorithms can effectively help to detect and remove the motion artifacted BCG signals based on sequential detection and model-based parametric tracking and reconstruction.

In the next chapter, we will develop statistical models linking sleep quality with daytime performance parameters to identify important relationships between sleep quality, learning, and development in severely disabled autistic children using our proposed sleep quality indicator, restlessness.

Chapter 4

Relationship between Sleep Quality and Daytime Behaviors in Children with Autism Spectrum Disorder

Monitoring the sleep patterns of children with ASD and understanding how sleep quality influences their daytime behavior is an important issue that has received very limited attention. In this chapter, we evaluate an unobtrusive and inexpensive bed system for in-home, long-term sleep quality monitoring using BCG signals. Using the BCG signals from our designed smart bed system, we define "restlessness" as a surrogate sleep quality estimator. Using this sleep feature, we build predictive models to find the link between sleep quality and daytime behaviors over a timescale. Specifically, we use two supervised machine learning algorithms namely SVM and artificial neural network (ANN).

4.1 Related Work

ASD is a neuro-developmental condition, in which affected individuals: (1) have challenges with social communication; (2) have restricted interests, and (3) perform repetitive patterns of activities [59]. In addition to core social difficulties, prior research indicates that 64-93%

of affected inviduals exhibit at least one challenging behavior such as aggression, self injury, depression, tantrums, and sleep disturbances [10–14, 60, 61]. Among all conditions, sleep problems are among the most prominent conditions faced by children with ASD [62, 63]. Sleep disturbances such as reduced total sleep time, increased bedtime resistance, frequent night wakings, and decreased sleep efficiency have been reported in 50-80% of children with ASD [64, 65].

In typically developed (TD) children, sleep problems are associated with daytime behavior and cognitive functioning [66]. Specifically, previous studies indicate that poor sleep quality can affect TD child behaviors such as aggression, hyperactivity, and anxiety [15, 67]. It is possible that children with ASD may be more vulnerable to the negative impacts of poor sleep quality. Previous studies show that the link between poor sleep and behavioral problems in children with ASD is not well understood. Detailed investigation of the link requires the use of unobtrusive instrumentation for objectively assessing sleep quality in longitudinal studies.

Methods for identifying sleep problems in children with ASD can be categorized into subjective and objective measures. Subjective measures often utilized in the study of sleep in children with ASD generally include parent-report questionnaires, Japanese Sleep Questionnaire for Preschoolers (JSQ-P), Child Behavior Checklist (CBCL), or completion of a sleep diary record [68–72]. However, sleep analysis based on subjective measurements has a major limitation due to the fact that the subject with ASD maybe nonverbal or in state of loss of consciousness or in the case of questionaire, the report is dependent to individual's recall. In contrast, objective measures of sleep rely less on information from parents or caregivers, and instead directly measure aspects of sleep through various technologies. Some of the most common objective approaches used to assess sleep in children with ASD include PSG [73–76] and actigraphy [10, 77–81]. Although PSG provides the most accurate detailed information on sleep, it requires multiple intrusive on-body sensors and also it's difficult to use for longitudinal studies. These sensors affect the comfort level of the subject possibly influencing the sleep process. Therefore, PSG may not be the appropriate method for measuring sleep

quality since it is impractical outside a lab environment for long-term sleep monitoring. As an alternative approach, actigraphy employs accelerometers attached to one's body to index sleep and wake periods based on subject movements [82]. While less invasive than PSGs, this technology needs on-body sensors and thus it is not well-suited for long-term monitoring with children with ASD. An unmet need remains for a low-cost and unobtrusive technology to quantitatively measure sleep quality of disabled children. We have developed a bed-based system previously validated for measuring sleep quality [21, 29]. This smart bed system provide BCG data as a promising, unobtrusive and inexpensive methodology. In contrast to other cardiac monitoring technologies such as ECG and PSG, BCG signals can be recorded without any electrodes or sensors attached to the body. Also, compared to conventional actigraphy, which uses ankle or wrist-worn sensors, the bed-based BCG system allows actigraphy monitoring without requiring the subject to wear any sensors. Although not employed in this study, the BCG system further captures physiologic information, such as heart-rate and respiratory, which may help to yield refined estimates of sleep quality [83–85].

To date, findings based on the correlational association between challenging behaviors and sleep problems in individual with ASD are mixed. In some studies, sleep problems (such as reduced sleep efficiency and increased night awakenings) were found to have a negative impact on the rate of daytime behaviors (such as aggression and self-injurious behaviors) [86–88] using subjective questionnaires and actigraphy to measure sleep quality. Lambert et al. [72] studied sleep problems and daytime functioning in both TD and ASD children based on one-night PSG and questionnaire-based sleep quality measurements and interestingly, assessment with PSG found sleep issues even in ASD children who did not report sleep complaints from sleep habit questionnaires. Goldman et al. [89] reported that there was an association between poor sleepers and behavioral problems using Children's Sleep Habits Questionnaire but the directionality of this relationship could not be determined. Cohen et al. [90] investigated sleep patterns predictive models of daytime behaviors in individuals with low-functioning autism using manually measured sleep pattern for more than 20,000 nights of sleep. Since the study uses a caregiver to collect measurements related to

sleep quality, it is difficult to scale this approach beyond clinical settings. Therefore, an unobtrusive and autonomous sleep quality monitoring system is needed. Thus, although the association between sleep and behavior has been investigated in children and adults with ASD [70, 72, 87, 89, 91–93], but there still exists limitations to get unobtrusive sleep data from these individuals for a long-term home monitoring environment.

The aim of this chapter is to develop and assess a methodology for assessing the link between longitudinal sleep quality in children with autism and daytime challenging behavior. Using our previously validated bed system, we determine periods of motion/restlessness based on a bed-based BCG sensor suite and use them as one of the main sleep quality features along with other metrics. This study describes an effort in collaboration with Heartspring located in Wichita, KS to develop and evaluate a toolset for monitoring and assessing children with ASD well-being. The objectives of this study are to: (a) investigate the utility of our bed-based unobtrusive system for collecting sleep metrics; (b) develop predictive models to find the relationship between sleep quality and daytime behavioral data; and (c) evaluate these metrics for data gathered from a group of children at Heartspring. Here, we analyze over 200 nights of sleep measurements from two individuals with ASD. We develop predictive models for daytime behavioral changes using night time sleep quality changes obtained from our smart bed system. Additionally, we investigate the influence of history of 2-8 nights sleep on daytime behaviors. Two different supervised machine learning classifiers are used to help build the predictive models for daytime behaviors. Furthermore, we study the predictive models for sleep quality using daytime behavioral features over a history of previous days information and also the classification accuracies for predicting sleep quality based on both night-time and daytime features are evaluated.

4.2 Materials and Methods

The overall processing procedure of night-time and daytime features are illustrated in Fig. 4.1. First, the BCG data are collected using smart bed-based system with EMFi sensors placed on it [29] for each subject during sleep time. Second, all BCG data are analyzed through our previously proposed motion detection approach [20] in order to detect motion artifact. These detected motion artifacts are further used to define a new sleep quality metric named as restlessness. Finally, predictive models are designed for daytime behaviors based on sleep quality metrics and sleep quality based on daytime behaviors. Each step is described in detail in the following sections.

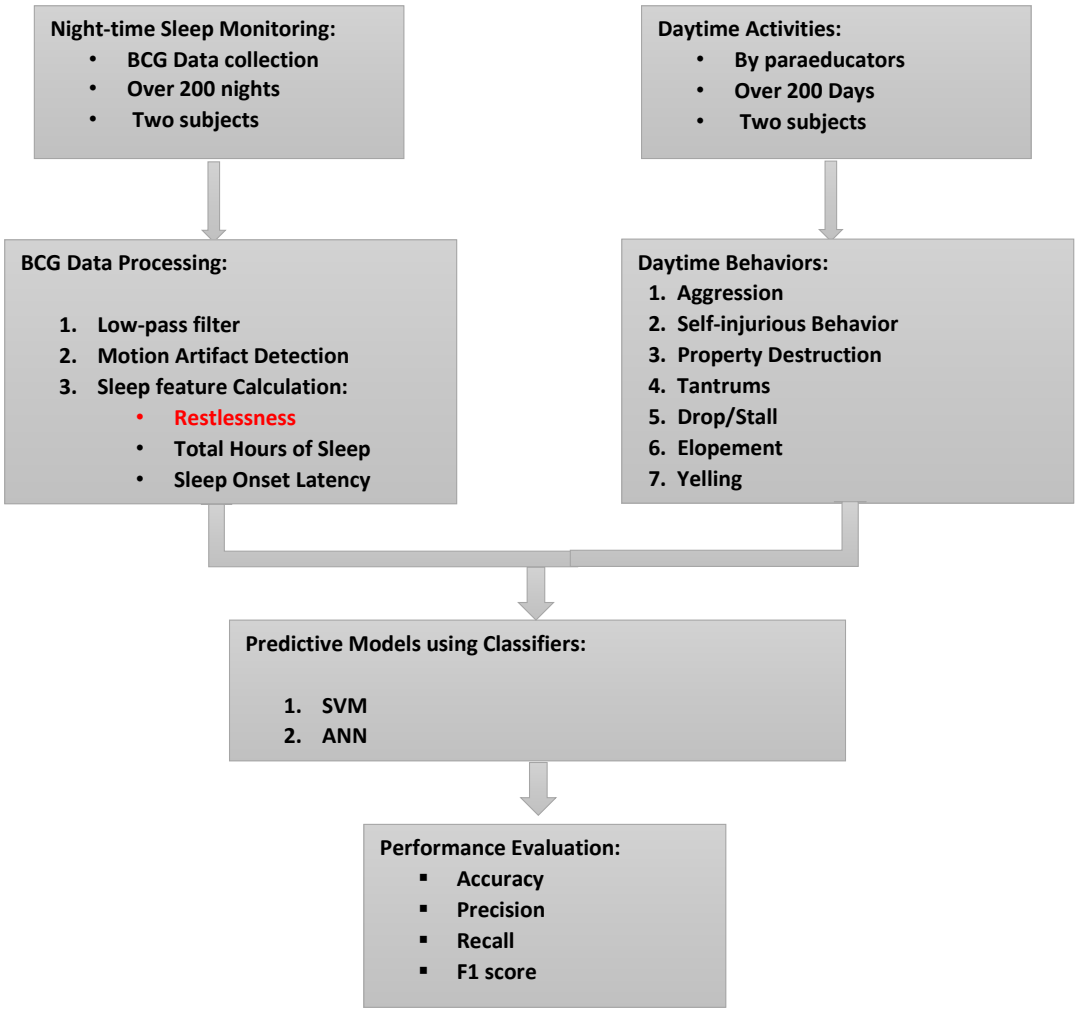

Figure 4.1: System presenting sleep data collection to predictive models.

4.2.1 Participants

In this study, two male children with severe ASD are chosen from Heartspring, a residential school located in Wichita, KS. The sensor-laden bed systems were placed in each child's residential room as their sleeping bed, while our team from Kansas State University were remotely collecting force sensor data (BCG data) overnight for more than 200 nights of sleep. Black and white images (no video recordings were allowed in order to protect the privacy and dignity of the children) were recorded through with a camera, which show the position of the subjects and the times when they are moving. Note that the data was collected under

Kansas State University IRB protocol #7783.

4.2.2 Sleep Quality Measures

The night-time monitoring system is a multi-parameter bed sensor system populated with sensing devices that provide sleep quality parameters [29]. It is important to note that this system is fully unobtrusive, meaning that each child thinks he is sleeping on his normal bed and he has no interactions with the sensors. The latter is important, as these children might be otherwise inclined to play with any device that is not part of their normal living environment. In our previous study, we proposed a method to automatically detect motions and measure restlessness as a surrogate sleep quality indicator [20] as described in Chapter 3. As a summary, in this method, the parametric distribution of the measurements for clean and motion corrupted BCG data is estimated based on the training data. Then, a $LLRT$ test is formulated and a binary decision is made as:

$$\delta_S = \begin{cases} 1 & \text{if } LLRT \geq A \qquad \text{(Motion-corrupted)} \\ \text{No Decision} & \text{if } B \leq LLRT \leq A \\ 0 & \text{otherwise } LLRT \leq B \qquad \text{(Clean)} \end{cases} \tag{4.1}$$

These two thresholds were chosen based on desired probability of detection P_D and probability of false alarm P_{FA}, which are defined as:

$$A = log(\frac{P_D}{P_{FA}}) \quad , \quad B = log(\frac{1-P_D}{1-P_{FA}}) \tag{4.2}$$

Based on prior literature, we define any continued movements longer than one minute as "restlessness" stage. Otherwise subject is considered to be in "sleep" stage (summarized in Fig. 4.2). This makes it possible to automatically estimate a sleep quality metric using the smart bed system rather than the classical approach of manually checking the subject every 15 or 30 minutes during night. Other sleep features are computed from each night of

sleep such as *Total Sleep Time*, defined as the length of the time spent sleeping; and *Sleep Onset Latency*, defined as the length of time that it takes from wakefulness to sleep. These two features are measured based on observational data which were black and white images acquired through the thermal camera in each individual's room.

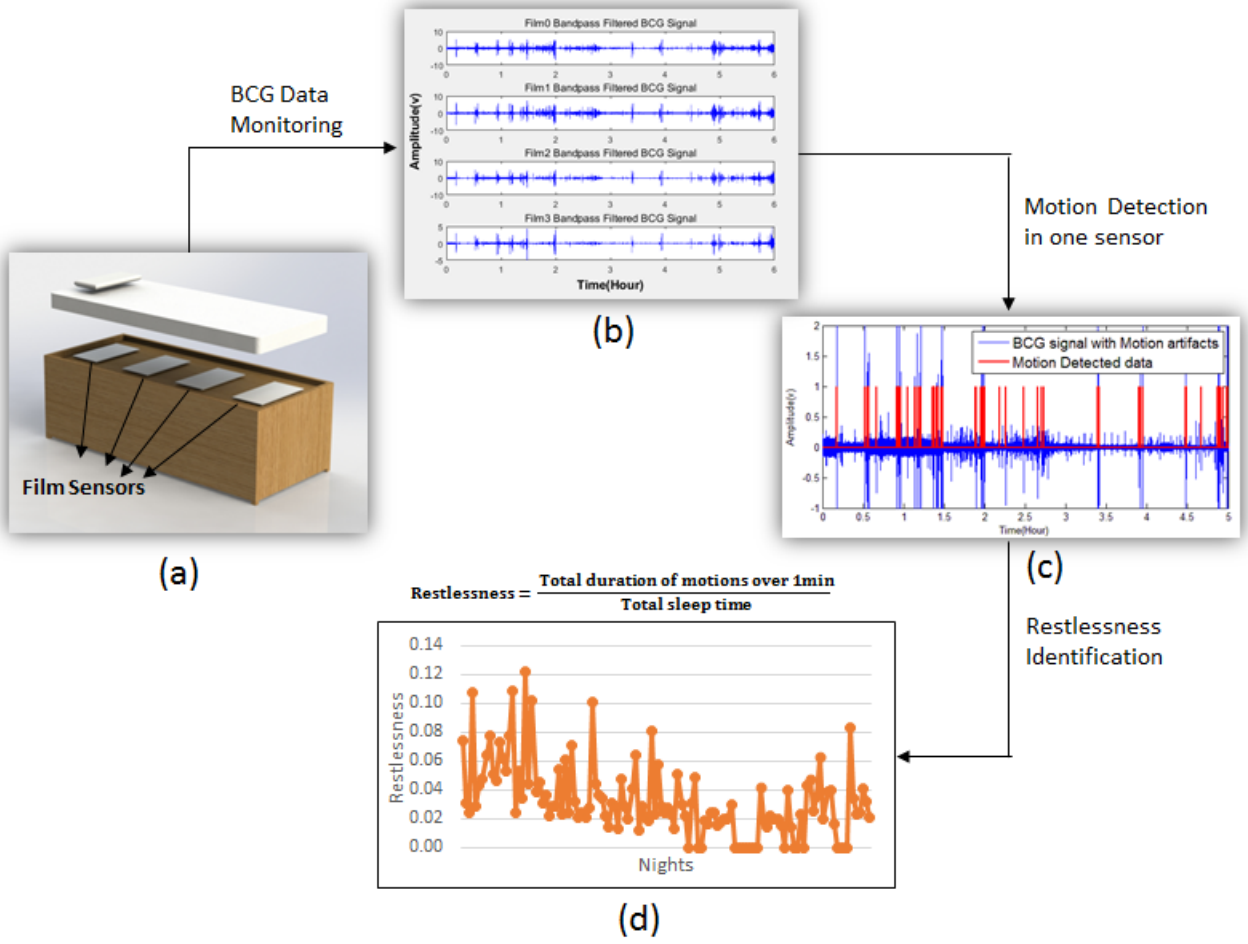

Figure 4.2: From smart bed system to restlessness identification: (a) our designed smart bes with four EMFI sensors on top of it; (b) four acquired BCG data from four film sensors; (c) motion artifact detection for BCG data in one film sensor; and (d) obtained restlessness from (c) over 200 nights of sleep.

4.2.3 Daytime Behavioral Data

Daytime child wellness data are obtained from the school databases, which include demographic information (such as age, gender, level of severity in autism), medical information such as seizure frequency, medications (such as nights with and without medication), and more importantly child behaviors during day. Each child is assigned a paraeducator who manually records all the child's behaviors during day. Out of the total of 35 different behaviors, in this paper, we analyze the two most commonly exhibited behaviors: (a) *aggression (AGG)*, defined as kicking, hitting, biting, grabbing, throwing objects at, or any other behavior that could cause injury to another person; and (b) *self-injury (SIB)*, defined as hurting or damaging one's own body. We analyze the presence or absence of each of these behaviors separately. The daytime behaviors were tracked and totals were generated for each day. Moreover, we measure all behaviors including aggression, property destruction, self-injury, tantrums, yelling, splints and mitts, and spitting on or at staffs, to arrive at an overall behavior score during class time. This cumulative metric is referred to as *Total behaviors in class (CL)* and is the third daytime feature of interest.

The descriptive statistics for all the sleep parameters and daytime behaviors used in this study are summarized in Table 4.1.

Table 4.1: Descriptive Statistics for Sleep parameters and Daytime behaviors.

Parameters	Possible Range	Mean	SD
Restlessness	0 - 23	6.85	3.5
Total hours of Sleep(h)	7.36 - 11.96	10.22	1.57
Sleep Onset Latency (h)	0.1- 3.08	1.37	0.57
AGG	0 - 73	7.39	11.92
SIB	0 - 191	22.16	32.52
CL	0 - 100	7.58	13.72

4.3 Hypothesis 1: Predictive Models for Daytime Behaviors

4.3.1 Classification Models

The goal here is to build a predictive model for daytime behavioral changes using night-time sleep quality features. For each individual, the behavioral patterns would vary over time. Also, the optimal number of nights utilized for determining the daytime-nighttime relationship tends to vary. All sleep metrics including restlessness, total sleep time, and sleep onset latency are z-score normalized prior to training and testing procedure. Standardization or z-score is the most commonly used method for normalizing data which converts all indicators to a common scale with an average of zero and standard deviation of one. In this study, we use two supervised machine learning algorithms namely SVM and ANN to help predict behavioral outcome based on sleep features. All the samples in the data-set are over-sampled to enable balanced learning using both SVM and ANN.

SVM classifier

We use a SVM classifier with a linear kernel [94] in order to learn sleep patterns for multiple nights and predict the presence or absence of a daytime behavior for the following day. First, we binary score the daytime behaviors based on presence or absence of that specific behavior. We repeat this classification procedure for each subject and each of three daytime behavior metrics (CL, AGG, and SIB). By considering the sleep quality over previous nights (1-8 nights) as input to the SVM, we aim to identify the influence of history of sleep on daytime behaviors. Additionally, we design the SVM classifier with and without the restlessness behavior metric to determine the value of our unobtrusive bed-based sleep quality measurement.For performance measurement, we used 100 randomly selected train and test sets and report the average performance. The ratio used for training and testing process is 70:30, which means that 70% of data is selected for training and 30% is used for testing.

ANN classifier

We use ANN classifier (as in Fig. 4.3) algorithm which implements a three-layer feed-forward neural network with 70:15:15 ratio as training, validation, and testing sets and Scaled Conjugate Gradient (scg) as the network training function. As in Fig. 4.3, the number of neurons in the input layer (f) is the number of sleep features of the input data. The number of neurons in the output layer is 2 which corresponds to the number of classes. The number of hidden layer neurons (d) is chosen by trial and error using different features and different activation functions to get the best performance.

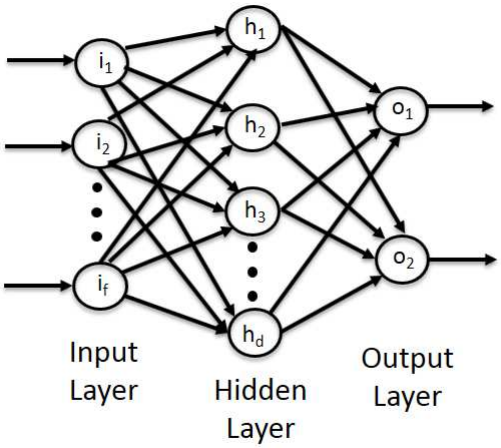

Figure 4.3: Schematic of three-layer feed-forward ANN classifier.

System Evaluation

In order to compare aforementioned classification efforts, we calculate a confusion matrix for each round of validation from which we drive the values for true positive (TP), false positive (FP), true negative (TN), and false negative (FN) cases. Then, we evaluate the performance of each approach by the following metrics: *Accuracy, Recall, Precision*, and F_1 *score*, which are commonly used for classification purposes and defined as below:

$$Accuracy = \frac{\Sigma TP + \Sigma TN}{\Sigma(Total)}$$
$$Precision = \frac{TP}{(TP + FP)}$$
$$Recall = \frac{TP}{(TP + FN)}$$
$$F_1 = \frac{2TP}{(2TP + FP + FN)}$$

where TP is the number of correctly identified presence of a daytime behavior, TN is the number of correctly identified absence of a daytime behavior, and FP and FN are the numbers of mis-classification for each class, respectively. We use F_1 score to compare the two classifier's performance which shows how robust and how precise each classifier is. Since our work primarily relies on average values based on the subjects and different training and testing sets, we report the mean and standard deviation for each model.

4.3.2 Impact of Restlessness Feature

As one of the main contributions of this study, we investigate the usefulness of our bed-based BCG in quantifying sleep quality by extracting one sleep feature named as "restlessness" from smart bed. In order to evaluate the system performance with this night-time sleep measure, we compare the performance in daytime behavior predictive models using restlessness as one feature, with models without restlessness as input feature. The results are shown in Fig. 4.4 for comparison for all three behaviors over a timescale of 2-14 previous nights. For AGG as in Fig. 4.4a, accuracy outperforms in our system compared to when restlessness is not among the night-time sleep features which can be seen in predictions over a history of sleep nights from 2-14 nights with over 6% difference in average. Additionally, for CL in 4.4c, significant improvement (about 8%) have achieved in classification performance by having restlessness as one night-time feature to predict CL behavior. It is also important to note that an exact

comparison with prior work [90] on using SVM to predict daytime behavior is not possible as the dataset used to quantify restlessness is different. In this work [90], sleep patterns in lower functioning autistic children were measured manually in order to find the the predictive models for daytime behaviors based on these sleep parameters using SVM. However, in their study, an autonomous sleep quality home monitoring system is need which can provide night-time sleep measurements unobtrusively. We have shown that our bed-based system is capable of recording motions and heart activities in an objective, unobtrusive, and robust way with high precision.

Moreover, we investigate importance of sleep features in driving behavioral predictions as it is shown in Fig. 4.5. For each subject, feature importance is measured in each predictive model and the average value across subjects and behavior predictive models are demonstrated. The values are showing the importance in the model and the sign is indicating whether values are positively associated with each behavior or negatively. We can conclude from Fig. 4.5 that restlessness has higher positive association with daytime behavior compared to other two sleep features. Also, sleep onset latency has negative relationship with daytime behavior across subjects with high level of impact.

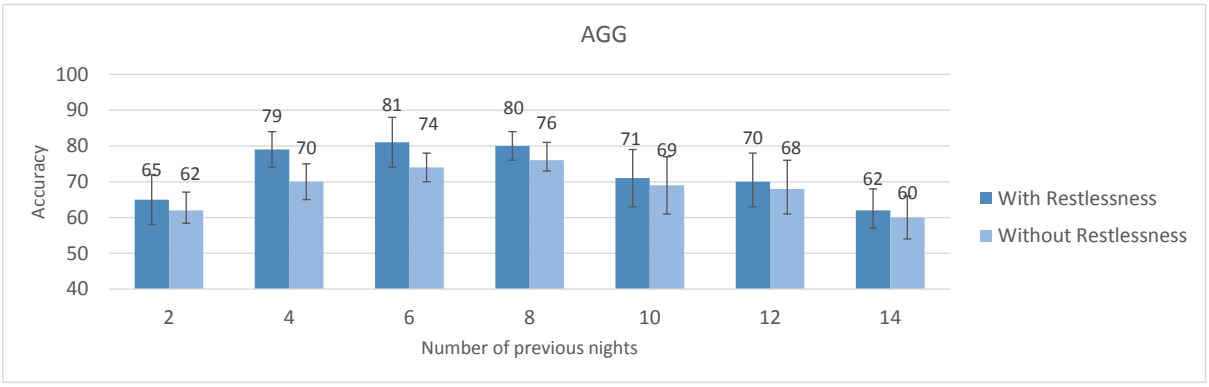

(a)

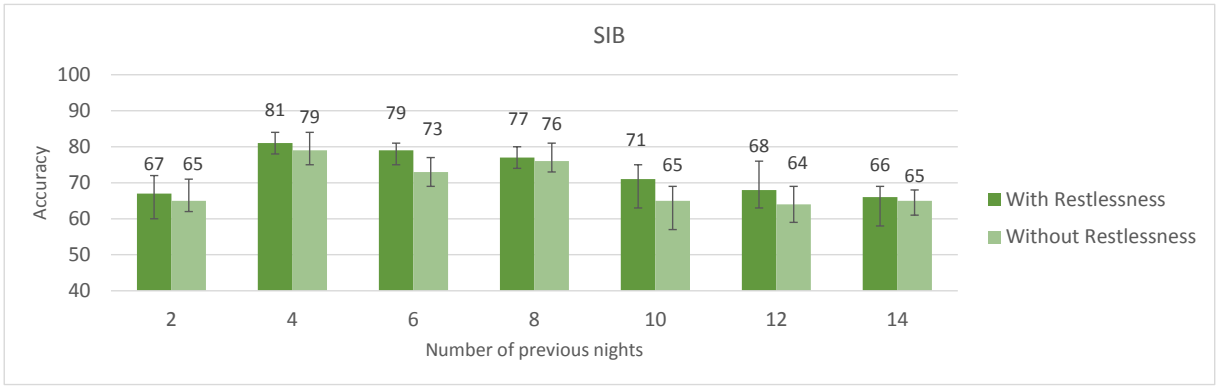

(b)

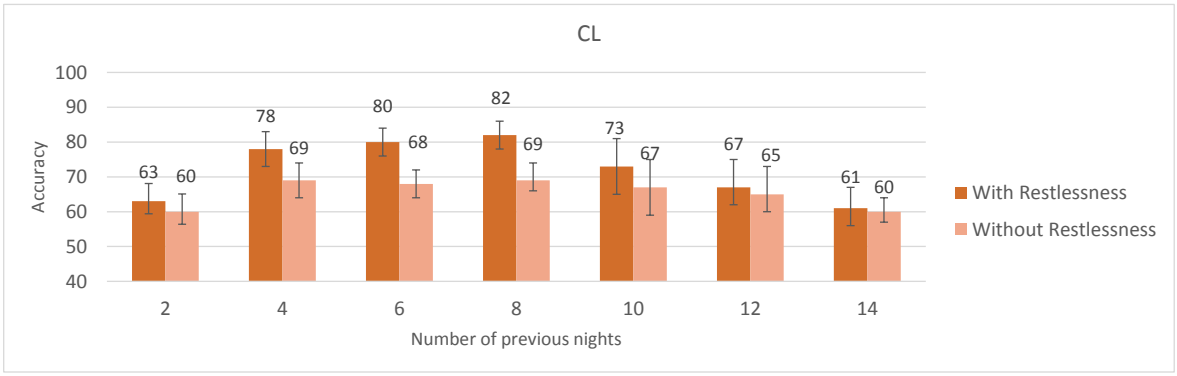

(c)

Figure 4.4: Evaluation of predictive models for challenging daytime behaviors as (a) AGG , (b) SIB ,and (c) CL using previous nights sleep quality data.

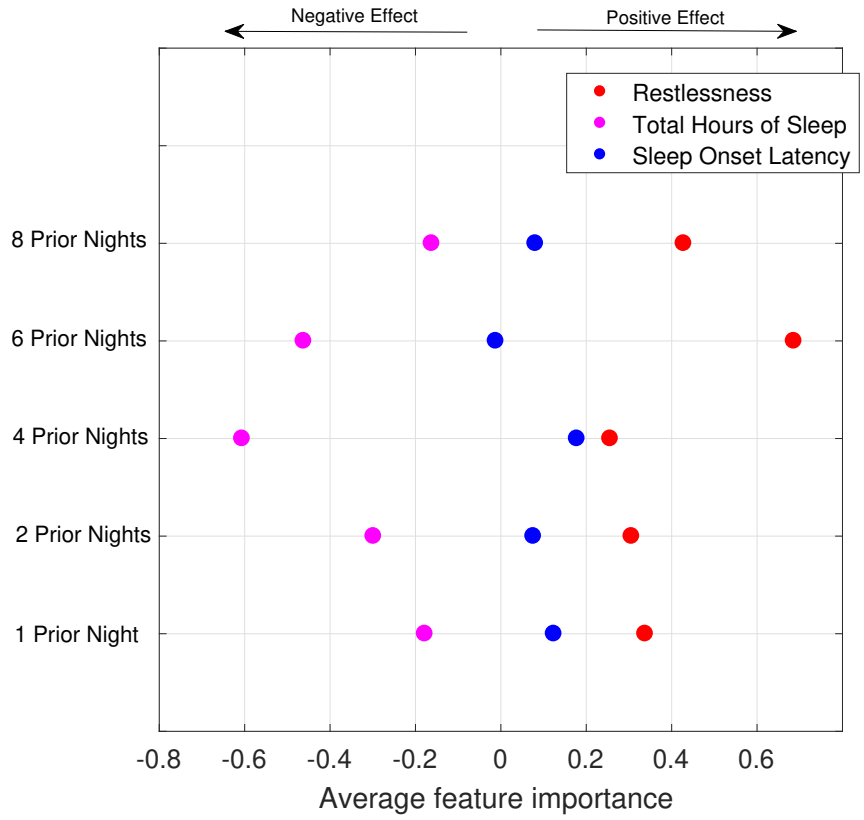

Figure 4.5: Measure of sleep feature importance averaged across successful predictive model for all daytime behaviors.

4.3.3 Impact of Sleep History on Predictive Performance

Next, we study the relationship between prior sleep history and the challenging daytime behavior in children with ASD. The goal is to predict the pressence or absence of daytime behaviors including AGG, SIB, and CL using sleep features from previous nights. After considering a range of sleep history windows, i.e., 2-14 prior nights of sleep features for prediction, we identify 4, 6, and 8 nights sleep data are the most informative based on the better performances (shown in Fig. 4.4). Surprisingly, the first 2 nights of sleep were not strongly predictive for the following day behavioral pattern because we notice meaningful accuracies resulting from our classification models. For brevity, we report the performance of each behavior based on 4, 6, and 8 prior nights features in Figs 4.6, 4.7, and 4.8. For each behavior, a total of three sleep features per night are selected which means for 4 previous nights $\sim$

12 features, for 6 nights $\sim$ 18, and for 8 nights $\sim$ 24 features are extracted as sleep quality features. We repeat the same analysis for all behaviors across subjects and the reported values are the average metrics over individuals with two different classifiers for 100 randomly chosen training and testing sets. The corresponding means and standard deviations are also shown in the figures for each classification based on the mean and standard deviation of the results. In this study, we find a significant predictive relationship with higher average accuracy of 83%, 86%, and 84% for AGG, SIB, and CL , respectively. The performance are evaluated using precision and recall metrics and all the average values are acceptable. This relationship is much strong for AGG behavior and as it was mentioned in [95, 96], sleep problems lead to aggressive behavior in children with ASD.

However, for some of the behaviors the prediction results improve with more prior sleep data, but we do not claim that sleep history over longer timescales would improve all daytime behaviors predictions. Many different internal and external factors can affect sleep and behaviors. As it is shown, for these subjects SIB is highly related to sleep quality compared to AGG and CL.

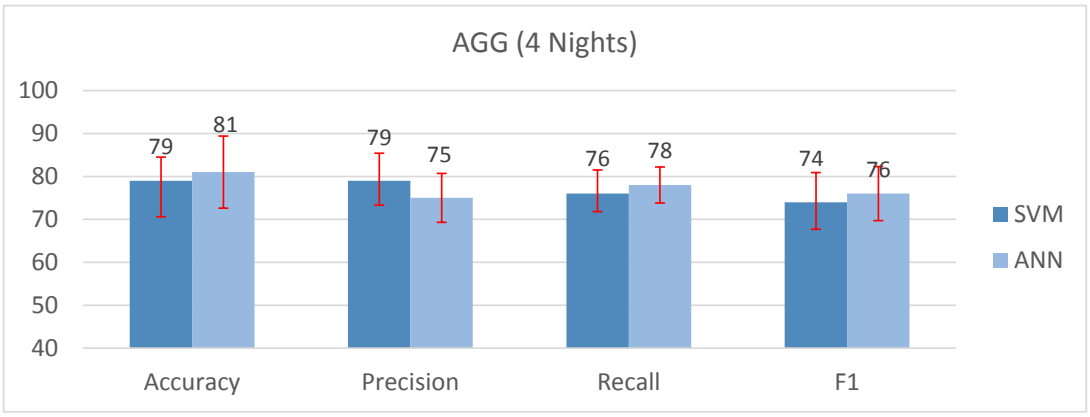

(a)

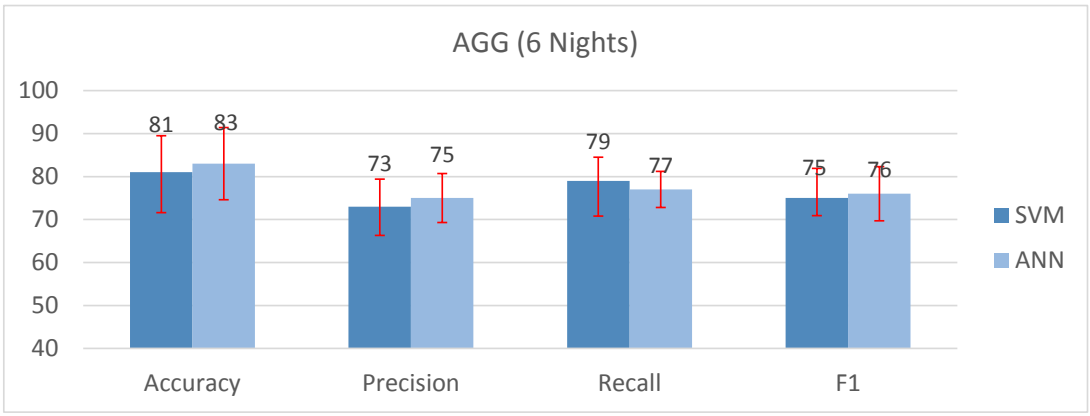

(b)

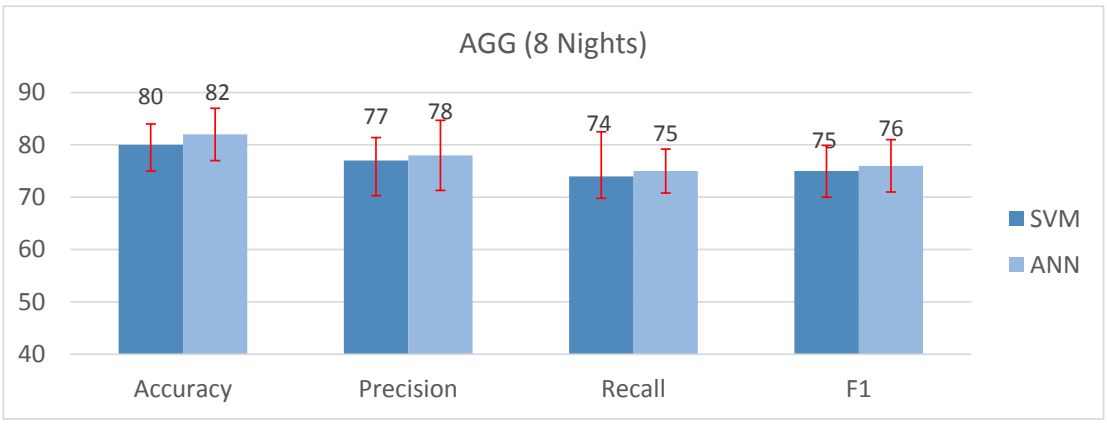

(c)

Figure 4.6: Evaluation of predictive models for AGG behavior over (a) 4 , (b) 6 ,and (c) 8 nights of prior sleep.

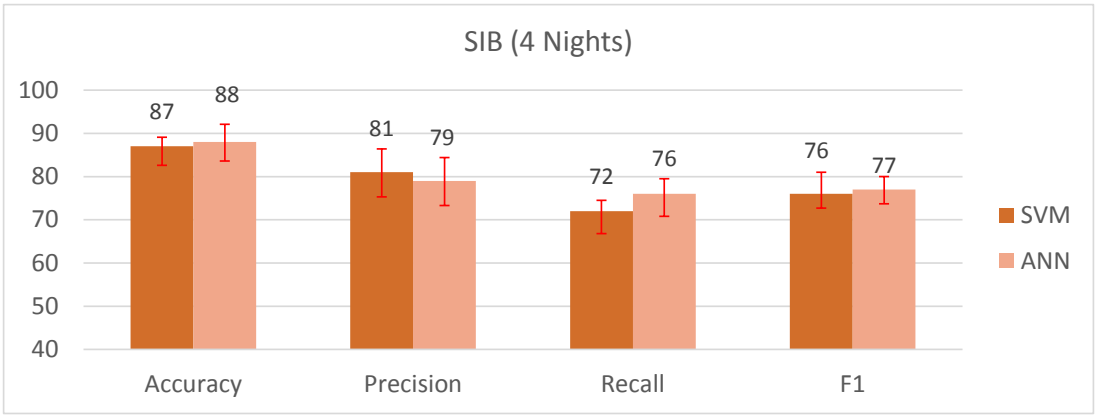

(a)

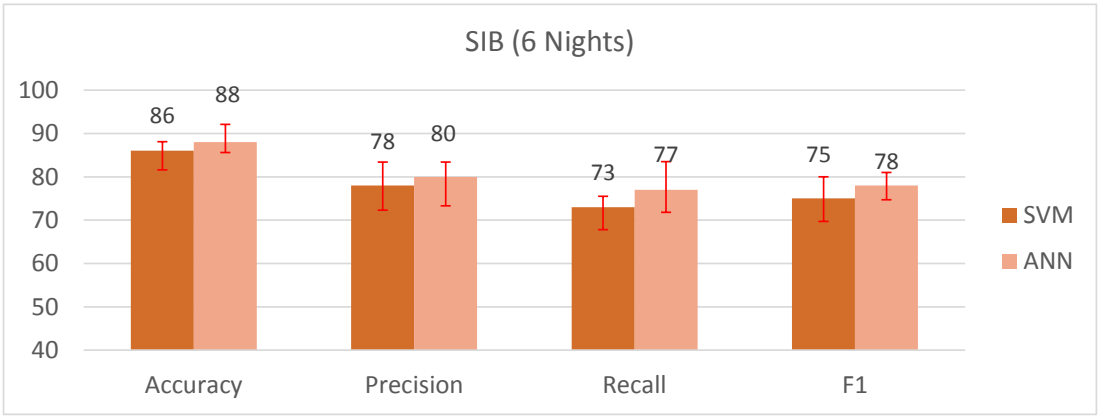

(b)

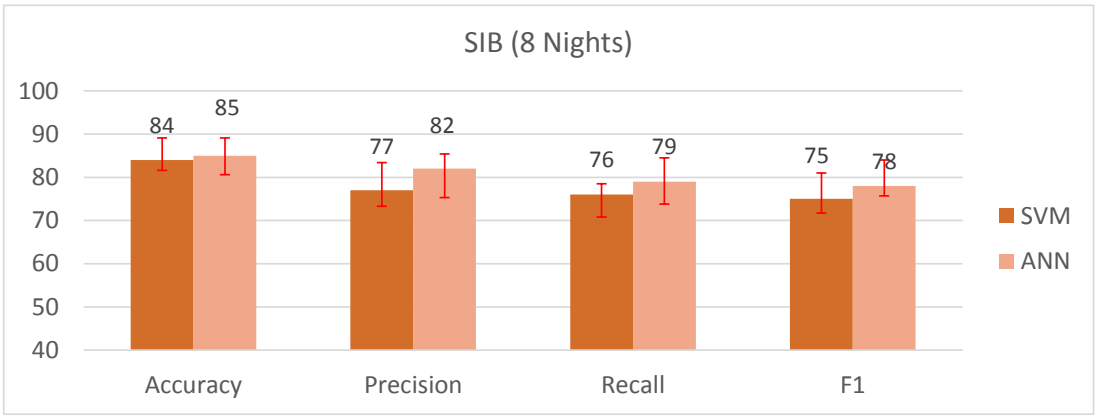

(c)

Figure 4.7: Evaluation of predictive models for SIB behavior over (a) 4 , (b) 6 ,and (c) 8 nights of prior sleep.

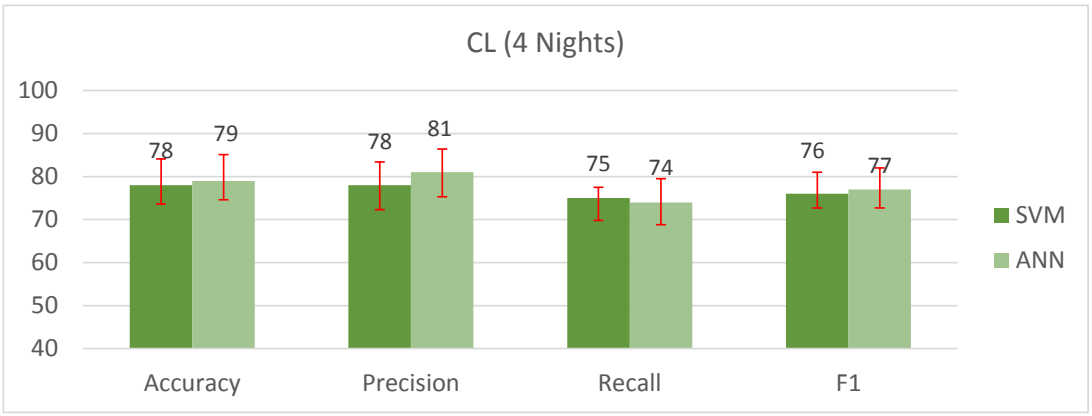

(a)

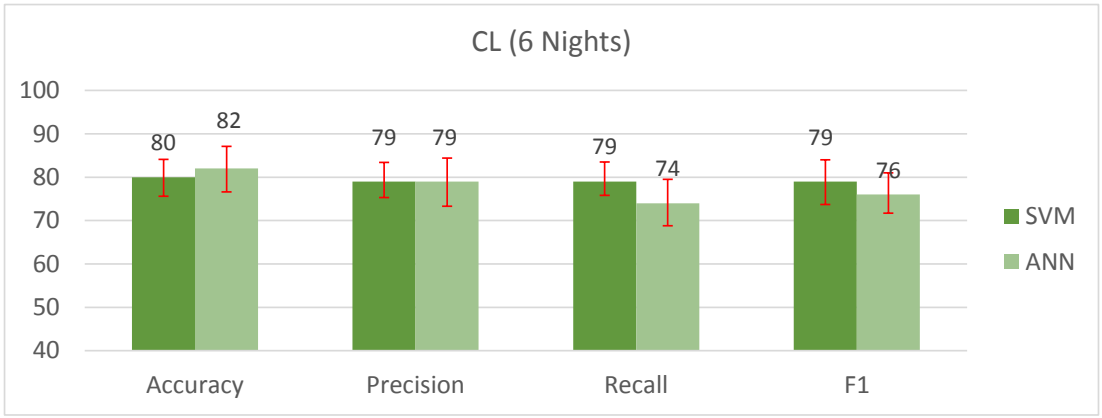

(b)

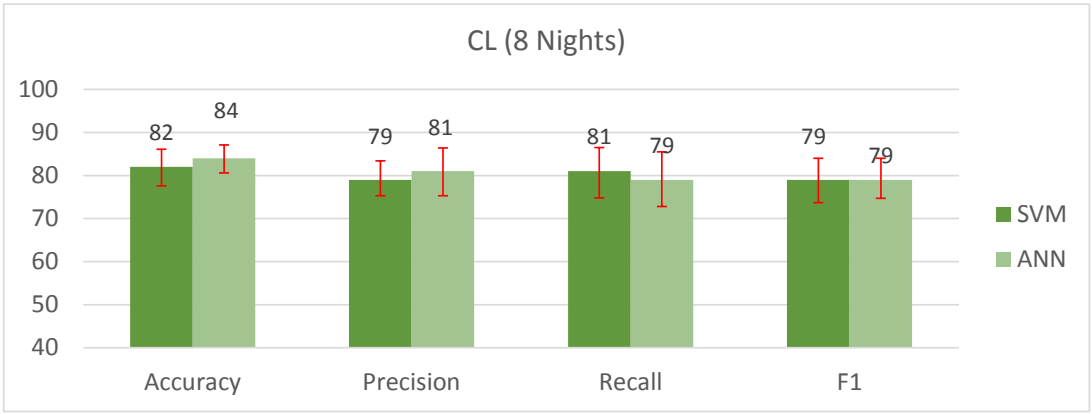

(c)

Figure 4.8: Evaluation of predictive models for CL behavior over (a) 4 , (b) 6 ,and (c) 8 nights of prior sleep.

4.3.4 Comparison between Classifiers

In this subsection, we aim to compare classifiers SVM and ANN on the given dataset, for which all we need is the measured F_1 score. The results using our proposed predictive models using both ANN and SVM classifiers are given in Figs 4.6, 4.7, and 4.8, where F_1 score is used to enable a single measure of performance which is a harmonic mean of the precision and recall metrics with its best value at 1 and worst at 0. ANN outperforms SVM in almost all three daytime behaviors predictive models by 2% different overall. For AGG behavior, specifically, the average $F1$ score of 76% from ANN is close to those from SVM at 75%. Also, this slightly difference (around 2%) is occurring for SIB behavior models. Thus, based on F_1 values for the three behavioral predictive models, ANN generates slightly better results than SVM. However, from the training time aspect, SVM has less time complexity compared to ANN. This is because the ANN requires a considerable amount of time to adjust and determine the network parameters that best has best training and testing performance. However, in general, both SVM and ANN showed an acceptable time complexity in all predictive models.

4.4 Hypothesis 2: Predictive Models for Sleep Quality

In the second hypothesis, we analyze the predictive models for night-time sleep quality variations. The daytime behavior features include AGG, SIB, property destruction (PDE), total behaviors at home (HM), and CL. All behaviors are defined in Chapter 4.2.3 except *property destruction*, which includes throwing objects not meant to be thrown (but not at someone), tearing objects not meant to be torn (i.e., -task, books), kicking objects not meant to be kicked, and dumping/tipping objects over. Sleep measures are the same as hypothesis 1 as *Total Sleep Time*, *Sleep Onset Latency*, and *Restlessness* which are defined in Chapter 4.2.2. We convert our sample's raw scores to z scores separately for each subject within the sample. In this way, we are able to obtain a common metric for all of them. In this section, we analyze the level of restlessness, sleep onset latency, and total hours of sleep for each

subject, thus we need to group the data in two classes for each sleep feature based on the average variation. For example, the nights with restlessness less than the average value of restlessness for each subject are considered as "Good Sleepers", and those with restlessness of greater than mean value are considered as "Poor Sleepers". We categorize the sleep measurements for each subject separately, since the level of sleep and restlessness is different for each individual especially for children with ASD.

4.4.1 Classification Models

The objective here is to build a predictive model for sleep quality changes based on daytime behavioral variations. In this study, we use the same classifiers as previous hypothesis as SVM and ANN. All the samples in the dataset are over-sampled to enable balanced learning using both SVM and ANN.

System Evaluation

We have a binary hypothesis testing problem for each sleep measure which we define one of them here. In the hypothesis problem for restlessness, H_0 corresponds to low restlessness during night, and H_1 corresponds to high value of restlessness. That is,

$$\begin{aligned} H_0 &: Restlessness \leq mean \quad \text{[Good Sleepers]} \\ H_1 &: Restlessness > mean \quad \text{[Poor Sleeper]} \end{aligned} \tag{4.3}$$

The same as hypothesis 1, for both classifiers, we use *Accuracy, Recall, Precision*, and F_1 *score* as the performance metrics.

4.4.2 Impact of Sleep History on Predictive Performance

First, we study the classification performance for sleep quality based on only daytime behaviors as input features for a timescale of 1-6 previous days. The results of the predictive models are illustrated in Fig. 4.9. For all three night-time metrics as restlessness, sleep onset latency, and total hours of sleep, the accuracies using two classifiers as SVM and ANN are shown in this figure. The accuracy has higher and more acceptable values for models using only 1 previous day behaviors as input features which have more than 71% as using both classifiers. Based on our findings, the reported performances for more than 2 previous days in this case are low and we can conclude that sleep quality is mostly predictable based on only previous day challenging behavioral data using data from these two subjects.

4.4.3 Daytime and Night-time Sleep Measures as Input Features

Having demonstrated a better predictive model for sleep quality measures using daytime behaviors based on only one previous day information, we next investigate whether using both daytime and night-time features as input features are outperforming the predictive models for sleep quality based on only one previous day and night data. Therefore, in our model we use both daytime behaviors and night-time sleep quality as input features to predict level of sleep quality (which can be below average or above the average for each subject) for the following night. Again, we average the evaluation metrics across subjects to get a single overall score to evaluate the system and we report the mean and standard deviation for each model. The results are illustrated in Fig. 4.10. For all three sleep quality metrics, ANN outperforms SVM and accuracy has greater improvement from ANN compared to SVM classifier with average of 2% difference. We have shown that our bed-based system is able to record sleep quality in an unobtrusive manner and these measurements can help in better analyzing the relationships between sleep quality and daytime behavior in children with ASD.

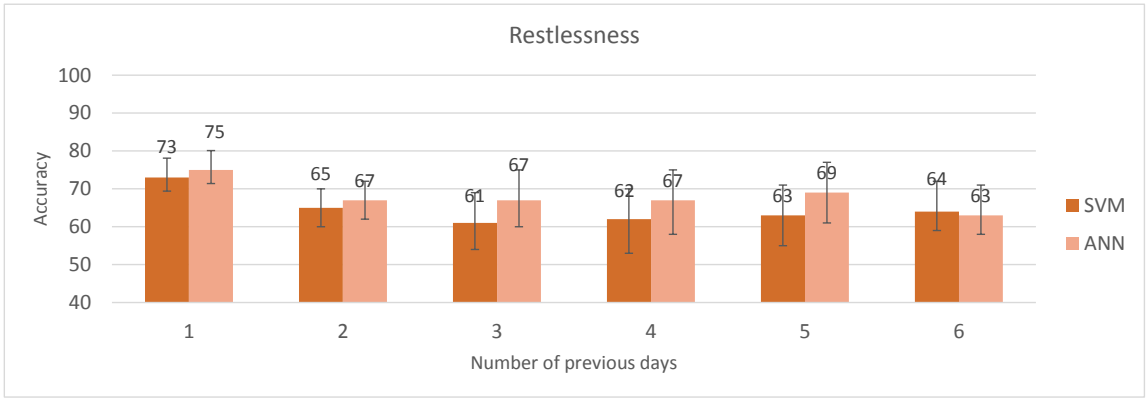

(a)

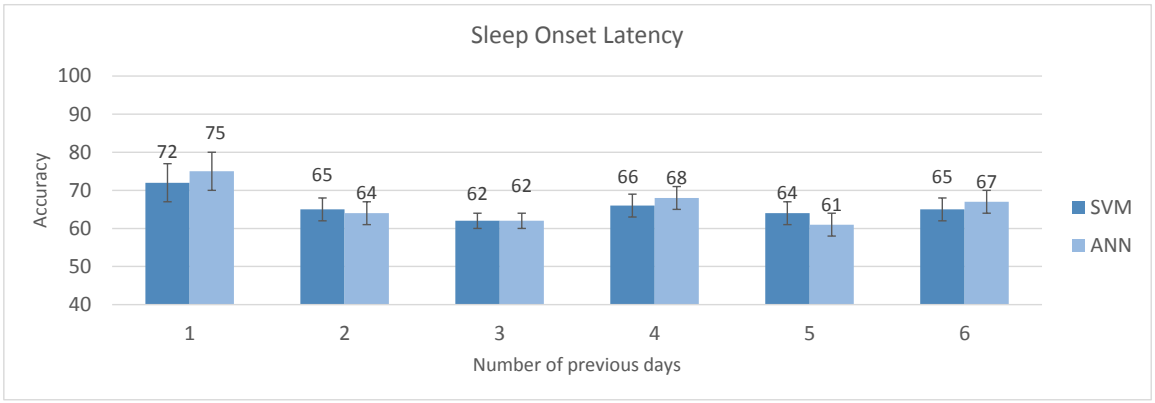

(b)

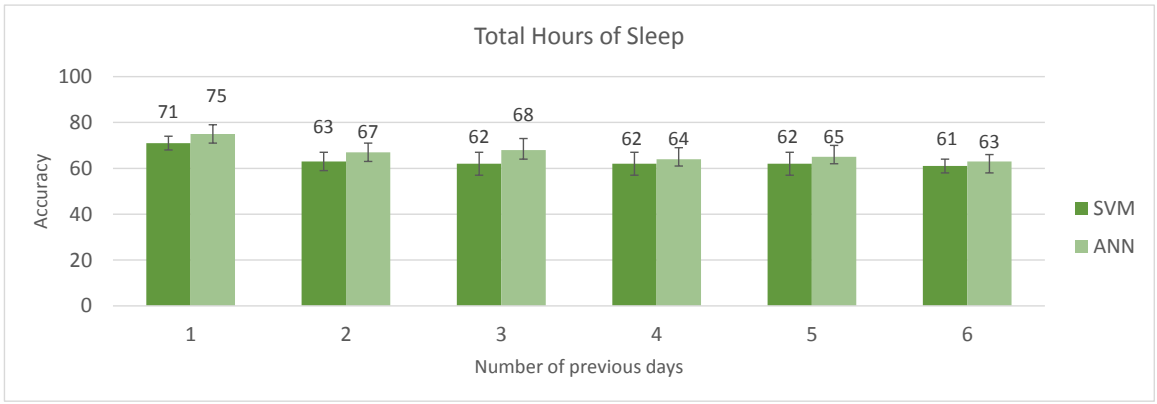

(c)

Figure 4.9: Evaluation of predictive models for Sleep quality metrics as (a) Restlessness , (b) Total Hours of Sleep ,and (c) Sleep Onset Latency using previous challenging daytime behaviors data.

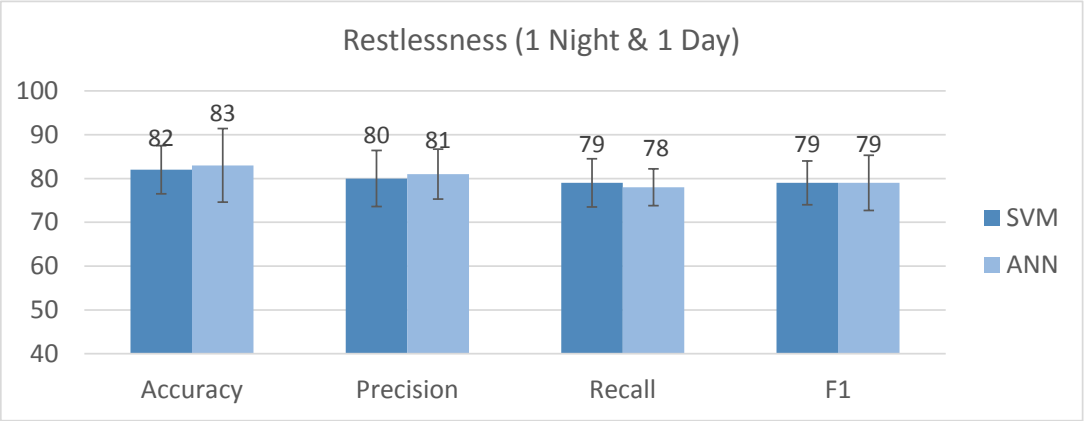

(a)

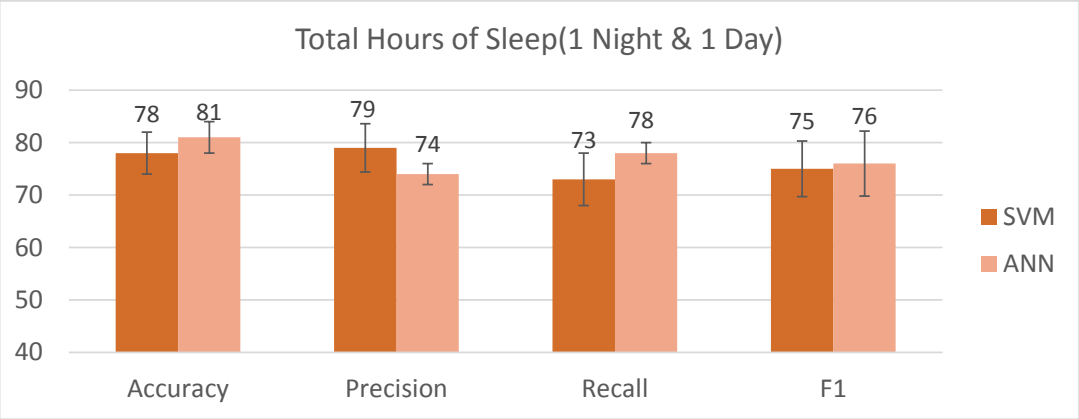

(b)

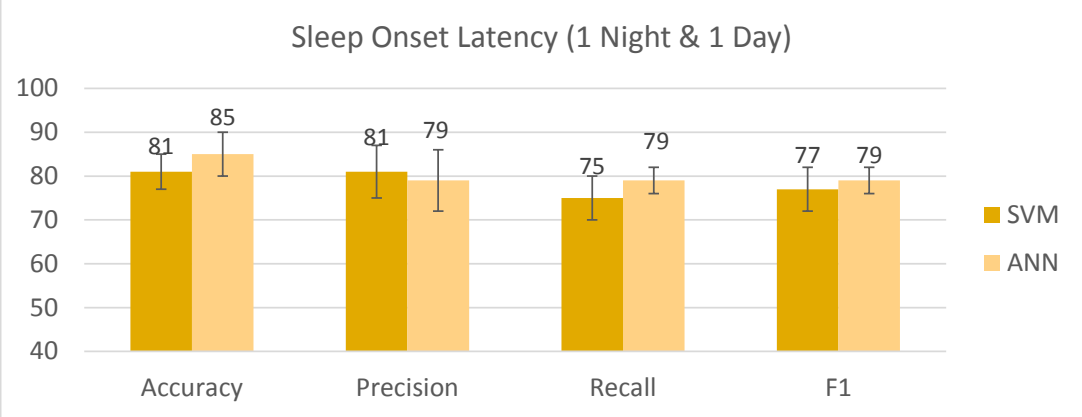

(c)

Figure 4.10: Evaluation of predictive models for Sleep Quality (a) Restlessness, (b) Total hours of Sleep , and (c) Sleep Onset Latency using previous day and night features.

4.4.4 Comparison between Classifiers

As it is shown in Fig. 4.10, all four metrics are having better performances in ANN compared to SVM in all three models. Comparing the F1 scores indicate that also ANN is better classifying the measurements using daytime and night-time features for total hours of sleep and sleep onset latency. Only for restlessness, both classifiers are having the same average with different ranges for F1 score. The exact reason for this improvement is difficult to pin-point and could simply be due to the parameter selection or the non-linear nature of data or even both. They each have their own advantages and disadvantages for a particular set of data and their mutual comparison could show us the best way forward, which essentially depends on the nature of data.

While we achieve high overall performances through both SVM and ANN for both hypotheses, the exact solution to what is the relationship between sleep quality and daytime behaviors in individuals with ASD, is still not fixed and based on different sets of data from various subjects, these results may change. However, the takeaway message from our system and models is that using smart bed system make it possible and simple to collect sleep quality measurements semi-automatically and help clinicians and paraeducators for predicting child's behaviors based on the these measurements.

4.5 Summary

In this chapter, we propose an objective and unobtrusive approach to measure sleep quality and use this measure to find the relationship between sleep quality and challenging daytime behaviors in children with ASD. Specifically, we use a bed-based monitoring system embedded in child's sleep environment without any sensors or wires connected to subject's body. From the smart bed, we automatically extract a sleep feature named as restlessness. The restlessness feature along with other sleep parameters over a period of 1-8 nights is used by machine learning engines (SVM and ANN) to predict daytime behaviors on the

following day. Additionally, we use previous night sleep quality and daytime behaviors to predict the following night sleep quality. The findings show that using the proposed sleep feature (restlessness) improves the prediction performance and make it possible for paraeducators/parents to automatically obtain the sleep quality of the child without the need for manual night-time checks every 15 or 30 minutes. Additionally, we study the classification performance using daytime behaviors and nigh-time sleep quality as input features to predict sleep quality for the following night/nights. Since each child with ASD is unique, the SVM and ANN algorithms are custom tuned to each individual to obtain the best predictive performance.

Chapter 5

Motion Correction in Heat-induced PRFS MR-Thermometry

In the previous chapters, we have focused on inferencing with motion artifact in bed based BCG signals. In this chapter, we study how to deal with temperature errors in PRFS MR thermometry caused by motion artifacts. Two robust model based and non-model based techniques are proposed and presented to improve performance of the temperature estimation in the presence of motion. Parts of this chapter have been published in [24] [1].

5.1 Introduction

Minimally invasive thermal therapies are in clinical use for image-guided treatment of cancer and other disease [97]. Thermal ablation involves tissue heating to temperatures in excess of 55 °C, resulting in cell death via coagulative necrosis, and is increasingly being used for treatment of tumors in the liver, lung, and other organs [98]. Mild hyperthermia, moderate heating in the range $39 \leq T \leq 45$ °C for 20-60 mins, has been shown to be a potent radio- and chemo-sensitizer [99]. Reliable temperature mapping is critical for measuring tissue heating

[1] A. Alivar, P. Faridi, P. Prakash, and B. Natarajan, "An enhanced hybrid mri thermometry technique for monitoring microwave thermal therapy," in *Medical Imaging 2019: Image-Guided Procedures, Robotic Interventions, and Modeling*, vol. 10951, p. 109512P, International Society for Optics and Photonics, 2019

during thermal therapies. Systems and devices employing a range of energy modalities have been developed for thermal therapies including radiofrequency current, microwaves, lasers, and ultrasound. Real-time quantitative estimations of spatial temperature profiles during thermal therapies enable monitoring and feedback-controlled energy-delivery with the objective of ensuring adequate thermal dose delivery to targeted tissues, while precluding thermal damage to adjacent critical structures [100].

MRI offers the ability to measure temperature noninvasively and visualize tissue during heating procedure. The goal of MR image-guided thermal therapy is to use real-time temperature mapping to monitor thermal profiles during therapy deliveries.

The PRFS has been widely used for measuring spatio-temporal temperature profiles during thermal therapy with MRI [16, 101–103]. Simplicity, real-time capability, high spatial resolution, and tissue independency are some of the key strengths of the PRFS technique compared to other MRI thermometry approaches [16]. The PRFS method estimates temperature from the phase difference between images acquired before and during treatment [101] by:

$$\Delta T = \frac{\phi(T) - \phi(T_0)}{\gamma \alpha (TE) B_0} \tag{5.1}$$

where $\phi(T)$ is the phase in the current image, $\phi(T_0)$ is the phase of a reference (baseline) image at a known temperature, γ is the gyromagnetic ratio, α is the PRF change coefficient, $B0$ is the magnetic field strength, and TE is the echo time. However, one of the main problems with the PRFS method is its sensitivity to inter-frame motions, nonlinear magnetic field changes induced by motion, tissue susceptibility changes, and magnetic field drifts. Each of these may result in non-temperature dependent phase changes and hence incorrect estimation of heat-induced temperature change. To address these challenges, several methods have been proposed to compensate and reduce temperature estimation errors [104] such as reference-less [17, 105, 106], multi-baseline [18], and hybrid [19] methods. In the general PRFS method, also referred to as conventional baseline subtraction, a phase image during heating is subtracted from a phase image prior to heating (i.e. a baseline image). Due to its

sensitivity to between scan motions, multi-baseline method has been proposed. In the multi-baseline method, multiple baseline images are taken before treatment, thereby providing a library of information of moving organs at various stages of the cardiac or respiratory cycle within a learning phase. Then, during heating, for each acquired phase image, subtraction is performed after determining the best fit baseline image from the pre-heating library [19]. It would be problematic when there are nonrigid motions, which are not included in the library anymore. To address this problem, the reference-less method was proposed. This technique determines the pre-treatment phase in a heated area based on the phase of the area surrounding the hot spot by fitting a polynomial distribution. In this case, the phase errors caused by tissue motion and perturbations in the external magnetic fields are minimized compared to the multi-baseline method. However, the polynomial fitting approach may be limited in regions with complex phase variations such as interfaces between different tissues. There are more limitations in this technique including, the assumption of a small zone of heating and the requirement of prior knowledge of the focal spot location. The hybrid method, which is the most comprehensive technique, exploits the strengths of the reference-less and multi-baseline techniques, and employs a mathematical-physical image model describing three different sources of phase changes: background anatomical phase, spatial phase changes, and heat-induced phase shift, to estimate temperature more robustly. Even though the hybrid method may be the most appropriate among currently available methods, based on its accuracy and computational load, there remain some limitations. The algorithm is based on the assumption of focal heating in an image, such that only a small subset of pixels in the image are heated i.e. small localization of hot spot. When the hot spot becomes diffuse, the hybrid method wold underestimate temperature error because of the spatial phase regularization assumption. The ability to extract the motion from the original signal without considering any model for the observations and it would have less computational complexity than hybrid method, and provides In this chapter, we propose two novel algorithm in temperature correction for MRI thermometry. The first study is to robustly correct MRI estimates of temperature variations during heating with applicators having diffuse patterns in the presence of motion. The second proposed approach is a

non-model based motion correction in temperature estimation using robust principal component analysis. The details of both proposed techniques are provided in the following sections.

5.2 Enhanced Hybrid Model

While the hybrid method has demonstrated the best performance, it assumes focal heating, which may be valid when using energy modalities such as high intensity focused ultrasound (HIFU)(as in Fig. 5.1), but does not hold for heating using diffuse sources such as needle- and catheter-based microwave applicators (as in Fig. 5.2), which have a relatively broad radiation pattern, and are widely used for thermal ablation of tumors in the liver, kidney, and lung. In this study, we enhance the original hybrid method by using the sparsity of heat-induced phase shift based on the wavelet transform, and assess its suitability for monitoring temperature profiles with a 2.45 GHz microwave applicator.

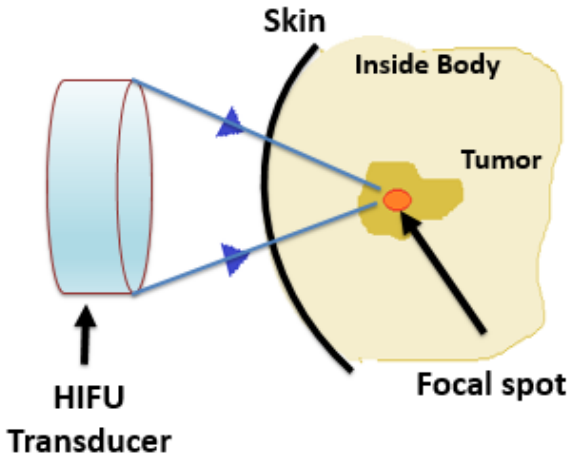

Figure 5.1: Focused hot spot from a HIFU transducer.

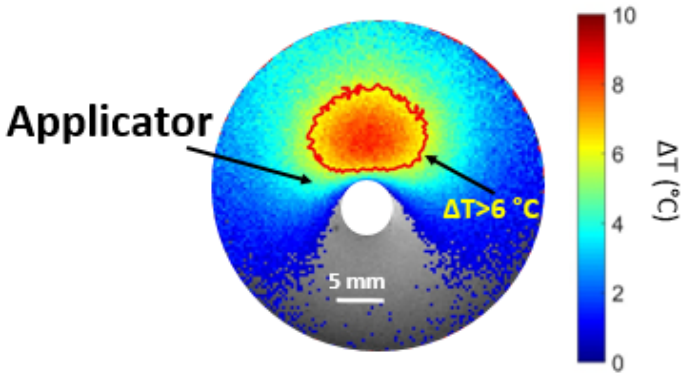

Figure 5.2: Temperature profile from 2.45 GHz directional microwave applicator in a tissue mimicking phantom.

5.2.1 Proposed Method

The proposed method estimates temperature changes by fitting a constrained image model to the acquired data[24]. This model comprises a weighted combination of baseline images acquired prior to heating, a polynomial phase shift to model frequency drift and other bulk phase shifts unrelated to heating, and a spatially-sparse heating-induced phase shift [19, 107]. These unwanted sources can either capture phase variations due to motions such as respiration and cardiac cycles or main field drifts. Smooth magnetic field shifts can be modeled as a linear combination of some basis functions by fitting a set of smooth, low-order polynomial functions to the surrounding phase (Ac). On the other hand, a library of baseline images (x_b) , which are acquired prior to heating, can be used to model the various stages of the respiratory cycle. The signal model for voxel j during treatment is defined as:

$$y_j = (\sum_{b=1}^{N_b} x_{b,j} w_b) e^{i(Ac_j + \theta_j) - \alpha_j} + \epsilon_j \tag{5.2}$$

where, y_j is one acquired data sample, N_b is the number of complex baseline images x_b ac-

quired prior to heating, $\boldsymbol{w_b}$ are baseline images weights, Ac_j is the polynomial fitted image including A as a matrix of polynomial basis functions, and c as polynomial coefficients, θ_j is heat-induced phase variation, α_j is heat-induced magnitude changes, and ϵ_j is i.i.d complex Gaussian noise samples.

In this study, we propose a hybrid model that considers the sparsity of $\boldsymbol{\theta}$ by transforming the correlated data into the wavelet domain [108]. For this, we transform the $\boldsymbol{\theta}$ values into the wavelet domain with wavelet coefficients $\boldsymbol{r}$ as in $\boldsymbol{\theta} = \boldsymbol{\psi r}$. Once the wavelet transform basis is generated based on orthogonal filters, the coefficients r can be obtained that well represent the sparsity in wavelet domain. To estimate $\boldsymbol{\theta}$, the proposed constrained minimization problem is:

$$\begin{aligned} minimize \quad & \frac{1}{2}\sum_{j=1}^{N_s}\left|y_j - (\sum_{b=1}^{N_b} x_{b,j}w_b)e^{i(Ac_j+\theta_j)-\alpha_j}\right|^2 + \lambda||\ \boldsymbol{r}\ ||_1 \quad , \\ & \boldsymbol{\theta} = \boldsymbol{\psi r} \\ Subject \quad to \quad & \\ & \boldsymbol{\alpha} \geq 0, \quad \boldsymbol{\theta} \leq 0 \\ & \sum_{b=1}^{N_b} w_b = 1, \quad \boldsymbol{w} \geq 0 \end{aligned} \tag{5.3}$$

where, the first term in the objective function is proportional to the negative log-likelihood, λ is a regularization parameter that controls the sparsity of r in $\lambda||\ \boldsymbol{r}\ ||_1$. Here, the ℓ_1 penalty on r is used to emphasize sparse estimates, ψ is wavelet basis transform matrix, and r are wavelet coefficients. In our analysis, the sparsifying basis ψ is defined using the Haar mother wavelet. This problem is solved by alternately updating each of the model parameters $\boldsymbol{w}, \boldsymbol{c}, \boldsymbol{\theta}, \boldsymbol{\alpha}$ while holding the other three; given initial of $\boldsymbol{w}, \boldsymbol{c}, \boldsymbol{\theta}, \boldsymbol{\alpha}$:

1: **repeat**

2: Update $\boldsymbol{w}$: By fixing $\boldsymbol{c}, \boldsymbol{\theta}, \boldsymbol{\alpha}$, a quadratic programming problem need to be solved to find optimal $\boldsymbol{w}$,

$$\begin{aligned} minimize \quad & \frac{1}{2}\sum_{j=1}^{N_s}\left|y_j e^{-i(Ac_j+\theta_j)-\alpha_j} - \sum_{b=1}^{N_b} x_{b,j}w_b\right|^2 \\ Subject \quad to & \\ & \sum_{b=1}^{N_b} w_b = 1 \\ & \boldsymbol{w} \geq 0 \end{aligned} \tag{5.4}$$

3: Update $\boldsymbol{\theta}$: By solving the nonlinear convex problem as:

$$\begin{aligned} minimize \quad & \frac{1}{2}\sum_{j=1}^{N_s}\left|y_j - (\sum_{b=1}^{N_b} x_{b,j}w_b)e^{i(Ac_j+\theta_j)-\alpha_j}\right|^2 + \lambda||\ \boldsymbol{r}\ ||_1 \quad , \\ Subject \quad to & \\ & \boldsymbol{\theta} \leq 0 \end{aligned} \tag{5.5}$$

The same procedure is done for updating $\boldsymbol{\alpha}$ and $\boldsymbol{c}$.

4: Until stopping criterion met.

The convergence or stopping criterion was chosen based on relative error in the objective function of less than 0.1% between consecutive iterations. The initial values for all parameters are solved using the same method used in the original hybrid approach and a detailed description of this initialization procedure is given in [19]. The final corrected temperature change can be obtained from changes in $\boldsymbol{\theta}$ using PRFS method defined as in equation (5.1) in which, γ is the proton gyro-magnetic ratio; and $\alpha = -0.01 ppm/^{\circ}C$ is the PRF change

coefficient.

5.3 Non-model Based Temperature Correction using RPCA

The objective here is to formulate our motion correction problem as the robust principal component analysis (RPCA) problem without considering any model for our observations, in which one aims to extract one or multiple structured signals from number of noisy observations [109–111]. Assumming that the image intensity is highly correlated in the time dimension, low-rank matrix and sparse noise can be recovered using compressive sensing (CS) based signal recovery algorithm. We consider the idealized robust PCA problem of recovering a low rank matrix L from corrupted observations $M = L + S$. The matrix S is assumed to be sparsely supported which affect only a fraction of the entries. Basically, robust PCA is the joint problem of low-rank matrix recovery in the presence of sparse corruption [112–115]. Robust PCA enhances the performance and improves the robustness of classical PCA against sparse outliers, which are captures in the sparse component S. This methodology has been successfully used and applied to different applications such as computer vision [112], image reconstruction in 4DCT [116], and image registeration and alignment [117]. Gao et al.[118] has worked on dynamic MRI to reconstruct undersampled cardiac data sets and separate motion affected data from background among frames.

Here, we wish to recover a clean temperature profile map as the low rank matrix L from sparsely corrupted observation M. The background component corresponds to the highly correlated information among frames that is slowly changing over time. Thus, each clean temperature temporal image is considered as low rank matrix and the motion artifacts are assumed to be sparse since substantial differences between consecutive frames are limited to small number of voxels.

Theory:

The main robust PCA approach aims to decompose matrix M as a superposition of a low rank matrix L (few non-zero singular values) and a sparse matrix S (few non-zero entries). L is formed by rearranging the spatiotemporal data into a matrix whose row diemnsion spans space and column dimension spans time. This problem can be solved by exploiting the low-rankness of M by the following formulation [109]:

$$\begin{aligned} \underset{L,S}{minimize} \quad & G_1(L) + \lambda G_2(S) \\ Subject \quad to \quad & M = L + S \end{aligned} \tag{5.6}$$

where G_1 and G_2 are penalties for low rank and sparsity promotion, respectively. λ is a tuning parameter to balance the contribution of G_1 term relative to G_2 term. Choosing $G_1(L) = || \ L \ ||_*$ as the nuclear norm or sum of singular values of matrix L and $G_2(S) = || \ S \ ||_1$ as the ℓ_1-norm or sum of absolute values of the entries of S, this problem can be solved with appropriate value of λ. Another version of equation (5.6) is the unconstrained formulation using regularization as follows:

$$\underset{L,S}{minimize} \quad \lambda_L \ || \ L \ ||_* + \lambda_S \ || \ S \ ||_1 + \frac{1}{2} || \ M - L - S \ ||_F{}^2 \tag{5.7}$$

where, the parameters λ_L and λ_S trade off data consistency versus the complexity of the solution given by the sum of two norm terms.

5.3.1 Proposed Method

The proposed method estimates true temperature from a non-model based RPCA decomposition approach. To apply RPCA to temperature map images, the time-series of images are converted to a matrix M in which each column is a temporal frame. The application

of using RPCA decomposition will have a matrix L as a background component and clean temperature image and a matrix S as the noise and corruption. In order to apply equation (5.7) to our problem, we solve the optimization problem using iterative soft thresholding of the singular values of matrices L and S. We can define the proximity operator or shrinkage operator for soft thresholding [109] as:

$$\Lambda_\lambda(x) = \frac{x}{\mid x \mid} max(\mid x \mid -\lambda, 0) \tag{5.8}$$

where x is a complex and λ is a real valued numbers. Then, singular value thresholding (SVT) operator is defined based on $SVT_\lambda(M) = U\Lambda_\lambda(\Sigma)V^H$ in which $M = U\Sigma V^H$ as the singular value decomposition of M. The entire procedure is summarized in Fig. 5.3. This approach is a combination os singular value thresholding that is used for matrix completion [119] and iterative soft thresholding as it is used for sparse reconstruction [120]. At each k iteration, we need to apply singular value thresholding to $M_{k-1} - S_{k-1}$ to find the value of L_k. Then, the soft thresholding is applied to $M_{k-1} - L_{k-1}$ to update S_k values. By having updated matrices L_k and S_k, we can obtain the new M_k. This algorithm terminates when the relative error in the solution is less than 10^{-5}. The relative error is defined as:

$$|| \ L_k + S_k - (L_{k-1} - S_{k-1}) \ ||_2 \leq 10^{-5} || \ L_{k-1} - S_{k-1} \ ||_2 \tag{5.9}$$

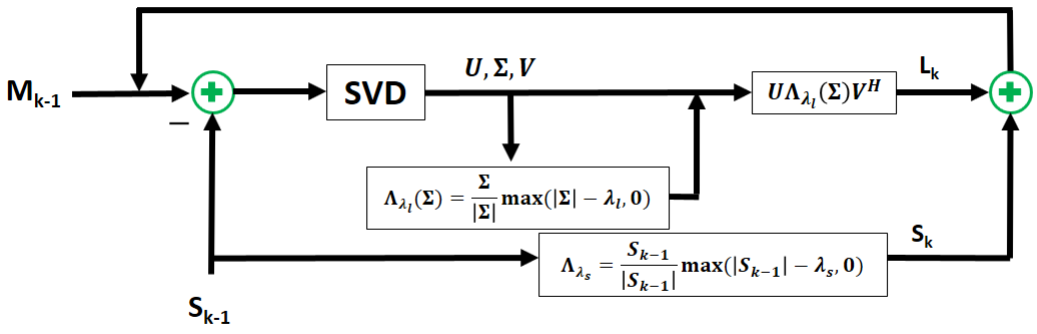

Figure 5.3: Sequence of operations for the k^{th} iteration of the RPCA algorithm.

5.4 Experimental Validation and Results in Tissue-mimicking Phantom

The proposed methods are evaluated for temperature estimation during microwave heating of a tissue-mimicking phantom with a 2.45 GHz directional microwave antenna integrated with 14.1 T high-field MRI (Bruker Avance III) (see Fig. 5.4). For validation, we use a phantom experiment in which temperature measurements from three fiber-optic probes (T1, T2, and T3 as a gold standard) were compared to MR thermometry as illustrated in Fig. 5.5b with antenna power of 10W over 5 min microwave exposure [121]. MR data were acquired with a FLASH sequence with parameters: $TR/TE = 30.15/4.0$ ms, $FOV = 30$ mm, image size $= 128 \times 128$, flip angle $= 15$ °, slice thickness $= 1$ mm, three axial slices, scanning duration $= 3.87$ s and PRF temperature coefficient $\alpha = -0.01 ppm/^{\circ}C$. Two 8×8 regions of interest (ROI) close to temperature probes T1 and T3 are chosen for further analysis and comparison to temperature measurements from the fiber optic sensors (see Fig. 5.5b).

Figure 5.4: Photograph of a vertical MRI scanner.

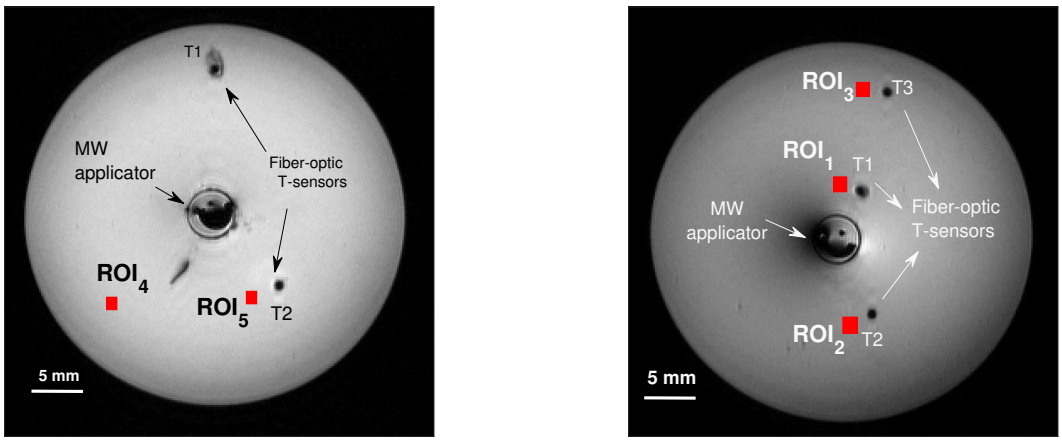

(a) (b)

Figure 5.5: T1-RARE magnitude images illustrating the water-cooled microwave applicator positioned within a phantom, and (a) the position of 2 fiber optics, (b) the position of 3 fiber optic temperature sensors used for validation of MRI thermometry.

Additionally, we evaluated the proposed method's robustness to motion in another phantom experiment with two fiber optic sensors for 15 min and same parameters as the previous experiment (see Fig. 5.5a). In this additional heating experiment, a 5 min scan was conducted without heating and cooling followed by 5 min only cool down period, and then 20W power was applied for another 5 min. During the whole 15 min experiment, motion was introduced by displacing the phantom within the imaging coil at specific times. This experiment was done for further investigating how is the quality of temperature estimation without heating in the presence of motion.

5.4.1 Enhanced Hybrid Model

The proposed method is compared to the original hybrid method and conventional PRFS (phase subtraction). Temperatures estimated by the two algorithms (original hybrid method and our proposed one) and the fiber-optic temperature sensors at two positions in the phantom, (i) 1.6 mm away (ROI_1) and the other (ii) 9 mm away from the hot spot center (ROI_3),

are plotted in Fig. 5.6. Here the root-mean-square-error (RMSE) of the temperature within ROI are calculated for quantitative comparison. The results illustrate that the proposed algorithm is able to better follow the temperature change in fiber-optic compared to the original hybrid method in both ROIs. The proposed method can estimate temperature with considerably smaller RMSE than the original hybrid method when using the same choice of $\lambda = 0.001$ in two different ROIs.

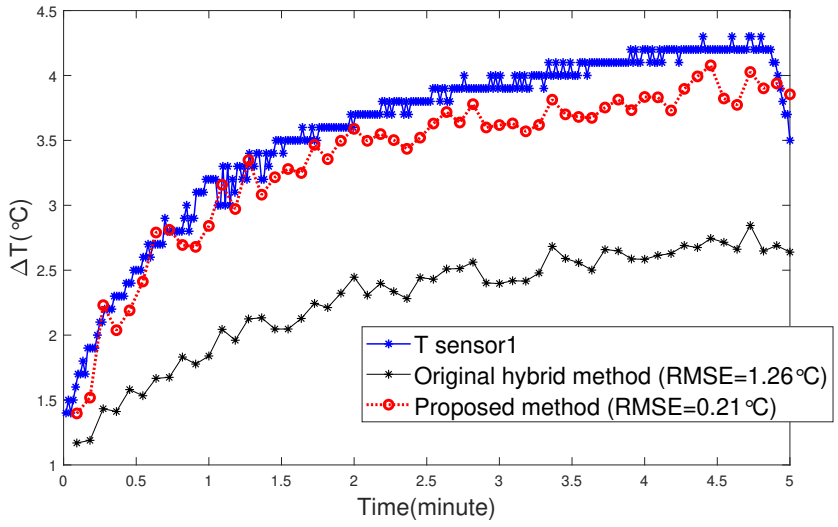

(a)

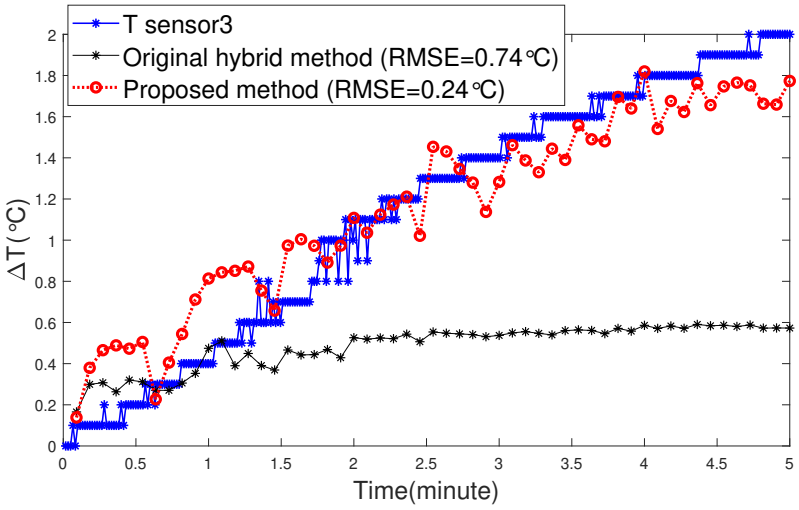

(b)

Figure 5.6: Temperature change measured at two location (a)ROI_1 and (b)ROI_3 with input power of 10 W.

To evaluate robustness to motion, one 8×8 ROI (named as ROI_4)(see Fig. 5.5a) is selected from the second MRI experiment for analysis since this was the region where greatest motion was observed. As it is illustrated in Fig. 5.7, the blue trace, using the conventional PRFS method shows a sudden rise in temperature around 1.7 minute (the pink rectangular box); the red plot, shows the estimated temperature using the proposed method. The estimated temperature change is approximately 0.1°C with the enhanced method, and the error due to motion is reduced by 0.9°C, compared to the original hybrid method. Therefore, our proposed estimated temperature is covering for both the motion and also the other external noises which caused temperature errors.

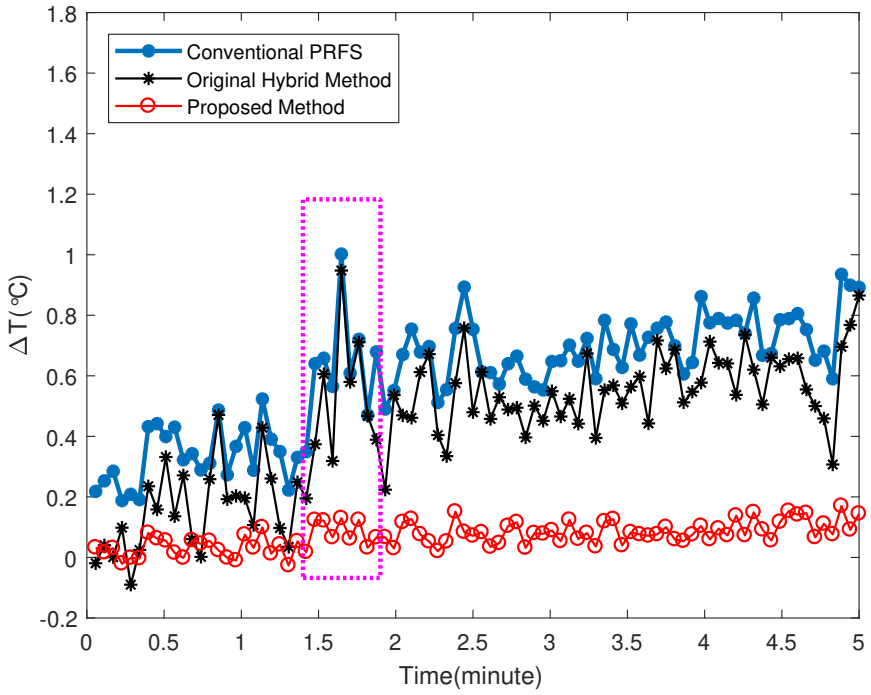

Figure 5.7: Temperature change in ROI_4 with input power of 0 W.

5.4.2 RPCA Method

In this subsection, we first analyze the efficacy of RPCA method to recover error-free temperature changes from motion artifacted one using the phantom experiment without motion

(Fig. 5.5b). To apply RPCA to MR temperature images, the time series of images are converted to a matrix in which each column presents a temporal frame. We validate the proposed method in three different regions close to the three fiber optic sensors. The method will produce a matrix L which is the background component free of motion and sparse noises. Since in this experiment we don't have any sparse noise or motion, we generate a sparse matrix whose support is chosen uniformly at random, and non zero entries are independent and uniformly distributed. This sparse matrix S is added to our observed temperature matrix M to produce an artificial motion corrupted temperature image as $M_{corrupted} = L+S$. We apply the proposed approach RPCA to this corrupted matrix to recover the original motion-free and low-rank matrix. The regularization parameters λ_L and λ_S are selected by comparing the performance for a range of values and the ones with the lowest RMSE are $\lambda_L = 0.005$ and $\lambda_S = 0.003$ that are employed. The results are presented in Fig. 5.8, 5.9, and 5.10. Our findings indicate that the estimated temperature changes are approximately matching with the temperatures from fiber optics in all three regions and we observe that the proposed algorithm is successful in recovering the low-rank (M or motion-free).

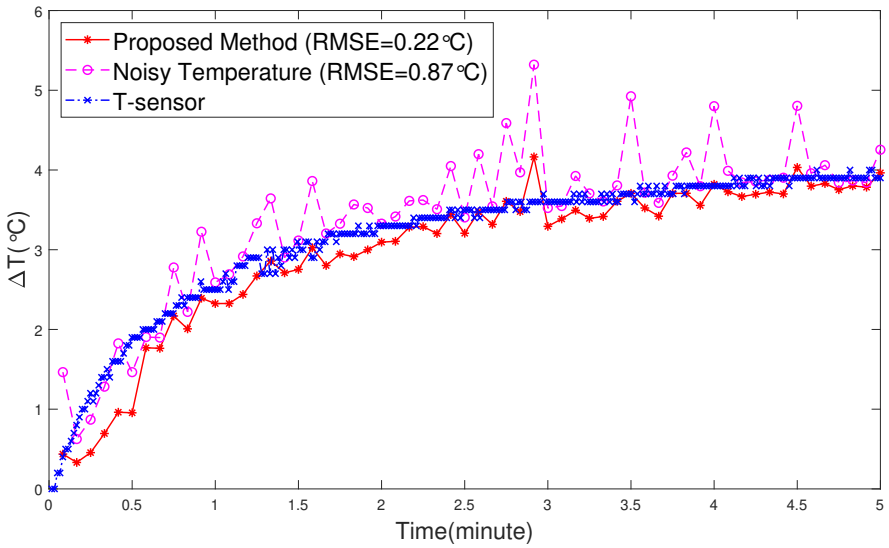

Figure 5.8: Temperature change in ROI_1 with input power of 10W.

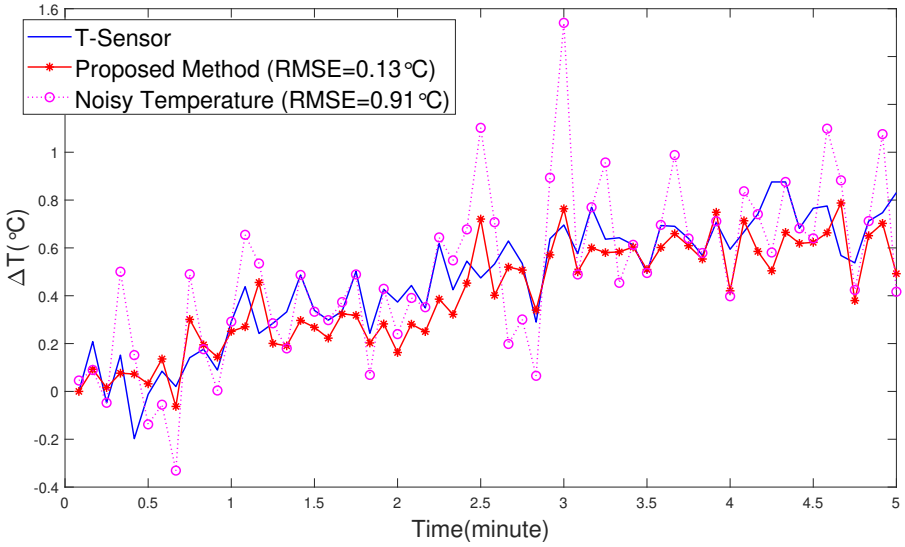

Figure 5.9: Temperature change in ROI_2 with input power of 10W.

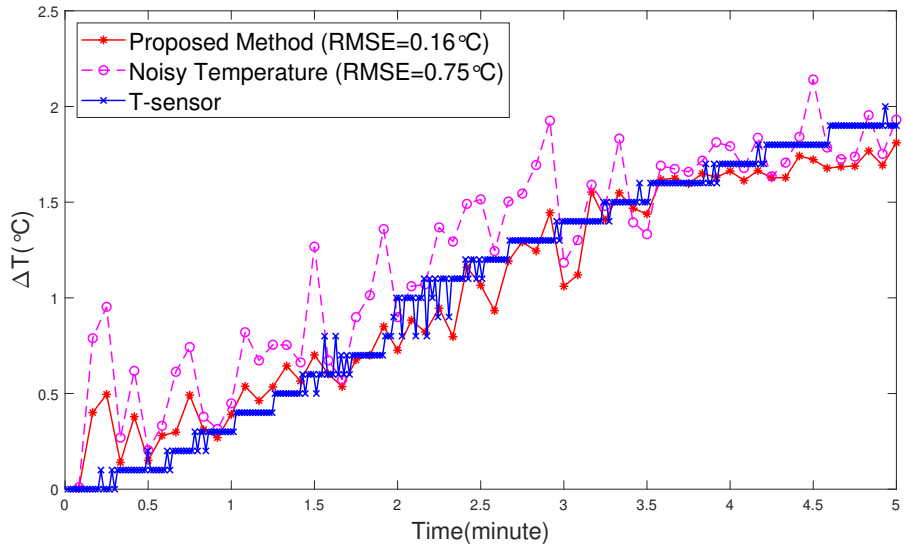

Figure 5.10: Temperature change in ROI_3 with input power of 10W.

To demonstrate the efficacy of the algorithm in minimizing the rank and sparsity of both unknown matrices, we generate the artificial sparse matrix with various number of non-zero entries. The results are demonstrated in Table 5.1 for the three regions of interest in three locations from hotspot. The proportion of nonzero elements are increased from 10%-60% and the number of iterations and reported simulation times are illustrated for each ROI.

We observe that the proposed algorithm is successful in recovering the low-rank matrix even when 60% of its entries are corrupted in all three regions. However, in ROI_1, since this is the region near the hotspot with higher temperature variations compared to other regions, the error in recovering the low-rank matrix takes more time for converging.

Table 5.1: Algorithm evaluation by growing in proportion to the number of nonzero entries of sparse matrix.

ROI	density	rank(L_0)	rank($\hat{L}$)	$\| S_0 \|_0$	$\| \hat{S} \|_0$	$iterations$	time(s)
ROI_1	0.1	26	24	152	176	251	12.3
	0.3	26	26	401	422	472	22.3
	0.6	26	21	700	742	980	85.7
ROI_2	0.1	23	22	138	144	187	2.3
	0.3	23	23	245	260	292	7.9
	0.6	23	22	616	670	681	16.3
ROI_3	0.1	27	26	146	158	150	2.8
	0.3	27	25	264	277	320	6.4
	0.6	27	22	663	672	496	18.5

5.4.3 Methods Comparison

There are a few factors that differentiate the two proposed algorithms. The enhanced hybrid approach solves many problems of reference-less, multi-baseline, and hybrid models. However, a certain number of user interactions are required to select the regularization parameter, polynomial order, wavelet transform, and baseline library size. Also, it is computationally complicated, which prevents its real-time application similar to the original hybrid algorithm [122]. The RPCA algorithm has less computational complexity and it only requires SVD calculation for each iteration. Additionally, it is only dependent on two user defined parameters which are the two regularization parameters for soft thresholding. Computational time

for both methods are approximately the same.

5.5 Summary

In this chapter, we studied how to deal with motion artifact in temperature change estimation in MR thermometry. Two different approaches were proposed. Firstly, we presented an enhanced hybrid MRI thermometry technique suitable for monitoring temperature profiles during microwave thermal therapy with diffuse hot spot or sources. Errors in thermometry are reduced by using a modified model-based phase correction procedure based on correlation structure of heat-induced phase shifts. Approximate sparsity is obtained by transforming the correlated phase variations into wavelet domain. Second method is a non model robust principal component analysis algorithm which aims to recover low-rank matrix from sparse noise in which low-rank matrix is a true temperature image and the motions are considered as sparse noise that happen only in some entries. Both approaches reduced errors duw to motion arifacts for estimating temperature profiles in phantom experiments.

Chapter 6

Conclusion and Future Directions

6.1 Summary

In this dissertation, we investigate inferencing strategies with motion artifacts in two biomedical signal and image modalities as 1D time series and 2D signal including ballistocardiogram (BCG) and proton resonance frequency shift (PRFS) MR-thermometry. Motion artifact has always been a significant concern in biomedical devices and technologies and there has been different software and hardware technologies to correct or reduce the impacts of these artifacts. Motivated by these factors, we studied the usefulness of identified motion artifacts from these two sensing modalities with different applications. In this regard, we summarize the contributions of this dissertation in two categories of 1D and 2D signals as follows:

1D signal or Bed-based BCG Signal:

- For the first case study, we proposed a motion detection algorithm to quantify restlessness during sleep via an unobtrusive contactless electromechanical film (EMFi) based BCG sensor integrated into a smart bed system. Extensive analysis of EMFi signals reveals that in time domain, variance measure and in frequency domain, out-of-band energy feature, are the two most discriminative features between clean and motion corrupted BCG data. Neyman-Pearson decision rule is formulated based on these two features. Alternately, a sequential decision rule is designed in which successive data

frames are compared to upper and lower thresholds to achieve a desired probability of detection and false alarm. The decisions from both approaches are shown to be reliable and efficient in distinguishing motion-corrupted and clean signals with high probabilities of detection of 95% and 96%.

- Additionally, the duration of motion corrupted frames can be used to infer the sleep and restlessness state of the subject. Any continued movements longer than one minute are typically classified as "restlessness" and all other periods during the night are classified as sleep. Using our proposed motion detection approach from Chapter 3, we segment restlessness and sleep phases of the subject and validate it using manual observation based ground truth data. 94% and 95.2% accuracies based on NP and sequential tests in distinguishing the child's sleep and wakefulness state demonstrate the effectiveness of the proposed motion detection algorithm.

- Using our validated bed system, we determined periods of motion/restlessness based on a bed-based BCG sensor suite and use them as one of the main sleep quality features along with other metrics. This study describes an effort in collaboration with Heartspring located in Wichita, KS to develop and evaluate a toolset for monitoring and assessing the well-being of children with ASD. We investigate the utility of our bed-based unobtrusive system for collecting sleep metrics and develop predictive models to find the relationship between sleep quality and daytime behavioral data. Furthermore, we evaluate these metrics for data gathered from a group of children with ASD at Heartspring. Here, we analyze over 200 nights of sleep measurements from two individuals with severe ASD. We develop predictive models for daytime behavioral changes using night time sleep quality variations obtained from our smart bed system. Additionally, we study the influence of history of 1-8 nights sleep on challenging daytime behaviors.The reverse problem is also studied which is classification models for sleep quality using daytime behaviors over 1-8 previous days.

- Following motion artifact detection algorithms, we proposed two motion artifact re-

construction techniques using autoregressive model-based tracking ad Wiener smoother based estimation. Each motion corrupted frame can be reconstructed by an approach that relies on a parametric model of the BCG signal. Exploiting the fact that the underlying BCG parameters (J-peak-to-J-peak interval, J-peak-to-K-peak amplitude, and the most significant frequency component) change slowly and are correlated across time. The high average coverage of 84% with over 90% precision for the estimated B-B intervals are achieved on recordings for 19 h of sleep from three subjects. Our novel motion detection and removal methods demonstrate the feasibility of using bed-based BCG signals for providing a reliable unobtrusive way to estimate the B-B interval in the presence of motion.

2D signal or Temperature images during MRI:

- For the second case study, we propose an enhanced hybrid model based method to correct temperature change errors caused by motion artifact in PRFS MR-thermometry. We present an enhanced hybrid method suitable for MRI thermometry in the presence of motion during microwave thermal therapy for heating using diffuse sources such as needle- and catheter-based microwave applicators. The presented model-based method uses the sparsity of wavelet coefficients of the phase shift based on the fact that heat-induced phase shifts exhibit a correlation structure due to smoothness. The presented enhanced hybrid method is compared to the previously presented hybrid and conventional PRFS methods for temperature estimation during microwave heating of a tissue-mimicking phantom. Experimental results demonstrate that the proposed method estimates microwave heating-induced temperature changes within 0.3-0.5 °C (mean error of 5.9 % over 5 min of heating) of fiber-optic temperature sensors, compared to 1.5 °C (mean error of 36.3% over 5 min of heating) with the hybrid technique.

- Furthermore, we propose a new non-model based temperature estimation for PRFS MR-thermometry using robust principal component analysis (RPCA). Since the temperature profile images have high correlation across time, we can consider each temporal frame as a low-rank matrix. When motion occurs with each frame, the motion can be

considered as sparse noise that has a limited number of non-zero elements. Thus, the algorithm enforces joint low-rank and sparsity to exploit temporal correlations and separate the background components without the need of modeling. The results illustrate that the proposed approach can well recover low-rank and sparse temperature images in the presence of motion. Both real-world motion corrupted temperature images and artificially corrupted images are tested and validated the algorithm can recover the low-rank matrix from sparse motion artifacts in PRFS MR-themrometry.

6.2 Future Directions

Based on the research accomplished in this dissertation, some possible future research directions are highlighted below:

- Chapter 3 of this dissertation develops a BCG motion reconstruction system followed by motion artifact detection method. In this method, we assumed that the subjects are not impacted by any kind of cardiac issues such as arrythmia. Cardiac arrythmias are conditions where individuals have irregular cardiac rhythms. Therefore, it would also be of particular interest to consider motion artifact detection and reconstruction in BCG signals considering subjects having arrythmia or other cardiac abnormalities.

- In this dissertation, for BCG signal analysis purposes, we first preprocessed the signal and removed the low frequency contents for further analysis. However, BCG signal analysis can be extended by considering respiration signal which can be used to detect pulmonary disorders such as sleep apnea.

- As we mentioned in Chapter 4, BCG as a non-intrusive methodology can help to monitor sleep quality and cardiac activity in children with ASD. Another common complication in individuals with ASD is epilepsy and seizures. Developing an unobtrusive system to predict seizures in this population using cardiac activity and/or heart rate variability from bed-based BCG signals can be pursued in the future.

- There are many other features that can help to improve the prediction model for challenging daytime behaviors in children with ASD including heartrate variability, seizure activities, age, gender, and level of autism. However, acquiring some of these information unobtrusively and objectively is so important. Therefore, it would be complementary to our predictive models to consider heart rate variability and seizure activities extracted from bed-based BCG data as sleep features.

- Chapter 5 develops a motion correction in PRFS MR-thermometry using (L+S) decomposition algorithm. We tested and validated the method on experiments with phantoms. It would be complementary to try this algorithm on in-vivo data with periodic motions like breathing and evaluate the proposed approach. Also, we consider the low-rank and sparsity conditions in time domain. This analysis can be extended as a low-rank tensor recovery by solving the optimization problem integrated the tensor nuclear norm and the ℓ_1 norm in a framework. By assuming that there is a correlation between temperature profile images either in spatial or temporal, we can use a structural tensor recovery by assuming a stack of 2-D images as a 3rd-order tensor.

Bibliography

[1] J. Paalasmaa and M. Ranta, "Detecting heartbeats in the ballistocardiogram with clustering," in *Proceedings of the ICML/UAI/COLT 2008 Workshop on Machine Learning for Health-Care Applications, Helsinki, Finland*, vol. 9, 2008.

[2] J. Deny, E. Muthukumaran, S. Ramkumar, and S. Kartheesawaran, "Extraction of respiratory signals and motion artifacts from ppg signal using modified multi scale principal component analysis," *International Journal of Pure and Applied Mathematics*, vol. 119, no. 12, pp. 13719–13727, 2018.

[3] T. Küstner, A. Liebgott, L. Mauch, P. Martirosian, F. Bamberg, K. Nikolaou, B. Yang, F. Schick, and S. Gatidis, "Automated reference-free detection of motion artifacts in magnetic resonance images," *Magnetic Resonance Materials in Physics, Biology and Medicine*, vol. 31, no. 2, pp. 243–256, 2018.

[4] M. Zaitsev, J. Maclaren, and M. Herbst, "Motion artifacts in mri: a complex problem with many partial solutions," *Journal of Magnetic Resonance Imaging*, vol. 42, no. 4, pp. 887–901, 2015.

[5] G. Takla, J. H. Petre, D. J. Doyle, M. Horibe, and B. Gopakumaran, "The problem of artifacts in patient monitor data during surgery: a clinical and methodological review," *Anesthesia & Analgesia*, vol. 103, no. 5, pp. 1196–1204, 2006.

[6] S. Malviya, T. Voepel-Lewis, O. P. Eldevik, D. T. Rockwell, J. Wong, and A. Tait, "Sedation and general anaesthesia in children undergoing mri and ct: adverse events and outcomes," *British journal of anaesthesia*, vol. 84, no. 6, pp. 743–748, 2000.

[7] M. A. Bernstein, K. F. King, and X. J. Zhou, *Handbook of MRI pulse sequences*. Elsevier, 2004.

[8] C. Hoog Antink, F. Schulz, S. Leonhardt, and M. Walter, "Motion artifact quantification and sensor fusion for unobtrusive health monitoring," *Sensors*, vol. 18, no. 1, p. 38, 2018.

[9] C. Lord, M. Elsabbagh, G. Baird, and J. Veenstra-Vanderweele, "Autism spectrum disorder," *The Lancet*, 2018.

[10] C. R. Johnson, K. S. Turner, E. Foldes, M. M. Brooks, R. Kronk, and L. Wiggs, "Behavioral parent training to address sleep disturbances in young children with autism spectrum disorder: a pilot trial," *Sleep medicine*, vol. 14, no. 10, pp. 995–1004, 2013.

[11] C. R. Johnson, K. S. Turner, E. L. Foldes, B. A. Malow, and L. Wiggs, "Comparison of sleep questionnaires in the assessment of sleep disturbances in children with autism spectrum disorders," *Sleep medicine*, vol. 13, no. 7, pp. 795–801, 2012.

[12] V. Hallett, L. Lecavalier, D. G. Sukhodolsky, N. Cipriano, M. G. Aman, J. T. McCracken, C. J. McDougle, E. Tierney, B. H. King, E. Hollander, *et al.*, "Exploring the manifestations of anxiety in children with autism spectrum disorders," *Journal of autism and developmental disorders*, vol. 43, no. 10, pp. 2341–2352, 2013.

[13] M. A. Hattier, J. L. Matson, B. C. Belva, and M. Horovitz, "The occurrence of challenging behaviours in children with autism spectrum disorders and atypical development," *Developmental Neurorehabilitation*, vol. 14, no. 4, pp. 221–229, 2011.

[14] J. L. Matson, S. Mahan, J. A. Hess, J. C. Fodstad, and D. Neal, "Progression of challenging behaviors in children and adolescents with autism spectrum disorders as measured by the autism spectrum disorders-problem behaviors for children (asd-pbc)," *Research in Autism Spectrum Disorders*, vol. 4, no. 3, pp. 400–404, 2010.

[15] A. Sadeh, R. Gruber, and A. Raviv, "Sleep, neurobehavioral functioning, and behavior problems in school-age children," *Child development*, vol. 73, no. 2, pp. 405–417, 2002.

[16] V. Rieke and K. Butts Pauly, "Mr thermometry," *Journal of magnetic resonance imaging*, vol. 27, no. 2, pp. 376–390, 2008.

[17] V. Rieke, A. M. Kinsey, A. B. Ross, W. H. Nau, C. J. Diederich, G. Sommer, and K. B. Pauly, "Referenceless mr thermometry for monitoring thermal ablation in the prostate," *IEEE transactions on medical imaging*, vol. 26, no. 6, pp. 813–821, 2007.

[18] K. K. Vigen, B. L. Daniel, J. M. Pauly, and K. Butts, "Triggered, navigated, multi-baseline method for proton resonance frequency temperature mapping with respiratory motion," *Magnetic resonance in medicine*, vol. 50, no. 5, pp. 1003–1010, 2003.

[19] W. A. Grissom, V. Rieke, A. B. Holbrook, Y. Medan, M. Lustig, J. Santos, M. V. McConnell, and K. B. Pauly, "Hybrid referenceless and multibaseline subtraction mr thermometry for monitoring thermal therapies in moving organs," *Medical physics*, vol. 37, no. 9, pp. 5014–5026, 2010.

[20] A. Alivar, C. Carlson, A. Suliman, S. Warren, P. Prakash, D. Thompson, and B. Natarajan, "Motion detection in bed-based ballistocardiogram to quantify sleep quality," in *GLOBECOM 2017-2017 IEEE Global Communications Conference*, pp. 1–6, IEEE, 2017.

[21] A. Alivar, C. Carlson, A. Suliman, S. Warren, P. Prakash, D. E. Thompson, and B. Natarajan, "Motion artifact detection and reduction in bed-based ballistocardiogram," *IEEE Access*, 2019.

[22] A. Alivar, C. Carlson, A. Suliman, S. Warren, P. Prakash, D. E. Thompson, and B. Natarajan, "Smart bed based daytime behavior prediction in children with autism spectrum disorder - a pilot study* (to be submitted to)," *Medical Engineering & Physics*, 2019.

[23] A. Alivar, C. Carlson, A. Suliman, S. Warren, P. Prakash, D. E. Thompson, and B. Natarajan, "A pilot study on predicting daytime behavior & sleep quality in children with asd (under review)," IEEE, 2019.

[24] A. Alivar, P. Faridi, P. Prakash, and B. Natarajan, "An enhanced hybrid mri thermometry technique for monitoring microwave thermal therapy," in *Medical Imaging 2019:*

Image-Guided Procedures, Robotic Interventions, and Modeling, vol. 10951, p. 109512P, International Society for Optics and Photonics, 2019.

[25] A. Alivar, P. Prakash, and B. Natarajan, "Reducing sparse motion artifacts in mr-thermometry using robust principal component analysis (to be submitted to)," in *International Symposium on Biomedical Imaging*, IEEE, 2020.

[26] I. Starr, A. Rawson, H. Schroeder, and N. Joseph, "Studies on the estimation of cardiac ouptut in man, and of abnormalities in cardiac function, from the heart's recoil and the blood's impacts; the ballistocardiogram," *American Journal of Physiology-Legacy Content*, vol. 127, no. 1, pp. 1–28, 1939.

[27] J. Gordon, "Certain molar movements of the human body produced by the circulation of the blood," *Journal of anatomy and physiology*, vol. 11, no. Pt 3, p. 533, 1877.

[28] T. Koivistoinen, S. Junnila, A. Varri, and T. Koobi, "A new method for measuring the ballistocardiogram using emfi sensors in a normal chair," in *Engineering in Medicine and Biology Society, 2004. IEMBS'04. 26th Annual International Conference of the IEEE*, vol. 1, pp. 2026–2029, IEEE, 2004.

[29] C. Carlson, A. Suliman, P. Prakash, D. Thompson, S. Wang, B. Natarajan, and S. Warren, "Bed-based instrumentation for unobtrusive sleep quality assessment in severely disabled autistic children," in *2016 IEEE 38th Annual International Conference of the Engineering in Medicine and Biology Society (EMBC)*, pp. 4909–4912, IEEE, 2016.

[30] S. H. Hwang, H. N. Yoon, Y.-J. G. Lee, D.-U. Jeong, K. S. Park, *et al.*, "Nocturnal awakening and sleep efficiency estimation using unobtrusively measured ballistocardiogram," *IEEE Transactions on Biomedical Engineering*, vol. 61, no. 1, pp. 131–138, 2014.

[31] A. Sivanantham, "Measurement of heartbeat, respiration and movements detection using smart bed," in *2015 IEEE Recent Advances in Intelligent Computational Systems (RAICS)*, pp. 105–109, IEEE, 2015.

[32] A. Vehkaoja, S. Rajala, P. Kumpulainen, and J. Lekkala, "Correlation approach for the detection of the heartbeat intervals using force sensors placed under the bed posts," *Journal of medical engineering & technology*, vol. 37, no. 5, pp. 327–333, 2013.

[33] Y. Zhu, H. Zhang, M. Jayachandran, A. K. Ng, J. Biswas, and Z. Chen, "Ballistocardiography with fiber optic sensor in headrest position: a feasibility study and a new processing algorithm," in *2013 35th Annual International Conference of the IEEE Engineering in Medicine and Biology Society (EMBC)*, pp. 5203–5206, IEEE, 2013.

[34] C. Brüser, N. Strutz, S. Winter, S. Leonhardt, and M. Walter, "Monte-carlo simulation and automated test bench for developing a multichannel nir-based vital-signs monitor," *IEEE transactions on biomedical circuits and systems*, vol. 9, no. 3, pp. 421–430, 2015.

[35] D. C. Mack, J. T. Patrie, P. M. Suratt, R. A. Felder, and M. Alwan, "Development and preliminary validation of heart rate and breathing rate detection using a passive, ballistocardiography-based sleep monitoring system," *IEEE Transactions on Information Technology in Biomedicine*, vol. 13, no. 1, pp. 111–120, 2009.

[36] M. Liu, F. Jiang, H. Jiang, S. Ye, and H. Chen, "Low-power, noninvasive measurement system for wearable ballistocardiography in sitting and standing positions," *Computers in Industry*, vol. 91, pp. 24–32, 2017.

[37] M. Etemadi and O. T. Inan, "Wearable ballistocardiogram and seismocardiogram systems for health and performance," *Journal of Applied Physiology*, vol. 124, no. 2, pp. 452–461, 2017.

[38] C. Carlson, A. Suliman, A. Alivar, P. Prakash, D. Thompson, B. Natarajan, and S. Warren, "A pilot study of an unobtrusive bed-based sleep quality monitor for severely disabled autistic children," in *2018 40th Annual International Conference of the IEEE Engineering in Medicine and Biology Society (EMBC)*, pp. 4343–4346, IEEE, 2018.

[39] O. T. Inan, P.-F. Migeotte, K.-S. Park, M. Etemadi, K. Tavakolian, R. Casanella, J. Zanetti, J. Tank, I. Funtova, G. K. Prisk, *et al.*, "Ballistocardiography and seismocardiography: A review of recent advances," *IEEE journal of biomedical and health informatics*, vol. 19, no. 4, pp. 1414–1427, 2015.

[40] J. S. Paul, M. R. Reddy, and V. J. Kumar, "A transform domain svd filter for suppression of muscle noise artefacts in exercise ecg's," *IEEE Transactions on Biomedical Engineering*, vol. 47, no. 5, pp. 654–663, 2000.

[41] G. Lu, J.-S. Brittain, P. Holland, J. Yianni, A. L. Green, J. F. Stein, T. Z. Aziz, and S. Wang, "Removing ecg noise from surface emg signals using adaptive filtering," *Neuroscience letters*, vol. 462, no. 1, pp. 14–19, 2009.

[42] M. Ayat, M. B. Shamsollahi, B. Mozaffari, and S. Kharabian, "Ecg denoising using modulus maxima of wavelet transform," in *2009 Annual International Conference of the IEEE Engineering in Medicine and Biology Society*, pp. 416–419, IEEE, 2009.

[43] R. Sameni, M. B. Shamsollahi, C. Jutten, and G. D. Clifford, "A nonlinear bayesian filtering framework for ecg denoising," *IEEE Transactions on Biomedical Engineering*, vol. 54, no. 12, pp. 2172–2185, 2007.

[44] H. Kim, S. Kim, N. Van Helleputte, T. Berset, D. Geng, I. Romero, J. Penders, C. Van Hoof, and R. F. Yazicioglu, "Motion artifact removal using cascade adaptive filtering for ambulatory ecg monitoring system," in *Biomedical Circuits and Systems Conference (BioCAS), 2012 IEEE*, pp. 160–163, IEEE, 2012.

[45] A. M. Adami, M. Pavel, T. L. Hayes, and C. M. Singer, "Detection of movement in bed using unobtrusive load cell sensors," *IEEE Transactions on Information Technology in Biomedicine*, vol. 14, no. 2, pp. 481–490, 2010.

[46] R. Krishnan, B. Natarajan, and S. Warren, "Two-stage approach for detection and reduction of motion artifacts in photoplethysmographic data," *IEEE transactions on biomedical engineering*, vol. 57, no. 8, pp. 1867–1876, 2010.

[47] M. Raghuram, K. Sivani, and K. A. Reddy, "Use of complex emd generated noise reference for adaptive reduction of motion artifacts from ppg signals," in *Electrical, Electronics, and Optimization Techniques (ICEEOT), International Conference on*, pp. 1816–1820, IEEE, 2016.

[48] R. W. Wijshoff, M. Mischi, and R. M. Aarts, "Reduction of periodic motion artifacts in photoplethysmography," *IEEE Transactions on Biomedical Engineering*, vol. 64, no. 1, pp. 196–207, 2017.

[49] A.-M. Tăuţan, A. Young, E. Wentink, and F. Wieringa, "Characterization and reduction of motion artifacts in photoplethysmographic signals from a wrist-worn device," in *Engineering in Medicine and Biology Society (EMBC), 2015 37th Annual International Conference of the IEEE*, pp. 6146–6149, IEEE, 2015.

[50] J. W. Chong, D. K. Dao, S. Salehizadeh, D. D. McManus, C. E. Darling, K. H. Chon, and Y. Mendelson, "Photoplethysmograph signal reconstruction based on a novel hybrid motion artifact detection–reduction approach. part i: motion and noise artifact detection," *Annals of biomedical engineering*, vol. 42, no. 11, pp. 2238–2250, 2014.

[51] R. M. Wiard, O. T. Inan, B. Argyres, M. Etemadi, G. T. Kovacs, and L. Giovangrandi, "Automatic detection of motion artifacts in the ballistocardiogram measured on a modified bathroom scale," *Medical & biological engineering & computing*, vol. 49, no. 2, pp. 213–220, 2011.

[52] J. Paalasmaa, H. Toivonen, and M. Partinen, "Adaptive heartbeat modeling for beat-to-beat heart rate measurement in ballistocardiograms," *IEEE journal of biomedical and health informatics*, vol. 19, no. 6, pp. 1945–1952, 2015.

[53] J. Alametsä, A. Värri, J. Viik, J. Hyttinen, and A. Palomäki, "Ballistocardiogaphic studies with acceleration and electromechanical film sensors," *Medical engineering & physics*, vol. 31, no. 9, pp. 1154–1165, 2009.

[54] H. V. Poor, *An introduction to signal detection and estimation*. Springer Science & Business Media, 2013.

[55] A. Domingues, O. Adamec, T. Paiva, and J. M. Sanches, "Automatic annotation of actigraphy data for sleep disorders diagnosis purposes," in *2010 Annual International Conference of the IEEE Engineering in Medicine and Biology*, pp. 5081–5084, IEEE, 2010.

[56] J. Pan and W. J. Tompkins, "A real-time qrs detection algorithm," *IEEE Trans. Biomed. Eng*, vol. 32, no. 3, pp. 230–236, 1985.

[57] F. Scholkmann, J. Boss, and M. Wolf, "An efficient algorithm for automatic peak detection in noisy periodic and quasi-periodic signals," *Algorithms*, vol. 5, no. 4, pp. 588–603, 2012.

[58] V. X. Afonso, W. J. Tompkins, T. Q. Nguyen, and S. Luo, "Ecg beat detection using filter banks," *IEEE transactions on biomedical engineering*, vol. 46, no. 2, pp. 192–202, 1999.

[59] R. L. Spitzer and J. B. Williams, "Diagnostic and statistical manual of mental disorders," in *American Psychiatric Association*, Citeseer, 1980.

[60] A. V. Brereton, B. J. Tonge, and S. L. Einfeld, "Psychopathology in children and adolescents with autism compared to young people with intellectual disability," *Journal of autism and developmental disorders*, vol. 36, no. 7, pp. 863–870, 2006.

[61] L. Lecavalier, "Behavioral and emotional problems in young people with pervasive developmental disorders: Relative prevalence, effects of subject characteristics, and empirical classification," *Journal of Autism and Developmental disorders*, vol. 36, no. 8, pp. 1101–1114, 2006.

[62] C. D. Hoffman, D. P. Sweeney, J. E. Gilliam, and M. C. Lopez-Wagner, "Sleep problems in children with autism and in typically developing children," *Focus on Autism and Other Developmental Disabilities*, vol. 21, no. 3, pp. 146–152, 2006.

[63] X. Liu, J. A. Hubbard, R. A. Fabes, and J. B. Adam, "Sleep disturbances and correlates of children with autism spectrum disorders," *Child psychiatry and human development*, vol. 37, no. 2, pp. 179–191, 2006.

[64] A. Schwichtenberg, A.-M. Iosif, B. Goodlin-Jones, K. Tang, and T. Anders, "Daytime sleep patterns in preschool children with autism, developmental delay, and typical development," *American journal on intellectual and developmental disabilities*, vol. 116, no. 2, pp. 142–152, 2011.

[65] L. J. Meltzer and J. A. Mindell, "Relationship between child sleep disturbances and maternal sleep, mood, and parenting stress: a pilot study.," *Journal of Family Psychology*, vol. 21, no. 1, p. 67, 2007.

[66] R. G. Astill, K. B. Van der Heijden, M. H. Van IJzendoorn, and E. J. Van Someren, "Sleep, cognition, and behavioral problems in school-age children: A century of research meta-analyzed.," *Psychological bulletin*, vol. 138, no. 6, p. 1109, 2012.

[67] M. A. Stein, J. Mendelsohn, W. H. Obermeyer, J. Amromin, and R. Benca, "Sleep and behavior problems in school-aged children," *Pediatrics*, vol. 107, no. 4, pp. e60–e60, 2001.

[68] D. M. Sikora, K. Johnson, T. Clemons, and T. Katz, "The relationship between sleep problems and daytime behavior in children of different ages with autism spectrum disorders," *Pediatrics*, vol. 130, no. Supplement 2, pp. S83–S90, 2012.

[69] E. Limoges, C. Bolduc, C. Berthiaume, L. Mottron, and R. Godbout, "Relationship between poor sleep and daytime cognitive performance in young adults with autism," *Research in developmental disabilities*, vol. 34, no. 4, pp. 1322–1335, 2013.

[70] I. Hirata, I. Mohri, K. Kato-Nishimura, M. Tachibana, A. Kuwada, K. Kagitani-Shimono, Y. Ohno, K. Ozono, and M. Taniike, "Sleep problems are more frequent and associated with problematic behaviors in preschoolers with autism spectrum disorder," *Research in developmental disabilities*, vol. 49, pp. 86–99, 2016.

[71] D. Wachob and D. G. Lorenzi, "Brief report: Influence of physical activity on sleep quality in children with autism," *Journal of autism and developmental disorders*, vol. 45, no. 8, pp. 2641–2646, 2015.

[72] A. Lambert, S. Tessier, A.-C. Rochette, P. Scherzer, L. Mottron, and R. Godbout, "Poor sleep affects daytime functioning in typically developing and autistic children not complaining of sleep problems: A questionnaire-based and polysomnographic study," *Research in Autism Spectrum Disorders*, vol. 23, pp. 94–106, 2016.

[73] S. Miano, O. Bruni, M. Elia, A. Trovato, A. Smerieri, E. Verrillo, M. Roccella, M. G. Terzano, and R. Ferri, "Sleep in children with autistic spectrum disorder: a questionnaire and polysomnographic study," *Sleep medicine*, vol. 9, no. 1, pp. 64–70, 2007.

[74] M. G. Elrod, C. M. Nylund, A. L. Susi, G. H. Gorman, E. Hisle-Gorman, D. J. Rogers, and C. Erdie-Lalena, "Prevalence of diagnosed sleep disorders and related diagnostic and surgical procedures in children with autism spectrum disorders," *Journal of Developmental & Behavioral Pediatrics*, vol. 37, no. 5, pp. 377–384, 2016.

[75] B. A. Malow, M. L. Marzec, S. G. McGrew, L. Wang, L. M. Henderson, and W. L. Stone, "Characterizing sleep in children with autism spectrum disorders: a multidimensional approach," *Sleep*, vol. 29, no. 12, pp. 1563–1571, 2006.

[76] S. M. Doran, M. T. Harvey, and R. H. Horner, "Sleep and developmental disabilities: assessment, treatment, and outcome measures," *Mental Retardation*, vol. 44, no. 1, pp. 13–27, 2006.

[77] S. E. Goldman, K. Surdyka, R. Cuevas, K. Adkins, L. Wang, and B. A. Malow, "Defining the sleep phenotype in children with autism," *Developmental neuropsychology*, vol. 34, no. 5, pp. 560–573, 2009.

[78] F. Cortesi, F. Giannotti, T. Sebastiani, S. Panunzi, and D. Valente, "Controlled-release melatonin, singly and combined with cognitive behavioural therapy, for persistent in-

somnia in children with autism spectrum disorders: A randomized placebo-controlled trial," *Journal of sleep research*, vol. 21, no. 6, pp. 700–709, 2012.

[79] B. A. Malow, K. W. Adkins, A. Reynolds, S. K. Weiss, A. Loh, D. Fawkes, T. Katz, S. E. Goldman, N. Madduri, R. Hundley, *et al.*, "Parent-based sleep education for children with autism spectrum disorders," *Journal of autism and developmental disorders*, vol. 44, no. 1, pp. 216–228, 2014.

[80] B. Malow, K. W. Adkins, S. G. McGrew, L. Wang, S. E. Goldman, D. Fawkes, and C. Burnette, "Melatonin for sleep in children with autism: a controlled trial examining dose, tolerability, and outcomes," *Journal of autism and developmental disorders*, vol. 42, no. 8, pp. 1729–1737, 2012.

[81] T. Morgenthaler, C. Alessi, L. Friedman, J. Owens, V. Kapur, B. Boehlecke, T. Brown, A. Chesson Jr, J. Coleman, T. Lee-Chiong, *et al.*, "Practice parameters for the use of actigraphy in the assessment of sleep and sleep disorders: an update for 2007," *Sleep*, vol. 30, no. 4, pp. 519–529, 2007.

[82] A. Domingues, T. Paiva, and J. M. Sanches, "Sleep and wakefulness state detection in nocturnal actigraphy based on movement information," *IEEE Transactions on Biomedical Engineering*, vol. 61, no. 2, pp. 426–434, 2014.

[83] J. Paalasmaa, M. Waris, H. Toivonen, L. Leppäkorpi, and M. Partinen, "Unobtrusive online monitoring of sleep at home," in *2012 Annual International Conference of the IEEE Engineering in Medicine and Biology Society*, pp. 3784–3788, IEEE, 2012.

[84] K. S. Park, S. H. Hwang, H. N. Yoon, W. K. Lee, *et al.*, "Ballistocardiography for nonintrusive sleep structure estimation," in *2014 36th Annual International Conference of the IEEE Engineering in Medicine and Biology Society*, pp. 5184–5187, IEEE, 2014.

[85] S. H. Hwang, G. S. Chung, Y.-J. Lee, D.-U. Jeong, K. S. Park, *et al.*, "Estimation of sleep onset latency based on the blood pressure regulatory reflex mechanism," *IEEE journal of biomedical and health informatics*, vol. 17, no. 3, pp. 539–544, 2013.

[86] C. C. Fadini, D. A. Lamônica, A. C. Fett-Conte, E. Osório, G. M. Zuculo, C. M. Giacheti, and L. Pinato, "Influence of sleep disorders on the behavior of individuals with autism spectrum disorder," *Frontiers in human neuroscience*, vol. 9, p. 347, 2015.

[87] N. AlBacker and S. Bashir, "Assessment of parent report and actigraphy for sleep in children with autism spectrum disorders. pilot study," *Neurology, Psychiatry and Brain Research*, vol. 23, pp. 16–19, 2017.

[88] E. A. Abel, A. Schwichtenberg, M. T. Brodhead, and S. L. Christ, "Sleep and challenging behaviors in the context of intensive behavioral intervention for children with autism," *Journal of autism and developmental disorders*, pp. 1–14, 2018.

[89] S. E. Goldman, S. McGrew, K. P. Johnson, A. L. Richdale, T. Clemons, and B. A. Malow, "Sleep is associated with problem behaviors in children and adolescents with autism spectrum disorders," *Research in Autism Spectrum Disorders*, vol. 5, no. 3, pp. 1223–1229, 2011.

[90] S. Cohen, B. D. Fulcher, S. M. Rajaratnam, R. Conduit, J. P. Sullivan, M. A. St Hilaire, A. J. Phillips, T. Loddenkemper, S. V. Kothare, K. McConnell, *et al.*, "Sleep patterns predictive of daytime challenging behavior in individuals with low-functioning autism," *Autism Research*, vol. 11, no. 2, pp. 391–403, 2018.

[91] J. A. Hollway, M. G. Aman, and E. Butter, "Correlates and risk markers for sleep disturbance in participants of the autism treatment network," *Journal of autism and developmental disorders*, vol. 43, no. 12, pp. 2830–2843, 2013.

[92] M. O. Mazurek and K. Sohl, "Sleep and behavioral problems in children with autism spectrum disorder," *Journal of autism and developmental disorders*, vol. 46, no. 6, pp. 1906–1915, 2016.

[93] M. G. Elrod and B. S. Hood, "Sleep differences among children with autism spectrum disorders and typically developing peers: a meta-analysis," *Journal of Developmental & Behavioral Pediatrics*, vol. 36, no. 3, pp. 166–177, 2015.

[94] J. Friedman, T. Hastie, and R. Tibshirani, *The elements of statistical learning*, vol. 1. Springer series in statistics New York, NY, USA:, 2001.

[95] M. O. Mazurek, R. A. Vasa, L. G. Kalb, S. M. Kanne, D. Rosenberg, A. Keefer, D. S. Murray, B. Freedman, and L. A. Lowery, "Anxiety, sensory over-responsivity, and gastrointestinal problems in children with autism spectrum disorders," *Journal of abnormal child psychology*, vol. 41, no. 1, pp. 165–176, 2013.

[96] A. P. Hill, K. E. Zuckerman, A. D. Hagen, D. J. Kriz, S. W. Duvall, J. Van Santen, J. Nigg, D. Fair, and E. Fombonne, "Aggressive behavior problems in children with autism spectrum disorders: prevalence and correlates in a large clinical sample," *Research in autism spectrum disorders*, vol. 8, no. 9, pp. 1121–1133, 2014.

[97] P. Faridi, S. H. Bossmann, and P. Prakash, "Image-guided cancer thermal therapies," in *Magnetic Nanomaterials*, pp. 195–220, 2017.

[98] K. F. Chu and D. E. Dupuy, "Thermal ablation of tumours: biological mechanisms and advances in therapy," *Nature Reviews Cancer*, vol. 14, no. 3, p. 199, 2014.

[99] R. D. Issels, L. H. Lindner, J. Verweij, P. Wust, P. Reichardt, B.-C. Schem, S. Abdel-Rahman, S. Daugaard, C. Salat, C.-M. Wendtner, *et al.*, "Neo-adjuvant chemotherapy alone or with regional hyperthermia for localised high-risk soft-tissue sarcoma: a randomised phase 3 multicentre study," *The lancet oncology*, vol. 11, no. 6, pp. 561–570, 2010.

[100] L. Winter, E. Oberacker, K. Paul, Y. Ji, C. Oezerdem, P. Ghadjar, A. Thieme, V. Budach, P. Wust, and T. Niendorf, "Magnetic resonance thermometry: methodology, pitfalls and practical solutions," *International Journal of Hyperthermia*, vol. 32, no. 1, pp. 63–75, 2016.

[101] Y. Ishihara, A. Calderon, H. Watanabe, K. Okamoto, Y. Suzuki, K. Kuroda, and Y. Suzuki, "A precise and fast temperature mapping using water proton chemical shift," *Magnetic resonance in medicine*, vol. 34, no. 6, pp. 814–823, 1995.

[102] J. D. Poorter, C. D. Wagter, Y. D. Deene, C. Thomsen, F. Ståhlberg, and E. Achten, "Noninvasive mri thermometry with the proton resonance frequency (prf) method: in vivo results in human muscle," *Magnetic resonance in medicine*, vol. 33, no. 1, pp. 74–81, 1995.

[103] K. Kuroda, "Mr techniques for guiding high-intensity focused ultrasound (hifu) treatments," *Journal of Magnetic Resonance Imaging*, 2017.

[104] U. Kägebein, O. Speck, F. Wacker, and B. Hensen, "Motion correction in proton resonance frequency–based thermometry in the liver," *Topics in Magnetic Resonance Imaging*, vol. 27, no. 1, pp. 53–61, 2018.

[105] V. Rieke, K. K. Vigen, G. Sommer, B. L. Daniel, J. M. Pauly, and K. Butts, "Referenceless prf shift thermometry," *Magnetic resonance in medicine*, vol. 51, no. 6, pp. 1223–1231, 2004.

[106] W. A. Grissom, M. Lustig, A. B. Holbrook, V. Rieke, J. M. Pauly, and K. Butts-Pauly, "Reweighted ℓ_1 referenceless prf shift thermometry," *Magnetic resonance in medicine*, vol. 64, no. 4, pp. 1068–1077, 2010.

[107] P. Gaur, B. Werner, X. Feng, S. W. Fielden, C. H. Meyer, and W. A. Grissom, "Spatially-segmented undersampled mri temperature reconstruction for transcranial mr-guided focused ultrasound," *Journal of therapeutic ultrasound*, vol. 5, no. 1, p. 13, 2017.

[108] S. Mallat, *A wavelet tour of signal processing*. Academic press, 1999.

[109] F. Wen, L. Chu, P. Liu, and R. C. Qiu, "A survey on nonconvex regularization-based sparse and low-rank recovery in signal processing, statistics, and machine learning," *IEEE Access*, vol. 6, pp. 69883–69906, 2018.

[110] R. Otazo, E. Candès, and D. K. Sodickson, "Low-rank plus sparse matrix decomposition for accelerated dynamic mri with separation of background and dynamic components," *Magnetic Resonance in Medicine*, vol. 73, no. 3, pp. 1125–1136, 2015.

[111] J. Wright, A. Ganesh, S. Rao, Y. Peng, and Y. Ma, "Robust principal component analysis: Exact recovery of corrupted low-rank matrices via convex optimization," in *Advances in neural information processing systems*, pp. 2080–2088, 2009.

[112] E. J. Candès, X. Li, Y. Ma, and J. Wright, "Robust principal component analysis?," *Journal of the ACM (JACM)*, vol. 58, no. 3, p. 11, 2011.

[113] C. Croux and G. Haesbroeck, "Principal component analysis based on robust estimators of the covariance or correlation matrix: influence functions and efficiencies," *Biometrika*, vol. 87, no. 3, pp. 603–618, 2000.

[114] F. De la Torre and M. J. Black, "Robust principal component analysis for computer vision," in *Proceedings Eighth IEEE International Conference on Computer Vision. ICCV 2001*, vol. 1, pp. 362–369, IEEE, 2001.

[115] F. De La Torre and M. J. Black, "A framework for robust subspace learning," *International Journal of Computer Vision*, vol. 54, no. 1-3, pp. 117–142, 2003.

[116] H. Gao, J.-F. Cai, Z. Shen, and H. Zhao, "Robust principal component analysis-based four-dimensional computed tomography," *Physics in Medicine & Biology*, vol. 56, no. 11, p. 3181, 2011.

[117] Y. Peng, A. Ganesh, J. Wright, W. Xu, and Y. Ma, "Rasl: Robust alignment by sparse and low-rank decomposition for linearly correlated images," *IEEE transactions on pattern analysis and machine intelligence*, vol. 34, no. 11, pp. 2233–2246, 2012.

[118] H. Gao, S. Rapacchi, D. Wang, J. Moriarty, C. Meehan, J. Sayre, G. Laub, P. Finn, and P. Hu, "Compressed sensing using prior rank, intensity and sparsity model (prism): applications in cardiac cine mri," in *Proceedings of the 20th Annual Meeting of ISMRM, Melbourne, Australia*, p. 2242, 2012.

[119] J.-F. Cai, E. J. Candès, and Z. Shen, "A singular value thresholding algorithm for matrix completion," *SIAM Journal on Optimization*, vol. 20, no. 4, pp. 1956–1982, 2010.

[120] I. Daubechies, M. Defrise, and C. De Mol, "An iterative thresholding algorithm for linear inverse problems with a sparsity constraint," *Communications on Pure and Applied Mathematics: A Journal Issued by the Courant Institute of Mathematical Sciences*, vol. 57, no. 11, pp. 1413–1457, 2004.

[121] S. Curto, P. Faridi, T. B. Shrestha, M. Pyle, L. Maurmann, D. Troyer, S. H. Bossmann, and P. Prakash, "An integrated platform for small-animal hyperthermia investigations under ultra-high-field mri guidance," *International Journal of Hyperthermia*, vol. 34, no. 4, pp. 341–351, 2018.

[122] P. Wang and O. Unal, "Motion-compensated real-time mr thermometry augmented by tracking coils," *Journal of Magnetic Resonance Imaging*, vol. 41, no. 3, pp. 851–857, 2015.